AD NUMBER
AD045310
CLASSIFICATION CHANGES
TO: unclassified
FROM: confidential
LIMITATION CHANGES
TO: Approved for public release, distribution unlimited
FROM: Distribution authorized to U.S. Gov't. agencies and their contractors; Administrative/Operational Use; 01 MAY 1954. Other requests shall be referred to U.S. Naval Ordnance Lab., White Oak, MD.
AUTHORITY
15 Sep 1962, per doc markings; USNOL ltr, 29 Aug 1974

NAVORD REPORT 2987

AFSWP 484

THE SCALING OF BASE SURGE PHENOMENA OF SHALLOW UNDERWATER EXPLOSIONS

1 May 1954

U. S. NAVAL ORDNANCE LABORATORY
WHITE OAK, MARYLAND

PLEASE REPLACE PAGES 51 & 52 WITH NEW PAGES ATTACHED

NAVORD 2987

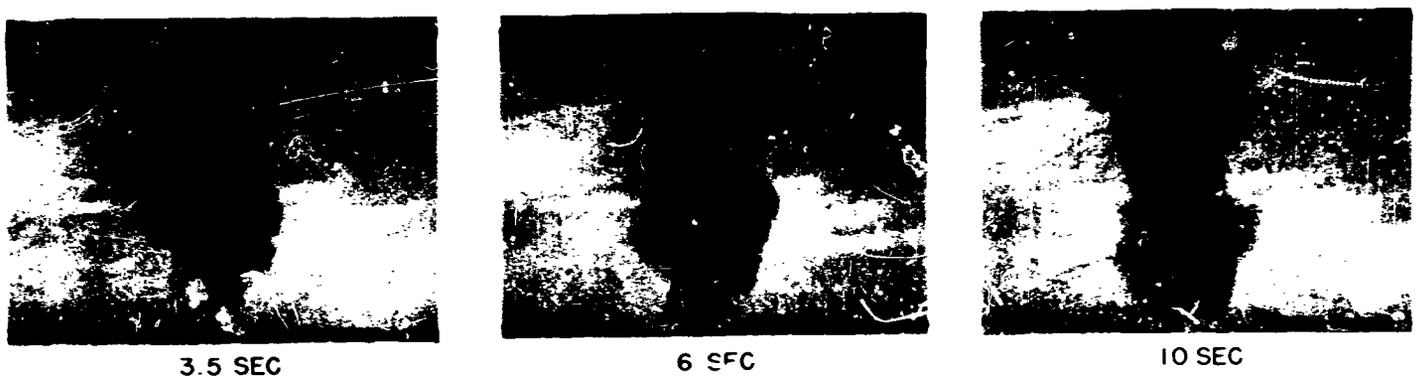

3.5 SEC 6 SEC 10 SEC

SHOT NO. 279
W = 4200 LB TNT

WATER DEPTH = 8.58 FT
λ_c = 0.307 FT/LB$^{1/3}$

2.5 SEC 5 SEC 10 SEC

SHOT NO. 216
W = 600 LB TNT

WATER DEPTH = 4.37 FT
λ_c = 0.257 FT/LB$^{1/3}$

FIG. 3.2 BASE SURGE FORMATION (TESTS SCALED TO BAKER)

4 SEC 7 SEC 16 SEC

SHOT NO. 280
W = 4200 LB TNT

WATER DEPTH = 1.83 FT
λ_d = 0.11⁶ FT/LB$^{1/3}$

4 SEC 7 SEC 12 SEC

SHOT NO. 221
W = 4200 LB TNT

WATER DEPTH = 9.25 FT
λ_d = 0.574 FT/LB$^{1/3}$

FIG. 3.3 BASE SURGE FORMATION (CHARGES ON BOTTOM)

CONFIDENTIAL
NAVORD Report 2987

INTERIM REPORT NO. 9
NOL PROJECT 152
AFSWP 484

THE SCALING OF BASE SURGE PHENOMENA OF SHALLOW UNDERWATER EXPLOSIONS

by
Mary L. Milligan
and
George A. Young

Approved by: E. Swift, Jr.
Chief, Explosion Hydrodynamics Division

ABSTRACT: A compilation and analysis of data collected in the study of the base surge and related surface phenomena resulting from shallow underwater explosions is presented. This includes a considerable body of data not reported elsewhere. Results of the firing of high explosive charges weighing up to 4200 lbs (TNT) at positions scaled to Test Baker in Operation CROSSROADS and at other depths are reported. The work includes studies of the effects of explosions at the water surface and explosions of partially buried charges.

Scaling laws are derived and the general problem of modeling nuclear surface phenomena with small scale experiments is discussed. A method is presented for predicting base surge growth from shallow underwater atomic explosions of various energy yields. Surface bursts are discussed qualitatively.

The results indicate that many of the surface phenomena observed at Bikini Baker are duplicated with high explosive charges and that considerable knowledge of the dynamics of column and base surge behavior can be obtained from small-scale tests. However, a major difference is the formation by high explosives of a central liquid jet, which rises above the column and as it collapses, greatly augments the radial growth of the base surge. The need for more information from shallow underwater atomic tests is emphasized.

U. S. NAVAL ORDNANCE LABORATORY
WHITE OAK, MARYLAND

NAVORD Report 2987 1 May 1954

This interim report presents the data and the conclusions concerning the surface phenomena from shallow underwater explosions which were obtained in the course of a general investigation of the scaling of the base surge effects of atomic weapons. The work was conducted at the Laboratory for the Armed Forces Special Weapons Project under Task NOL-152.

The new experimental work which is reported here was carried out by R. L. Willey, B. E. Cox, R. L. Marbury, C. E. Hopkins and D. L. Marks, principally at the Naval Proving Ground, Dahlgren, Virginia. The cooperation and assistance of Dahlgren personnel and the diving group from the Explosives Ordnance Disposal Unit, Indian Head, Maryland are gratefully acknowledged. Sincere thanks are due Dr. E. Swift, Jr. for his invaluable aid and suggestions during the program of investigation and the preparation of this report.

This report is intended for information only, and the opinions expressed are those of the authors.

EDWARD L. WOODYARD
Captain, USN
Commander

JAMES E. ABLARD
By direction

ILLUSTRATIONS (CONT.)

ILLUSTRATIONS (CONT.)

TABLES

THE SCALING OF BASE SURGE PHENOMENA OF SHALLOW UNDERWATER EXPLOSIONS

CHAPTER I

INTRODUCTION

1.1 Scope of Report. The base surge has been investigated under Naval Ordnance Laboratory Task NOL-152 since the fall of 1949 [1,2,3]*. The work was undertaken as a result of the observation of a base surge following the underwater atomic test (Baker) in Operation CROSSROADS and the subsequent concern over the possibility that the surge was a dangerous carrier of radioactivity. At NOL, the emphasis has been placed on studies of the base surge and other surface phenomena produced by underwater explosions at relatively shallow depths, but the program has also included investigations of the analogous surface effects of underground explosions [4,5]. In addition, it was possible to obtain data on other explosion effects, such as air blast [6] and cratering [7]. A liquid model of the base surge has been used with considerable success [1,2,3] and charges weighing 0.1 gram have been fired in a vacuum tank at various pressures in order to obtain a better understanding of column and jet formation [2]. With these experiments as a guide, a mathematical treatment of column formation was published [8].

At the present time a large amount of data has been accumulated on the base surge and related surface phenomena produced by underwater explosions. Preliminary results have been presented in References [1], [2] and [3] but the treatments were based mainly on the results of 21-lb and 100-lb explosion tests and were somewhat limited in scope.

---

* Such numbers refer to the list of references at the end of this report.

This report presents a summation of the currently available data on relatively shallow underwater explosion tests with charges weighing up to 4200 lbs and the formulas and conclusions presented herein will supersede those given previously. The report also includes a discussion of the general scaling problem and a summary of methods for the prediction of the base surge phenomena associated with atomic weapons, in accordance with the current state of knowledge.

1.2 Sources of Data. The primary sources of data on base surge are the programs of high explosive tests conducted by NOL. During the first two years of investigation, the emphasis was placed on charges weighing 21 lbs and 100 lbs, which were fired at the Stump Neck Annex of the Naval Powder Factory, Indian Head, Maryland. The principal data collected were radius measurements of the surge cloud as a function of time for explosions scaled geometrically to Test Baker in Operation CROSSROADS. A weapon with a 20 kiloton yield, fired at mid-depth in 180 ft of water was used as the prototype condition. However, recognition of the complex nature of base surge formation led to the measurement of all the visible surface phenomena. In addition, the range of firing conditions was extended in order to determine the effects of charge and water depth upon the surface effects.

Attempts to obtain instrumental data from within the surge clouds formed by the 21-lb and 100-lb charges were not highly successful, due to the small size and relatively brief durations of the surges. In addition, the duration of the surge was too limited for an adequate comparison with the scaled record of the growth of the Test Baker base surge.

It was therefore decided to shift the emphasis to larger charges, and experimental tests with 600-lb and 4200-lb

charges were conducted at the Naval Proving Ground, Dahlgren, Virginia.

Photographs of underwater explosion tests fired in the Potomac River from the EPCS-1413 in connection with other NOL projects were also obtained. Charge and water depth were different from those obtained at Stump Neck or Dahlgren.

The number of charges of each weight fired in the several NOL programs are listed in Table 1.1. For scaling purposes, charge weights given in the table were converted to the TNT equivalents given in Appendix A.

Motion picture films of the larger charges fired in the experimental programs at the Waterways Experiment Station, Vicksburg, Mississippi [9] were forwarded to NOL for analysis. In addition, data published by other investigators [10,11,12] have been incorporated into this report when appropriate.

1.3 Experimental Arrangements. For the smaller charges, water depths to about 5 ft were obtained in Chicamuxen Creek, which lies to the east of Stump Neck, Maryland, and deeper water, to a depth of 16 ft, was available in the Potomac River west of Stump Neck.

The underwater firing area at Dahlgren, Virginia, which was used for the larger charges, was located between Beabors Point and Black Marsh on the Pumpkin Neck peninsula. A broad beach with a gently sloping bottom was used for these tests. The bottom consisted of a firm clay or sand from the shore out to a water depth of about 5 ft but was covered with soft silt at greater depths [7].

The "21-lb" charges consisted of 7 tetrytol M2 demolition blocks, taped together to form a charge 12 in. long, 8 in. wide, and 4 in. high (see Fig. 1.1). (The tetrytol charges weighed 17.5 lbs but were considered to be equivalent to 21 lbs of TNT.) A 100-lb charge was formed by strapping two 50-lb TNT Mark 14 Demolition Blocks together to

TABLE 1.1

CHARGES FIRED IN NOL EXPERIMENTAL PROGRAMS

Shot Number	Dates	Location	Charge Weight (lb)																	
			1.6	7.5	10	12.5	15	17.5	20	20	20	20	20.2	31.5	35	83	100	100	600	3600	4200
			TNT	Tetrytol	TNT	Tetrytol	Tetrytol	Tetrytol	TNT	Tetrytol	Comp. B	Blasting Gelatin	Torpex	Comp. C-3	Tetrytol	Pentolite	Blasting Gelatin	TNT	TNT	TNT	TNT
1-99	2/15/50-6/13/50	Stump Neck	2	1	12	1		46	2	1	2		3					25	5		
100-105	6/27/50-6/28/50	Dahlgren																	6		
106-110	6/29/50-7/6/50	Stump Neck																5			
111-114	7/19/50-7/25/50	Dahlgren																			4
115-135	7/26/50-8/18/50	Stump Neck						11										10			
136-165	10/16/50-1/19/51	Stump Neck			1			2						1				26			
166-211	3/2/51-8/27/51	Stump Neck						10				5					5	26			
212-222	10/1/51-1/3/52	Dahlgren																	3		8
223-270	2/4/52-3/28/52	Stump Neck					1	26							2			20			
271-287	5/5/52-7/23/52	Dahlgren																	10		7
288-292	8/27/52-9/12/52	E.P.C.S.														5					
293-315	9/22/52-11/18/52	Dahlgren																12	1	1	9
316-322	7/9/53-7/22/53	E.P.C.S.																7			
Total number fired			2	1	13	1	1	95	2	1	2	5	3	1	2	5	5	131	25	1	28

Total Weight about 76 tons

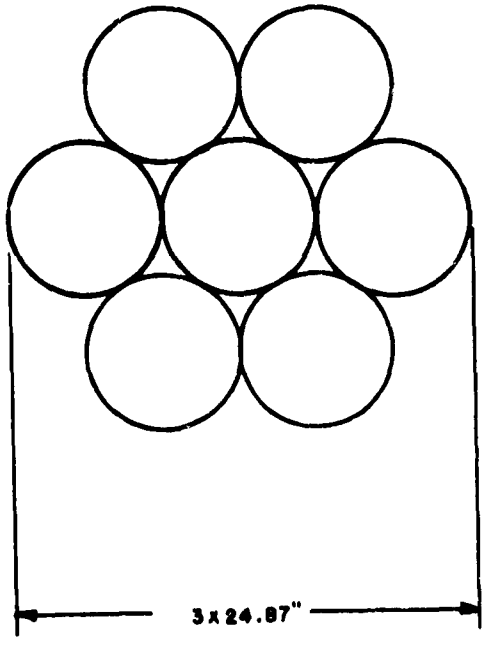

4200-LB TNT (TOP VIEW)
(SEVEN MK 7 DEPTH CHARGES)

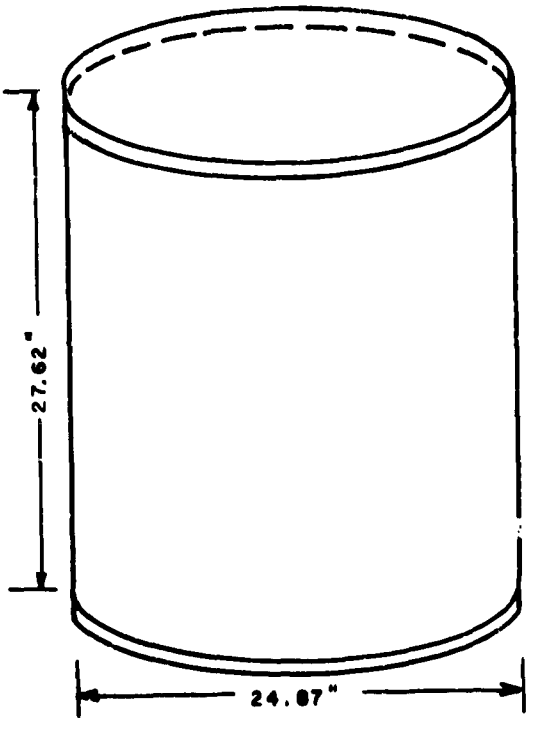

600-LB TNT
(MK 7 DEPTH CHARGE)

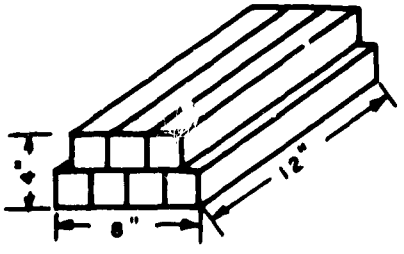

21-LB TNT EQUIVALENT
(SEVEN BLOCKS TETRYTOL)

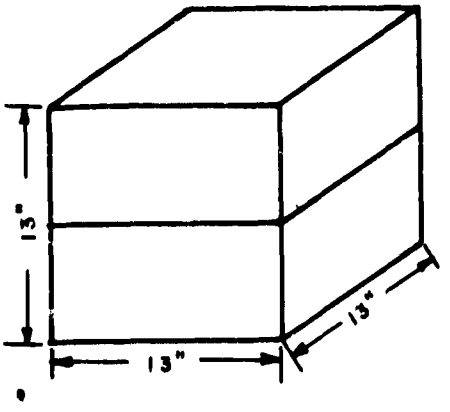

100-LB TNT
(TWO 50-LB MK 14 DEMOLITION BLOCKS)

FIG. 1.1 DIMENSIONS OF CHARGES FIRED IN EXPERIMENTAL PROGRAMS

form a cube, about 13 in. long on each side. For some experiments, 20-lb packages of 100% Blasting Gelatin, manufactured by the Atlas Powder Company, were used individually or combined to form 100-lb charges.

The 600-lb charges were Mark 7 depth charges, which are 24-7/8 in. in diameter and 27-5/8 in. long. The total length of the casing includes rims about one in. high, which sank into the bottom when the charges were placed on end for firing. The 3600-lb and 4200-lb charges consisted of 6 and 7 Mark 7 depth charges respectively, detonated in the central charge, which was encircled horizontally by the others. Thus, charge heights were the same as for the 600-lb charges, but diameters were about three times as large. The 3600-lb and 4200-lb charges, therefore, do not scale geometrically to the smaller charges and have a proportionately deeper layer of water above them than the smaller charges at the same scaled depth.

A small number of other charges of various weights and sizes were also included in the general program (see Table 1.1).

Composition C-3, a plastic explosive, was used as a booster for the TNT charges, and the charges were detonated with U. S. Army Engineers' Special Electric Blasting Caps.

The 21-lb and 100-lb charges were tied to a wooden pole or suspended from a float when it was necessary to fire these above the bottom. Wooden platforms, resting on the bottom, supported the larger charges when charge positions above the bottom were required. The placing and arming of the charges at Dahlgren in water depths greater than 5 ft was done by divers from the Explosive Ordnance Disposal Unit at Indian Head, Maryland.

At Stump Neck, one or two 35 mm Mitchell motion picture cameras, operating at 24 fps, were used to photograph each shot. For some of the tests, a 16 mm camera with Kodachrome film was mounted on a pole near the charge position

and aimed at the water surface to obtain close-up views of surge behavior.

At Dahlgren, two camera stations were used, generally with a total of five 35 mm Mitchell cameras operated at speeds ranging from 24 to 96 fps, two K-25 aerial cameras, and one 16 mm camera with Kodachrome film. Various positions were used, and the distances from the cameras to the charge varied from about 250 ft to 6600 ft. Timing for the Mitchells was provided by an electronic device which placed 100 dots per second on the margin of the film, or by a clock in the field of view of the camera. No timing was used in the 16 mm camera. The time interval between frames on the K-25 cameras was about 0.42 seconds.

A distance scale was established with markers placed a measured distance apart at the charge location, on a line perpendicular to the camera line of sight. Photoflash bulb scale markers were used for the larger charges (see Appendix B) and were visible from distances greater than 6000 ft.

The tide at Dahlgren is semidiurnal with a mean annual range of about 1.6 ft and is greatly affected by wind conditions. It was necessary to study these tidal effects and maintain a constant check on weather conditions. Predictions of tide and wind were made daily, and as two days were required to prepare instrumentation for each shot, a test was scheduled only when two consecutive days with satisfactory conditions were expected.

1.4 Analysis of Photographic Records. Measurements were made directly on continuous photographic prints of the 35 mm films, enlarged 5 times. The K-25 and 16 mm films were sometimes used to provide supplementary data; however, these were primarily useful for documentary purposes. K-25 prints are used as illustrations in this report when possible because of their superior quality.

The instant of detonation as seen on the films was taken as zero time. Length scales were corrected to compensate for the apparent vertical foreshortening in measurements of jet heights resulting from 600-lb and 4200-lb explosions. In addition, measurements were corrected for any horizontal motion due to the wind.

The measurements of each shot are summarized in Appendix A. Data obtained on temperatures, droplet and particle size distribution in the base surge, and meteorology at the test sites will be presented in NAVORD Report 2988 [13].

1.5 Symbols, Definitions and Units. The symbols used throughout this report are listed in Table 1.2.

TABLE 1.2
SYMBOLS, DEFINITIONS AND UNITS

Symbol	Units	Definition
t	sec	time
W	lb (TNT)	charge weight
d	ft	water depth
c	ft	charge depth, measured from the water surface to the center of the charge
λ_d	$ft/lb^{1/3}$	scaled depth, $d/W^{1/3}$, for charges on the bottom
λ_c	$ft/lb^{1/3}$	scaled depth, $c/W^{1/3}$, for charges not on the bottom
V	ft/sec	venting velocity
S	ft	smoke crown diameter
e_s	millibars	saturation water vapor pressure
e	millibars	water vapor pressure
T	ft	radial throwout diameter
D	ft	column diameter
C	ft	column height, measured to the base of the smoke crown

TABLE 1.2 (CONT.)

SYMBOLS, DEFINITIONS AND UNITS

Symbol	Units	Definition
J	ft	jet height
j	ft	jet diameter
Ω	ft	overall height
R	ft	base surge radius
H	ft	base surge height
r	dimensionless	scaled base surge radius, R/D_{max}
h	dimensionless	scaled base surge height, H/D_{max}
τ	$sec/ft^{1/2}$	scaled time, $t/D_{max}^{1/2}$
ρ	g/cm^3	density of moving fluid
ρ_o	g/cm^3	density of ambient fluid
σ	dimensionless	density ratio $\frac{\rho-\rho_o}{\rho}$
τ'	$sec/ft^{1/2}$	scaled time, $t\ C_{max}^{1/2}/D_{max}$, including effect of column height
h'	dimensionless	scaled base surge height, $H/(C_{max}\ D_{max})^{1/2}$, including effect of column height
A	ft	radius of underwater explosion bubble

1.6 Statistical Treatment of Data. It is not generally possible to fire shots in identical conditions in field experimentation. This might be accomplished with small charges in a tank or artificial pond [9,11]. However, the large scale of experiment required for the formation of surges of suitable size for measurement precludes this. Because of variations in bottom conditions and atmospheric effects, the nature of the phenomena, and the impossibility

of attaining complete objectivity in the measurement of records, a considerable degree of dispersion is usually found in the data. A discussion of the scatter of surface phenomena data has been presented in Reference [3] and additional material is given in Sec. 6.1 of this report.

The statistical terms and symbols used in this report are defined in Table 1.3.

TABLE 1.3

STATISTICAL SYMBOLS AND DEFINITIONS

Symbol	Definition
X	data expressed as individual items
N	total number of items
Σ	symbol meaning "sum of"
$\bar{X}$	arithmetic mean
x	deviation from arithmetic mean
σ	standard deviation of a single observation
σ_m	standard deviation of the mean
V	coefficient of variation (%)

$$\bar{X} = \frac{\Sigma(X)}{N}$$

$$x = X - \bar{X}$$

$$\sigma = \sqrt{\frac{\Sigma(x^2)}{N-1}}$$

$$\sigma_m = \frac{\sigma}{\sqrt{N}}$$

$$V = 100\ \frac{\sigma}{\bar{X}}$$

In the usual formula for σ, the sum of the squares of the deviations is divided by the total number of items. In this report, a correction is introduced by dividing by one less than the total number of items, as a relatively small amount of data is available in each category.

In many of the illustrations in this report, the standard deviation of a single observation and the standard deviation of the mean are indicated. This has been done only when at least 4 observations are available for the same or very similar firing conditions. A diagram showing the method of presentation is given in Fig. 1.2.

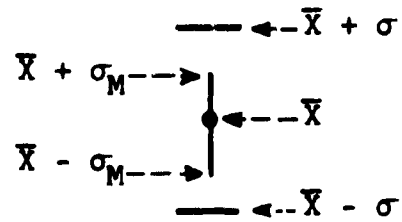

FIG 1.2 METHOD OF INDICATING SCATTER ON FIGURES

If the data have a Gaussian distribution, about 68% of all the observations will fall between $\bar{X}+\sigma$ and $\bar{X}-\sigma$ and over 95% of all the observations will lie between $\bar{X}+2\sigma$ and $\bar{X}-2\sigma$. If the extremes are disregarded $\bar{X}\pm2\sigma$ approximately represents the range of the data.

Throughout this report, the symbol $\bar{\lambda}$ is used to represent the arithmetic mean of a group of scaled depths.

CHAPTER II
SURFACE PHENOMENA

2.1 General Description. The appearance and structure of the surface phenomena produced by underwater explosions are markedly dependent upon charge depth and water depth. The results presented herein are limited to relatively shallow water conditions, where venting of the explosion bubble occurs during its initial expansion, but significant differences are observed in effects when firing conditions are varied even in this narrow range.

As an introduction it will be of interest to describe briefly the sequence of events above the water surface produced by the explosion of a 4200-lb TNT charge at a depth scaled to Test Baker. This represents an intermediate condition in the shallow charge range, and geometrical scaling is accomplished by placing the charge at mid-depth in 8.49 ft of water.

The first effect visible above the water surface is the vertical venting of a cloud of solid and gaseous explosion products mixed with a fine spray of water. This cloud grows rapidly into a roughly spherical shape and has been termed a "smoke crown". The smoke crown is followed by a cylindrical column of water, which rises beneath it and grows laterally to a maximum diameter of approximately 100 ft about 0.75 seconds after detonation (Fig. 2.1a). At the same time, the smoke crown rises and expands. The column enters the bottom of the smoke crown, but the extent of penetration is not known. For a 4200-lb shot scaled to Test Baker, the maximum height of the part of the column remaining visible beneath the smoke crown is about 140 ft.

Between 1.5 and 2 seconds after detonation, the leading edge of a high velocity jet appears above the expanding smoke crown, and rises to a height of 1000 ft (Fig. 2.1 b,c). This

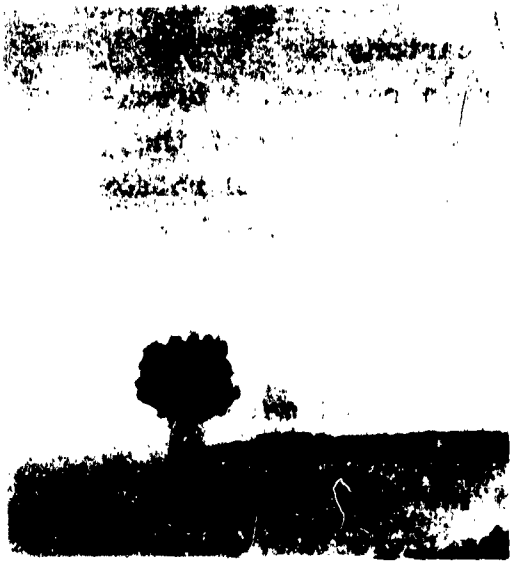

(a) 0.75 SEC

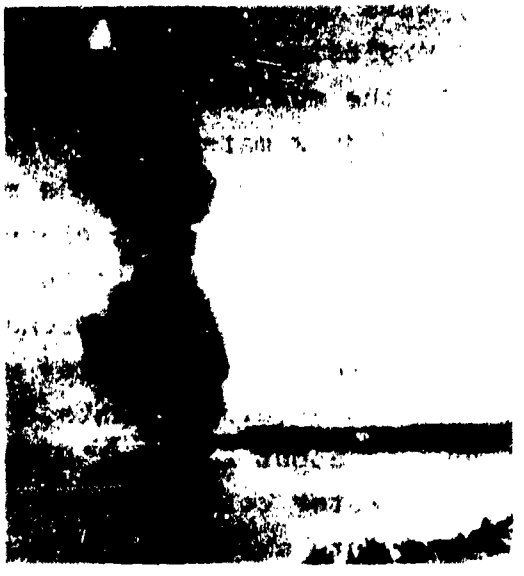

(c) 8.0 SEC

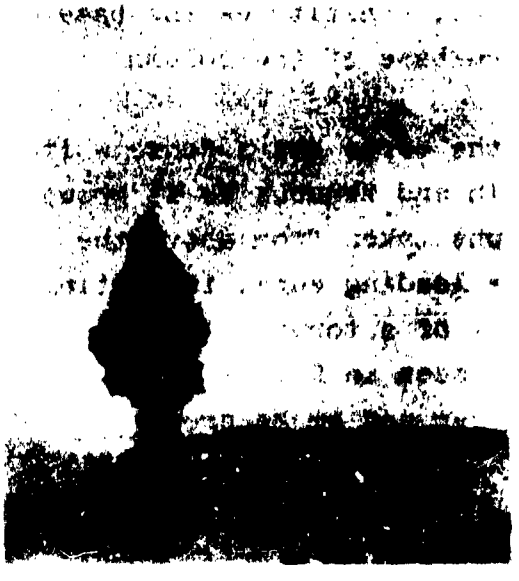

(b) 2.0 SEC

(d) 15 SEC

SHOT NO. 276
λ_c = 0.268 FT/LB$^{1/3}$

WATER DEPTH = 8.25 FT
CHARGE DEPTH = 4.33 FT

FIG. 2.1 SURFACE EFFECTS OF A 4200-LB TNT EXPLOSION SCALED TO TEST BAKER

jet appears to be predominantly liquid and is dark in color due to explosion products, probably carbon.

As the maximum column diameter is reached, a breakthrough of dark material is observed at the base of the column. This appears to be a mixture of water and bottom material ejected when the crater is formed and reaches a maximum height of 30-50 ft for shots scaled to the Baker geometry. After 8 to 10 seconds splashes may be observed from rocks and clumps of clay which were ejected by the explosion to greater heights. The maximum diameter of this throwout is about 200 ft.

The water column ejected into the air by the explosion breaks up into small droplets, giving the column a white appearance. When the column collapses the water droplets entrain the air in the column and the mixture of water and air descends and flows outward as if it were a homogeneous fluid*. This dense cloud, or aerosol, constitutes the base surge, which grows radially from the base of the column (Fig. 2.1c,d).

In the high explosive tests the surge has a dense white appearance at first and becomes thin and tenuous as it grows radially and vertically. Photographs taken from above the surge show a clear space behind the leading edge, indicating that the primary surge has the shape of a torus. (The torus-like form of the Baker surge may be seen in Fig. 3.1.) However, material falling from the jet and smoke crown propagates radially to form secondary surges, which may mix with the primary surge.

---

* The phenomenon of bulk subsidence of the column will be discussed more fully in Reference [13].

2.2 Smoke Crown. The smoke crown formed by an underwater explosion results from the initial venting of a cloud of smoke and fine spray directly above the charge. The venting velocity decreases with increasing charge depth. The relationship in feet per second can be expressed by the following formula, which is applicable to bottom shots only within the indicated range of scaled depths:

$$V = 2270 - 1580\ \lambda_d \quad (0.1 < \lambda_d < 1.1\ \text{ft/lb}^{1/3}) \qquad (1)$$

In general, shallow shots produce broad low bowl-shaped smoke crowns, which exhibit a rapid initial lateral expansion. Charges scaled to Test Baker ($\lambda_c = 0.26\ \text{ft/lb}^{1/3}$) produce smoke crowns which, except for their darker color, resemble the "cauliflower" cloud above the Baker column. (See Fig. 2.2). Smoke crowns formed by deeper explosions are narrow and extend to greater heights. They appear to consist mostly of a fine spray (Fig. 2.3).

A plot of maximum smoke crown diameter versus scaled charge depth for charges on the bottom is shown in Fig. 2.4, and indicates that within a scaled depth range from 0.1 $\text{ft/lb}^{1/3}$ to about 0.6 $\text{ft/lb}^{1/3}$ maximum smoke crown diameter is virtually independent of depth and is mainly a function of charge weight. For λ_d values greater than about 0.6 $\text{ft/lb}^{1/3}$ the maximum horizontal extent of the smoke crown decreases rapidly with increasing charge depth. At a scaled depth of 2.15 $\text{ft/lb}^{1/3}$, the smoke crown is narrow and elongated and apparently contains little carbon.

Maximum smoke crown diameters versus the cube root of charge weight for charges on the bottom within the scaled depth range of $\lambda_d = 0.1\ \text{ft/lb}^{1/3}$ to $\lambda_d = 0.6\ \text{ft/lb}^{1/3}$ are shown in Fig. 2.5. Using cube root scaling, the relationship in ft and lb is expressed by the formula:

t ≅ 0.5 SEC

SHOT NO. 280
WATER DEPTH = 1.83 FT
λ_d = 0.114 FT/LB$^{1/3}$

t ≅ 0.4 SEC

SHOT NO. 214
WATER DEPTH = 4.33 FT
λ_d = 0.269 FT/LB$^{1/3}$

FIG. 22 SMOKE CROWN FORMATION BY RELATIVELY SHALLOW 4200-LB EXPLOSIONS

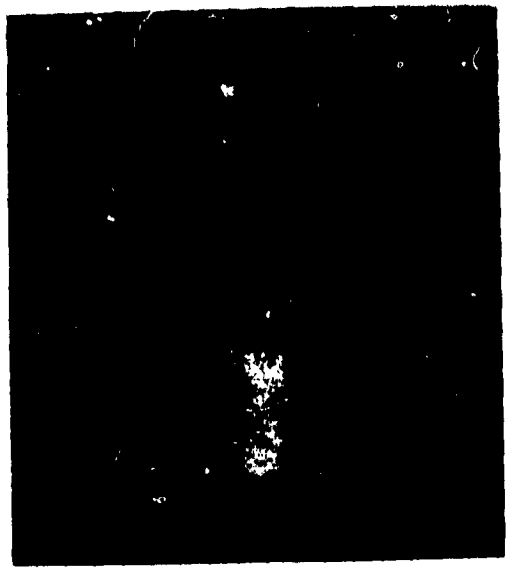

0.25 SEC

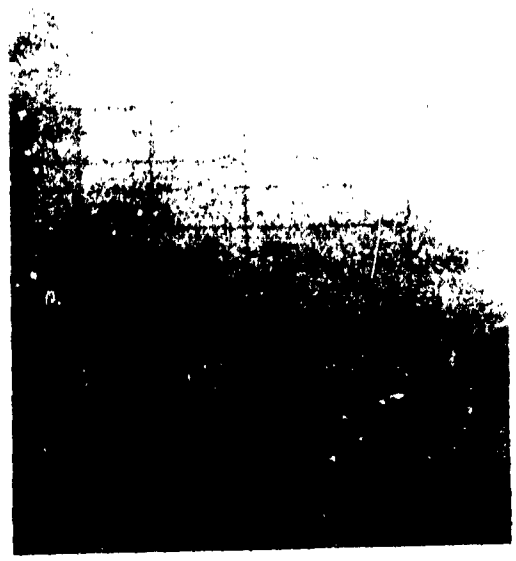

0.25 SEC

1.0 SEC

SHOT NO. 305
WATER DEPTH = 3.92 FT
λ_d = 0.845 FT/LB$^{1/3}$

1.0 SEC

SHOT NO. 262
WATER DEPTH = 4.83 FT
λ_d = 1.04 FT/LB$^{1/3}$

FIG. 2.3 SMOKE CROWN FORMATION BY RELATIVELY DEEP 100-LB EXPLOSIONS

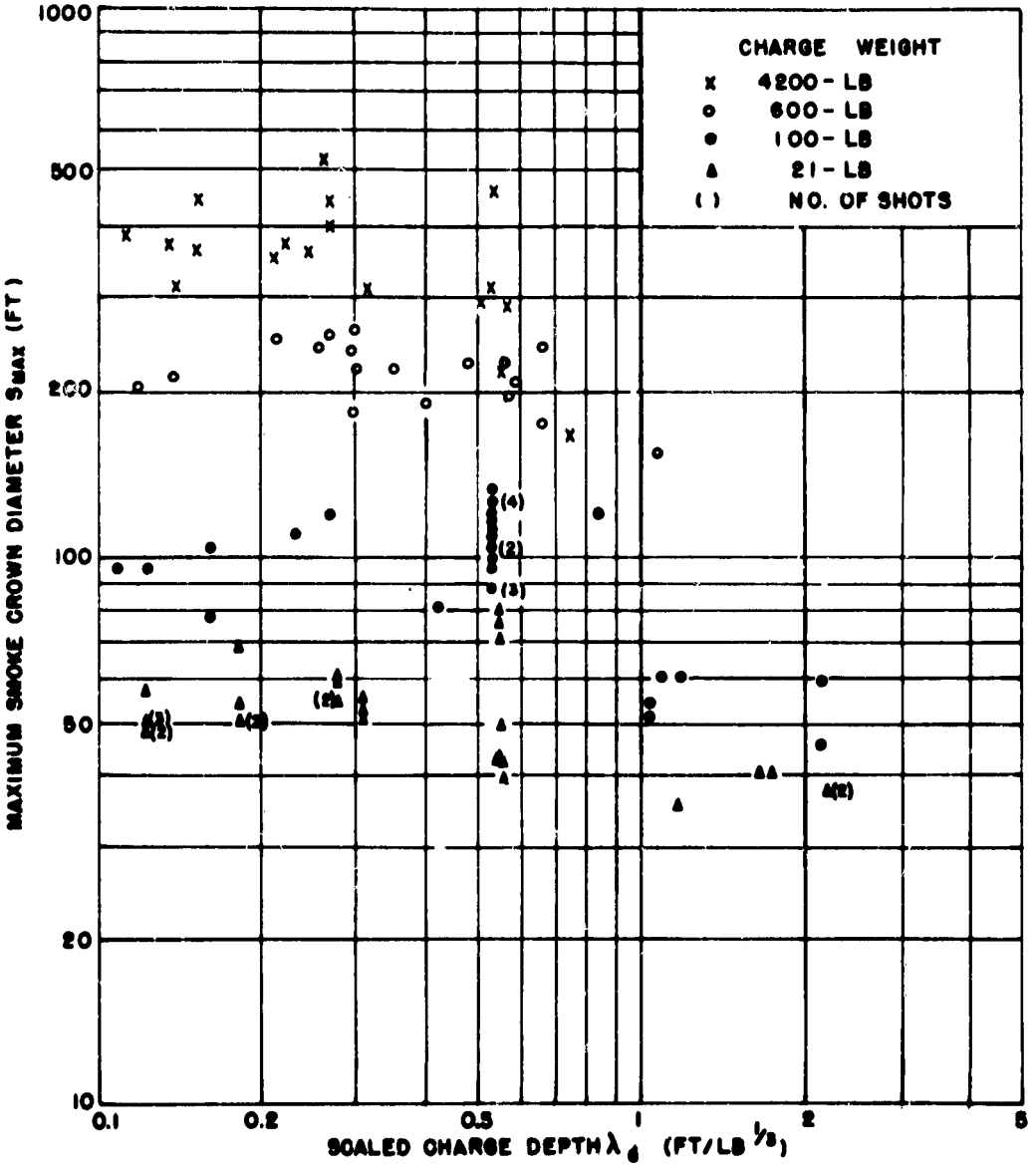

FIG. 2.4 MAXIMUM SMOKE CROWN DIAMETER
VS
SCALED CHARGE DEPTH
(CHARGES ON BOTTOM)

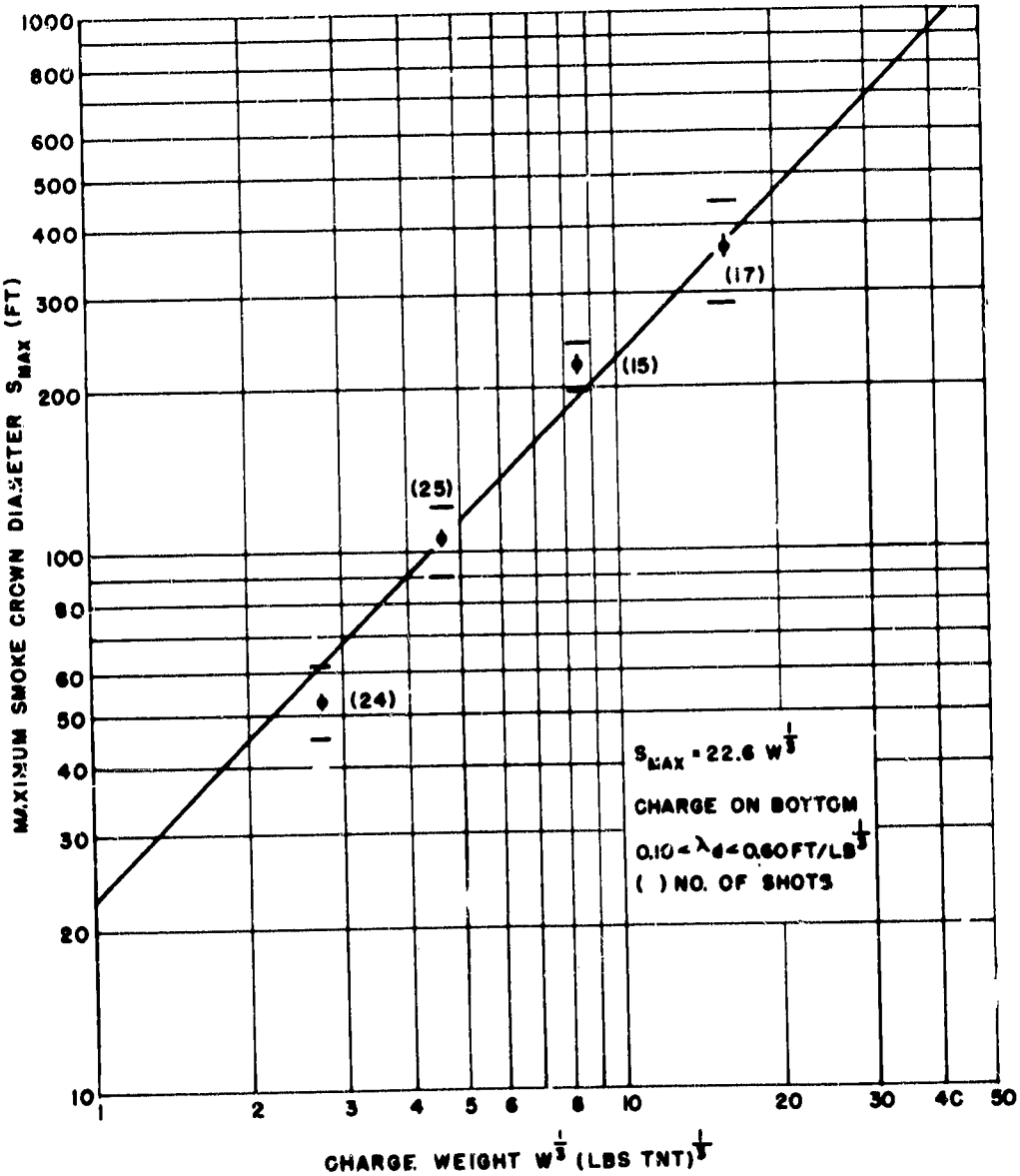

FIG. 2.5 MAXIMUM SMOKE CROWN DIAMETER
VS
CHARGE WEIGHT$^{\frac{1}{3}}$
(CHARGES ON BOTTOM)

$$S_{max} = 22.6\ W^{1/3} \qquad (0.1<\lambda_d<0.6\ \text{ft/lb}^{1/3}) \qquad (2)$$

The narrowness of the smoke crown formed by deeper shots indicates that the area of fallout is relatively small for explosions in deeper water. In very shallow water the fallout might extend farther than the base surge.

Extrapolation of formula (2) to a charge weight of 20 kilotons gives a smoke crown diameter of 7730 ft, which is consistent with the Test Baker cauliflower cloud diameter of 7340 ft [14]. The Baker value is the maximum recorded but was obtained before the cloud had reached its full size.

2.3 Condensation Cloud. When a shockwave passes through the atmosphere and is followed by a rarefaction wave, the ambient air in the rarefaction phase may be cooled adiabatically to saturation and the condensation of water vapor may occur. The cloud formed in this manner is brief in duration and evaporates when the atmospheric pressure returns to normal. The effect is similar to that observed in a cloud-chamber.

Condensation clouds have been observed on several of the 4200-lb explosions and one shallow 600-lb explosion. In almost all cases, the condensation started at the base of the smoke crown. A secondary phase often started at the surface of the water. The condensation cloud formed by Shot 222 is illustrated in Fig. 2.6. There was a slight development of the cloud in Shots 275, 214, 215, 219, and 297, but the formation of a hemispherical cloud was observed following Shots 293, 217, 222, and 283 (600-lb).

The development of condensation clouds is dependent upon the strength of the shockwave in air, which is greatest for underwater explosions when firing takes place at shallow depths. The formation is also strongly dependent upon the

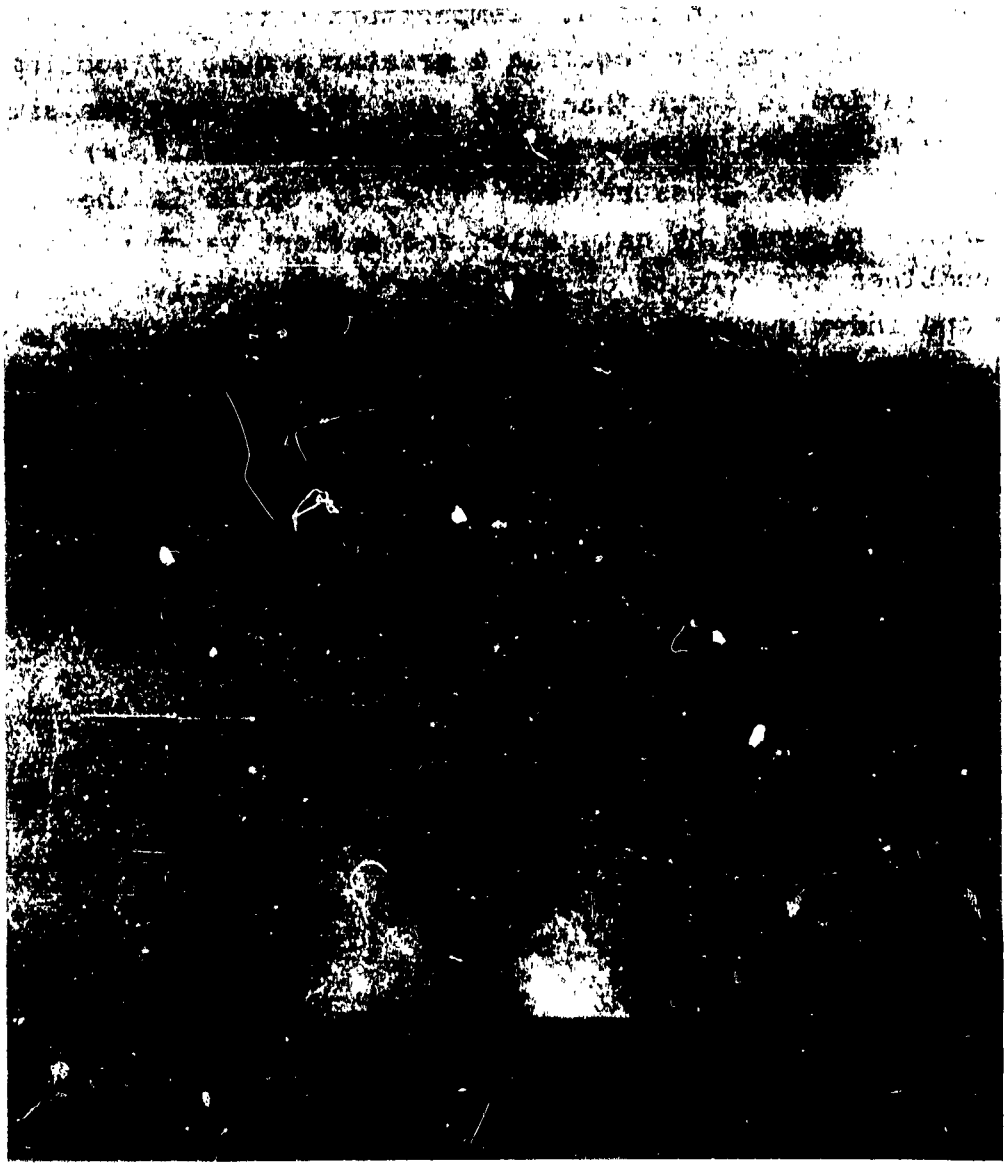

SHOT NO. 222
WATER DEPTH=8.50 FT
CHARGE DEPTH = 4.67 FT
$\lambda_c = 0.289$ FT/LB$^{1/3}$

FIG. 2.6 FORMATION OF CONDENSATION CLOUD BY 4200-LB EXPLOSION

amount of atmospheric moisture available for condensation.

Relative humidity alone is not an adequate index of the probability of condensation. Temperature effects are also important, as warm air requires a greater amount of cooling for saturation to occur than cool air, if both have the same relative humidity. A more satisfactory parameter is the atmospheric vapor pressure deficit (e_s-e), which is the difference between the saturation and ambient vapor pressures and combines the effects of temperature and relative humidity into one index number. Low values of (e_s-e) are favorable for condensation cloud formation.

For example, the data and results of Shots 281 and 293, both fired at 67% relative humidity, are compared in Table 2.1. Although firing conditions are almost identical, a complete hemispherical cloud formed on the cooler day while no cloud was observed on the warmer day.

TABLE 2.1
EXPERIMENTAL DATA FOR SHOTS 281 AND 293

Shot No.	281	293
Weight	4200 lbs	4200 lbs
Water Depth	2.17 ft	2.52 ft
Charge Position	Bottom	Bottom
Relative Humidity	67%	67%
Temperature	94.0°F	74.0°F
Vapor Pressure Deficit	18.0 mb	9.5 mb
Condensation Cloud Formation	None	Complete

The effects of charge depth and vapor pressure deficit on condensation cloud formation for the 4200-lb charges fired in the NOL programs are shown in Fig. 2.7, which indicates the tendency for clouds to form at low values of

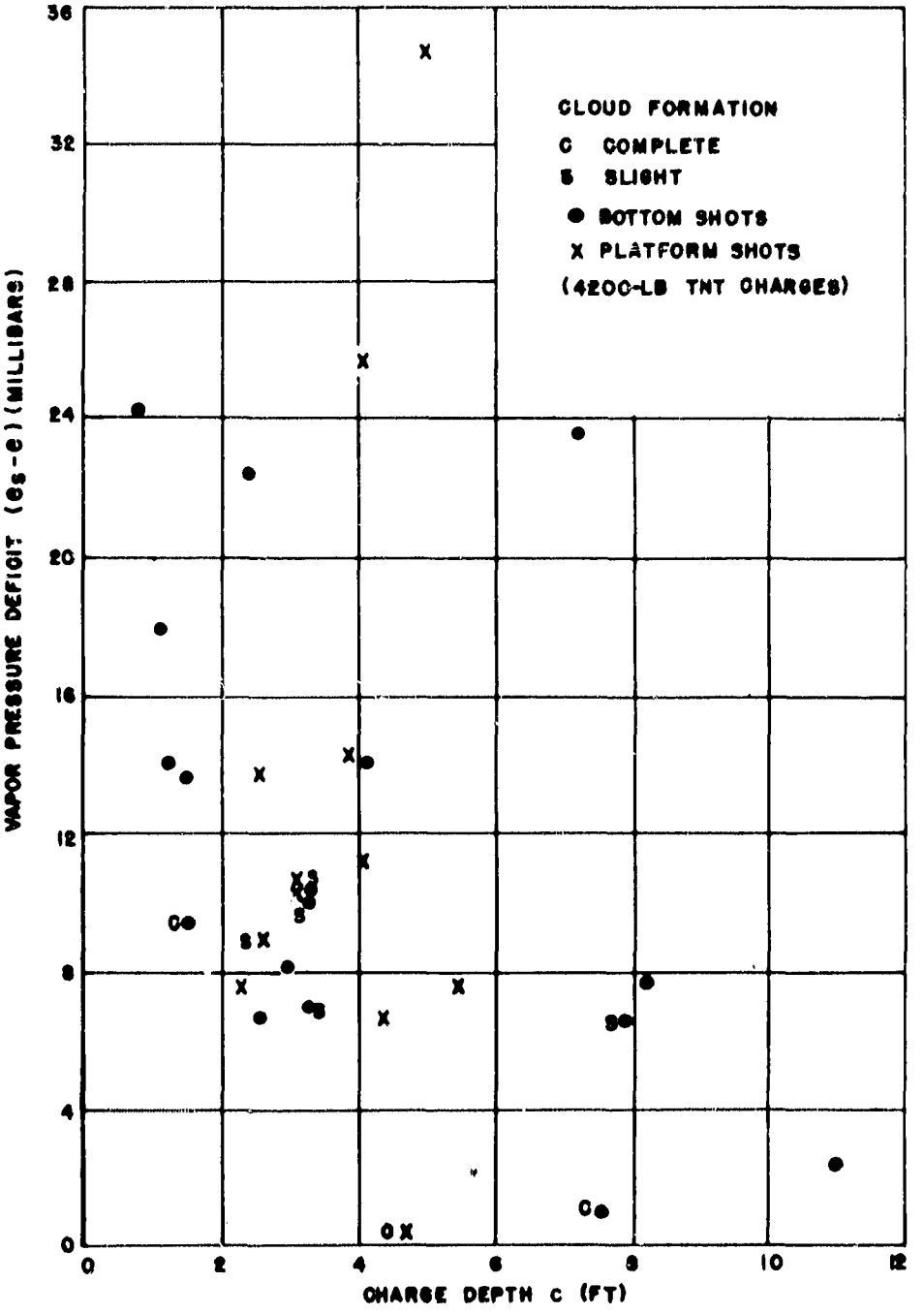

FIG. 2.7 EFFECTS OF CHARGE DEPTH AND ATMOSPHERIC CONDITIONS ON CONDENSATION CLOUD FORMATION

(e_s-e) and shows a greater probability of occurrence when charges are shallow.

The cloud chamber effect obscures the early stages of column development, which are important in the study of surface phenomena. However, it could possibly be used to study the growth of shockwaves at positions close to the explosions.

At Test Baker also, the condensation cloud began its formation at the junction of the smoke crown and the water column. A second part started below the first, about 500 ft above the water, and a third cloud formed at the water surface. All of these parts merged into one hemispherical cloud. The vapor pressure deficit during the Baker test was 8.0 mb.

2.4 Radial Throwout. When charges are exploded on or near the bottom in very shallow water, a spectacular radial throwout of bottom material occurs. The amount and extent depend upon the composition of the river bottom as well as upon charge weight and depth. Clay bottoms and bottoms covered by gravel or rocks give the greatest throwout effect. Debris and clumps of clay are ejected through the expanding water column and the smoke crown at high velocities. Figure 2.8 illustrates the throwout resulting from 4200-lb TNT charges fired on the bottom at various depths. Whenever possible, the maximum extent of the resulting splashes was measured for all charge weights. (See Appendix A.)

For a 4200-lb TNT charge fired at a depth of 1.83 ft, throwout material is first observed emerging through the column walls at about 0.1 second. The time of this initial appearance increases with increasing charge depth, and the throwout becomes smaller in magnitude. At a depth of 8.25 ft, a mixture of bottom material and smoke emerges through the column walls close to the water surface at about 0.5 second,

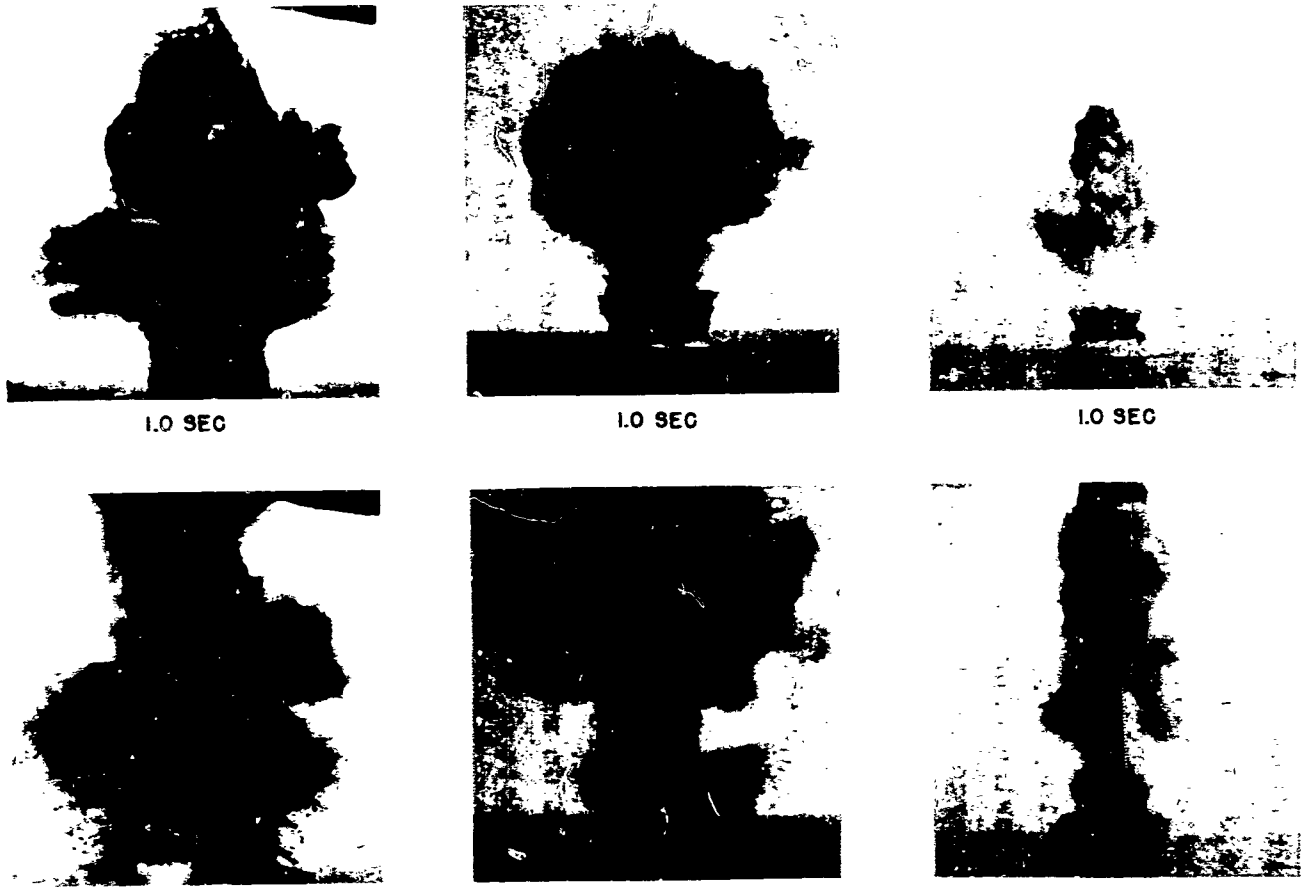

λ_d = 0.135 FT/LB $^{1/3}$
BOTTOM—CLAY
SHOT NO. 281

λ_d = 0.263 FT/LB $^{1/3}$
BOTTOM - CLAY
SHOT NO. 275

λ_d = 0.512 FT/LB $^{1/3}$
BOTTOM - SILT
SHOT NO. 274

FIG. 2.8 RADIAL THROWOUT FROM 4200-LB EXPLOSIONS

rising to a height of roughly 90 ft. This material is not ejected radially to great distances but falls into and mixes with the base surge, as can be seen in Fig. 2.8 (Shot 274).

Throwout diameter measurements are plotted against scaled charge depth in Fig. 2.9 for explosions on the bottom. The figure indicates that there is a high degree of scatter due to the differences in bottom conditions and the impossibility of measuring exact radial distances when the splashes were not on a line perpendicular to the camera line of sight.

The following expression for throwout diameter as a function of charge weight and depth can be obtained from the data, using the maximum values for each weight and scaled depth:

$$T_{max} = 59.6\ W^{0.457}\ d^{-1} \quad (0.1 < \lambda_d < 2.0\ \text{ft/lb}^{1/3}) \qquad (3)$$

The formula is assumed to be applicable to conditions well suited for throwout, such as explosions in areas covered with boulders or hard clay.

The effect on maximum throwout diameter of firing a charge off the bottom is shown in Fig. 2.10, a plot of T_{max} vs $W^{1/3}$ for charges on the bottom ($\lambda_d \cong 0.26$ ft/lb$^{1/3}$ and $\lambda_d \cong 0.53$ ft/lb$^{1/3}$) and charges at mid-depth ($\lambda_c \cong 0.26$ ft/lb$^{1/3}$). The relationships for these three cases are expressed by the following formulas, where T is in feet and W in pounds:

$$T_{max} = 229\ W^{0.124} \qquad (\lambda_d = 0.26\ \text{ft/lb}^{1/3}) \qquad (4)$$

$$T_{max} = 112\ W^{0.124} \qquad (\lambda_d = 0.53\ \text{ft/lb}^{1/3}) \qquad (5)$$

$$T_{max} = 88\ W^{0.124} \qquad (\lambda_c = 0.26\ \text{ft/lb}^{1/3}) \qquad (6)$$

Formulas (4) and (5) were obtained by substituting the indicated values of λ_d in formula (3). The relationships

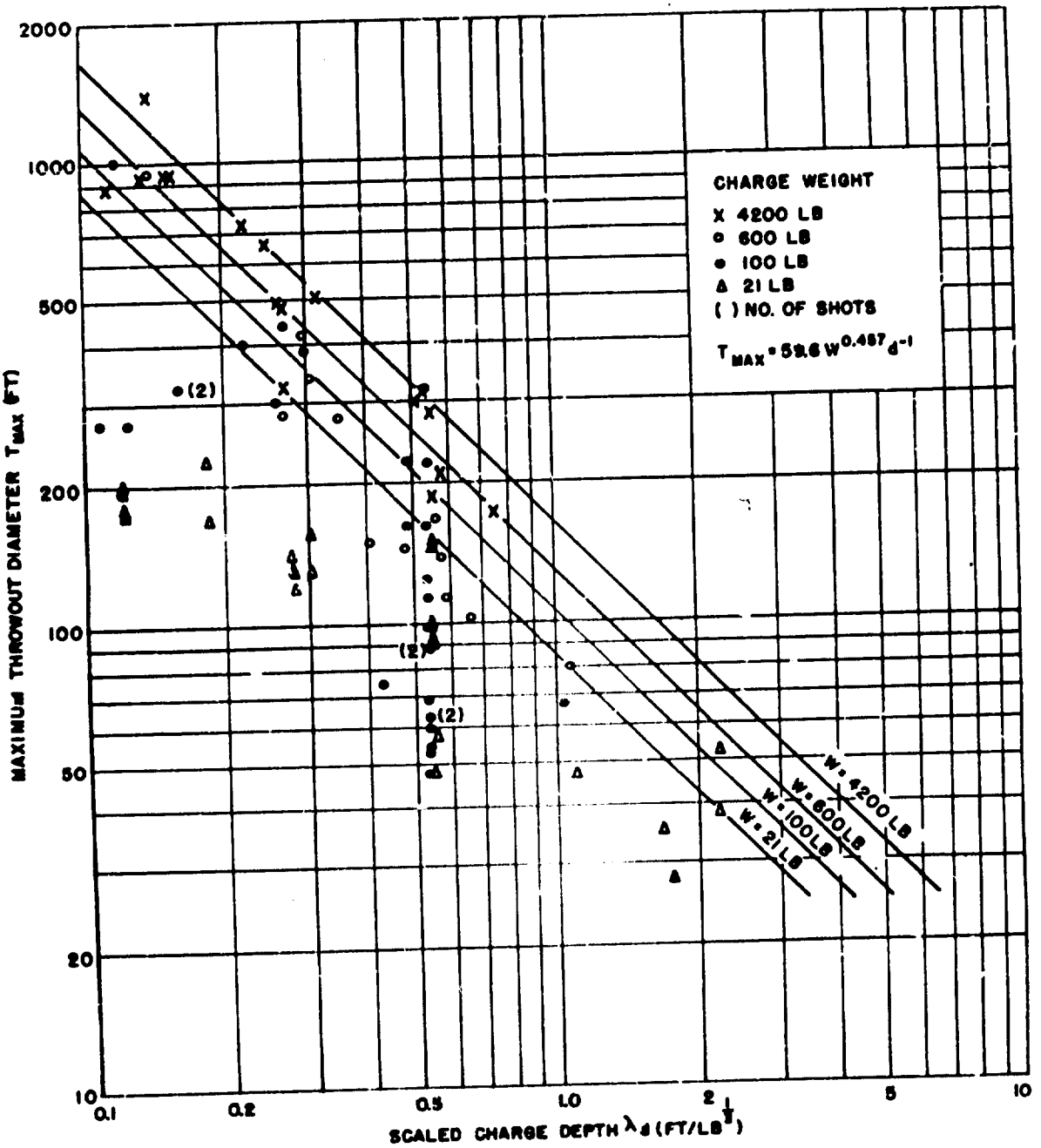

FIG. 2.9 MAXIMUM THROWOUT DIAMETER
VS
SCALED CHARGE DEPTH
(CHARGES ON BOTTOM)

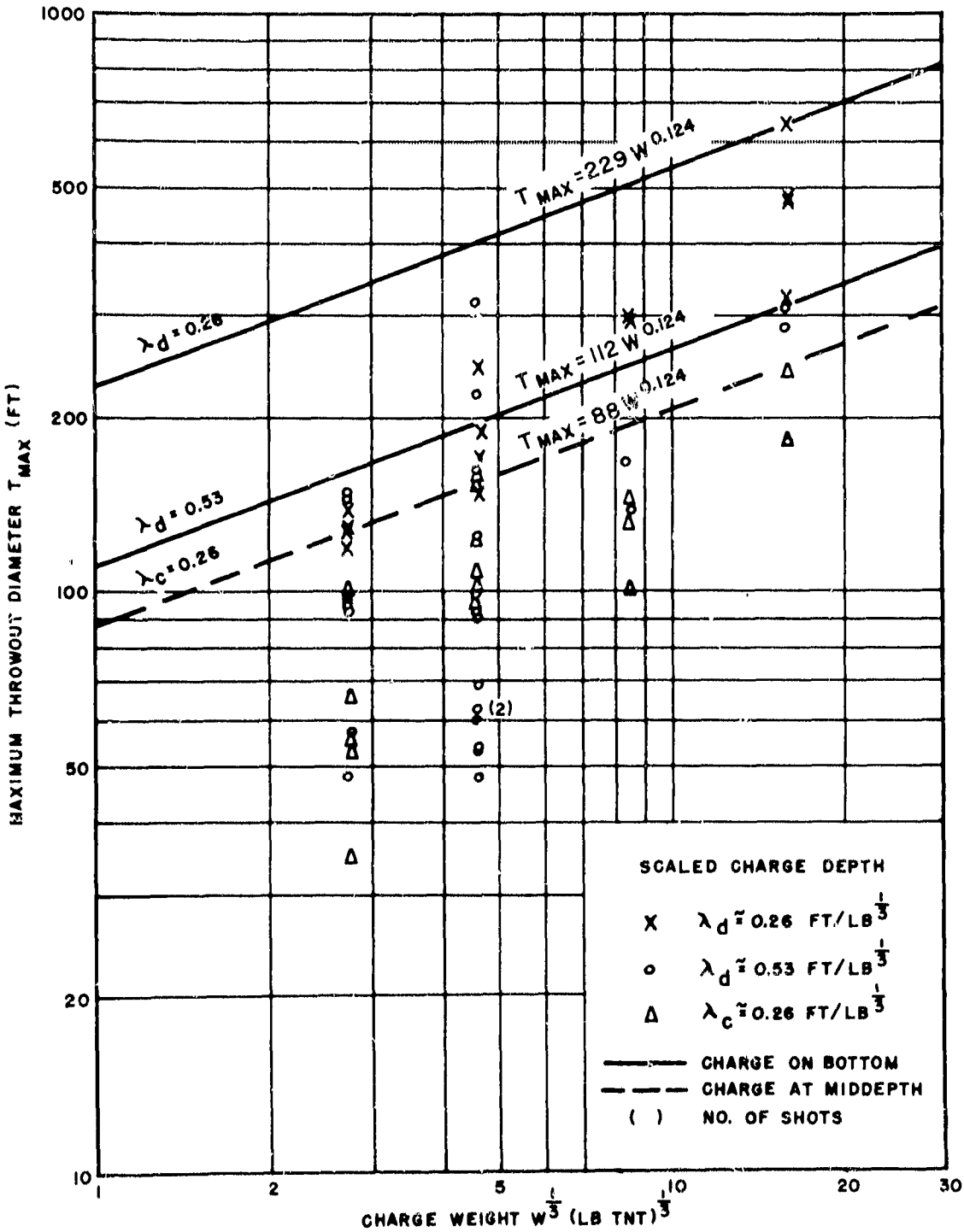

FIG. 2.10 MAXIMUM THROWOUT DIAMETER VS CHARGE WEIGHT$^{\frac{1}{3}}$

indicate that, for a given water depth, damage due to throwout is at a maximum when the charge is fired on the bottom.

The formulas are considered valid only within the investigated range of charge sizes. Extrapolation to nuclear weapons yields values that are obviously too low.

2.5 Column. The maximum column diameter, D_{max}, is measured at the completion of the rapid horizontal expansion of the cylindrical water column, while the outer edges are still sharply defined and prior to the appearance of "spikes". The differences in the appearance of the column at the time of maximum diameter for various firing conditions are shown in Fig. 2.11. In general, deeper charges produce broader, higher columns than shallow charges in the range of depths shown. Very shallow charges fired on the bottom at scaled depths $\lambda_d \leqq 0.2$ ft/lb$^{1/3}$ produce columns which contain considerable bottom material, e.g., Shot 281, Fig. 2.11.

A plot of maximum column diameter versus the cube root of charge weight for TNT explosions scaled to Test Baker ($\lambda_c \cong 0.26$ ft/lb$^{1/3}$) is shown in Fig. 2.12. Mean values for shots of the same weight are plotted and the standard deviation of a single observation and the standard deviation of the mean are indicated. The relationship between maximum column diameter and the cube root of charge weight is expressed by the formula:

$$D_{max} = 6.75\, W^{1/3} \qquad (\lambda_c \cong 0.26 \text{ ft/lb}^{1/3}) \qquad (7)$$

It should be noted that the Test Baker value of 2030 ft for maximum column diameter falls very close to the cube root line, and lies within the range of scatter of TNT results.

When D_{max} is plotted versus $W^{1/3}$ for charges on the bottom, grouped according to scaled depths, the following relationships are obtained:

SHOT NO. 281
W = 4200 LB
D_{max} = 87.7 FT

WATER DEPTH = 2.17 FT
CHARGE ON BOTTOM
λ_d = 0.135 FT/LB$^{1/3}$

SHOT NO. 221
W = 4200 LB
D_{max} = 114 FT

WATER DEPTH = 9.25 FT
CHARGE ON BOTTOM
λ_d = 0.574 FT/LB$^{1/3}$

SHOT NO. 277
W = 600 LB
D_{max} = 70.7 FT

WATER DEPTH = 9.12 FT
CHARGE ON BOTTOM
λ_d = 1.08 FT/LB$^{1/3}$

SHOT NO. 222
W = 4200 LB
D_{max} = 99.0 FT

WATER DEPTH = 8.50 FT
CHARGE DEPTH = 4.67 FT
λ_c = 0.289 FT/LB$^{1/3}$

FIG. 2.11 COLUMN FORMATION BY EXPLOSIONS AT DIFFERENT DEPTHS

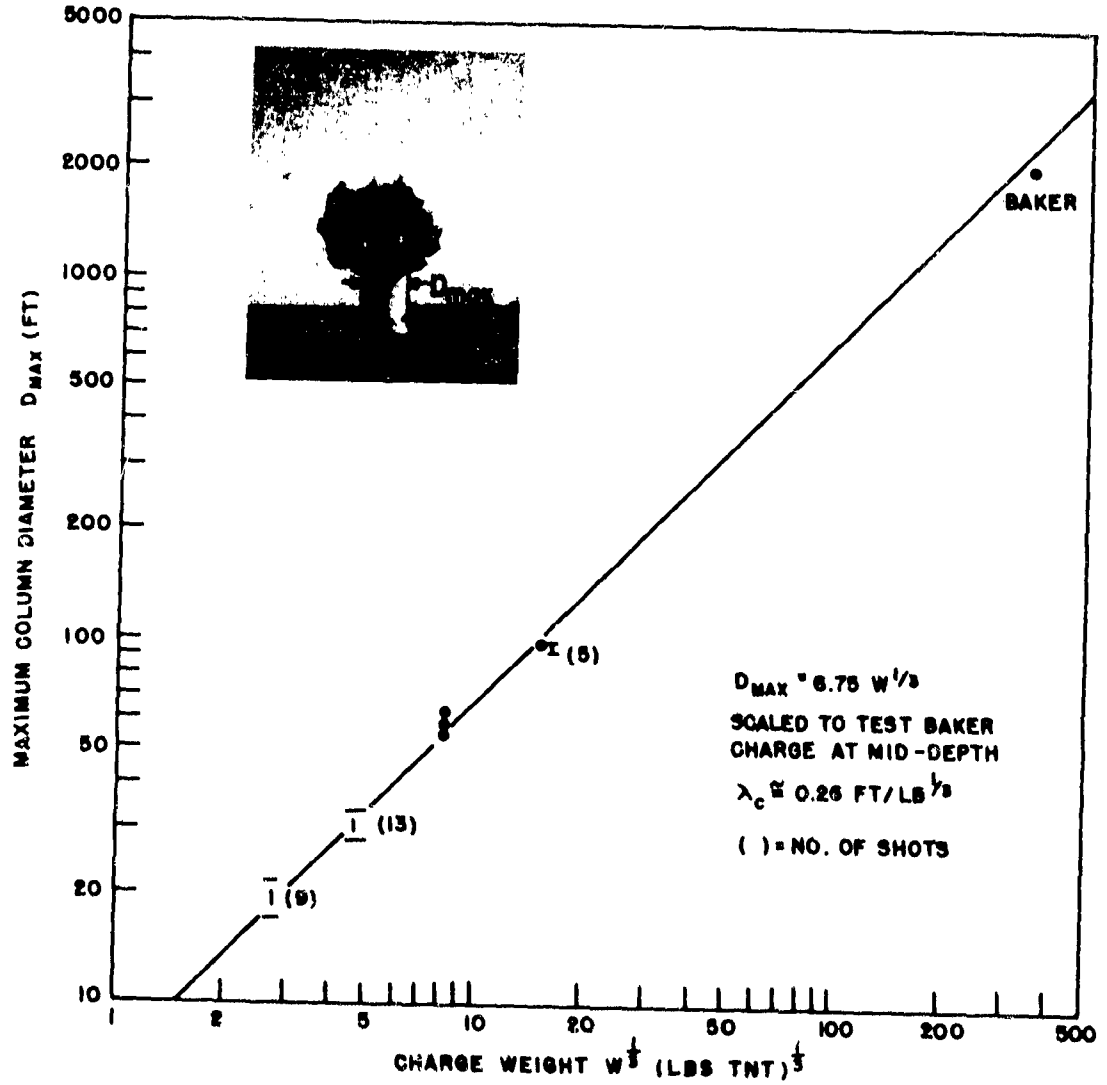

FIG. 2.12 MAXIMUM COLUMN DIAMETER
VS
CHARGE WEIGHT$^{\frac{1}{3}}$
(CHARGES SCALED TO TEST BAKER)

$$D_{max} = 6.45\ W^{1/3} \quad (0.25 < \lambda_d < 0.32) \quad \bar{\lambda}_d = 0.28\ ft/lb^{1/3} \quad (8)$$

$$D_{max} = 7.30\ W^{1/3} \quad (0.48 < \lambda_d < 0.66) \quad \bar{\lambda}_d = 0.55\ ft/lb^{1/3} \quad (9)$$

$$D_{max} = 8.55\ W^{1/3} \quad (0.75 < \lambda_d < 2.22) \quad \bar{\lambda}_d = 1.46\ ft/lb^{1/3} \quad (10)$$

The above formulas may be combined to express D_{max} as a function of charge weight and water depth:

$$D_{max} = 8.01\ W^{0.278}\ d^{0.166} \quad (0.25 < \lambda_d < 2.22\ ft/lb^{1/3}) \quad (11)$$

Equation (11) may be solved for different weights, as shown by the lines in Fig. 2.13, a plot of all D_{max} values for bottom charges as a function of scaled depth λ_d.

Shallow charge depths, at which "smog" surges are produced, are delineated for each charge weight, the limits varying with charge weight because of the shapes of the charges (see Sec. 1.3). Smog surges are defined as those that contain visible quantities of smoke, and will be discussed further in Chapter 4. Figure 2.13 indicates the trend towards increasing column diameters when charges are fired on the bottom in increasing depths of water. The extension of formula (11) beyond the indicated range may not be justified.

Measurements of maximum column diameter were made in several high explosive studies conducted in preparation for Operation CROSSROADS and were reported by J. W. Johnson in 1946 [10]. Using charge weights ranging from 0.35 lb to 600 lbs (TNT), Johnson obtained a formula for the "maximum base-width" of the plume for explosions scaled to the Baker geometry of:

$$D_p = 7.3\ W^{1/3} \quad (12)$$

where D_p is in ft and W is in lbs.

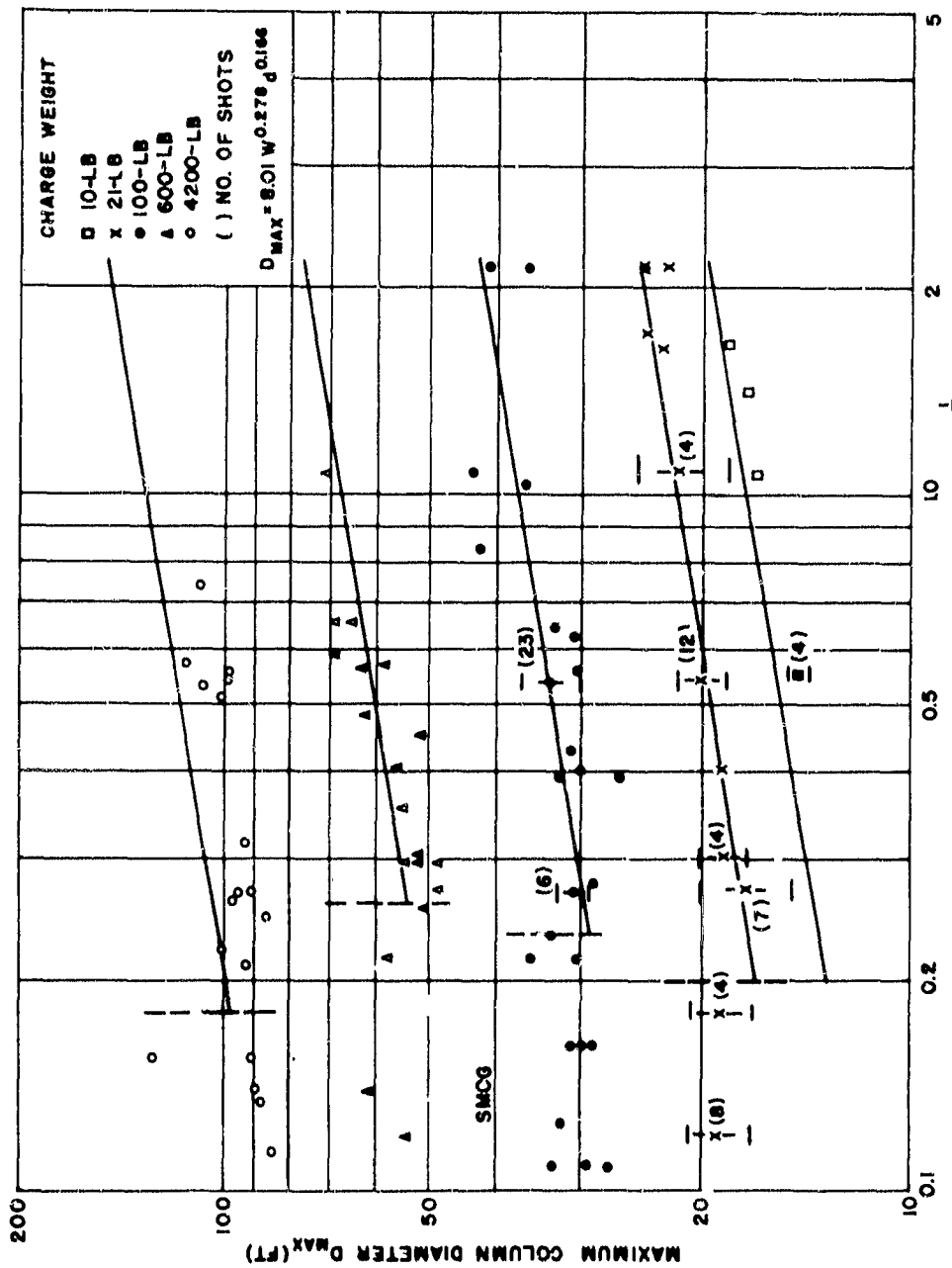

FIG. 2.13 MAXIMUM COLUMN DIAMETER
VS
SCALED CHARGE DEPTH
(CHARGES ON BOTTOM)

Johnson's "maximum base-width" coincides approximately with the maximum column diameter defined herein. His formula is the same as that obtained for bottom shots scaled to the Baker water depth in the NOL programs, which may indicate a different manner of measurement of maximum column size.

The height, C, of the water column resulting from a shallow underwater explosion is measured f om the water surface to the base of the roughly spherical smoke crown or "cauliflower" cloud. The maximum height is attained after the column has reached its maximum diameter.

For mid-depth explosions scaled to Test Baker the relationship between the maximum column height and the cube root of the charge weight is shown in Fig. 2.14 and is expressed by:

$$C_{max} = 8.50\ W^{1/3} \qquad (\lambda_c \cong 0.26\ ft/lb^{1/3}) \qquad (13)$$

It will be noted that the height of the Baker column, measured to the base of the cauliflower cloud, lies considerably below the cube root curve.

The dependence of maximum column height C_{max} upon charge weight and depth for charges on the bottom is illustrated in detail in Fig. 2.15, a plot of all available C_{max} values versus scaled depth. The relationship in ft and lbs can be expressed by:

$$C_{max} = 14.5\ W^{0.135}\ d^{0.593} \quad (0.24 < \lambda_d < 1.10\ ft/lb^{1/3}) \quad (14)$$

The formula is based on the assumption that maximum column height is a function of the energy yield and the scaled charge depth and is obtained from the following formulas:

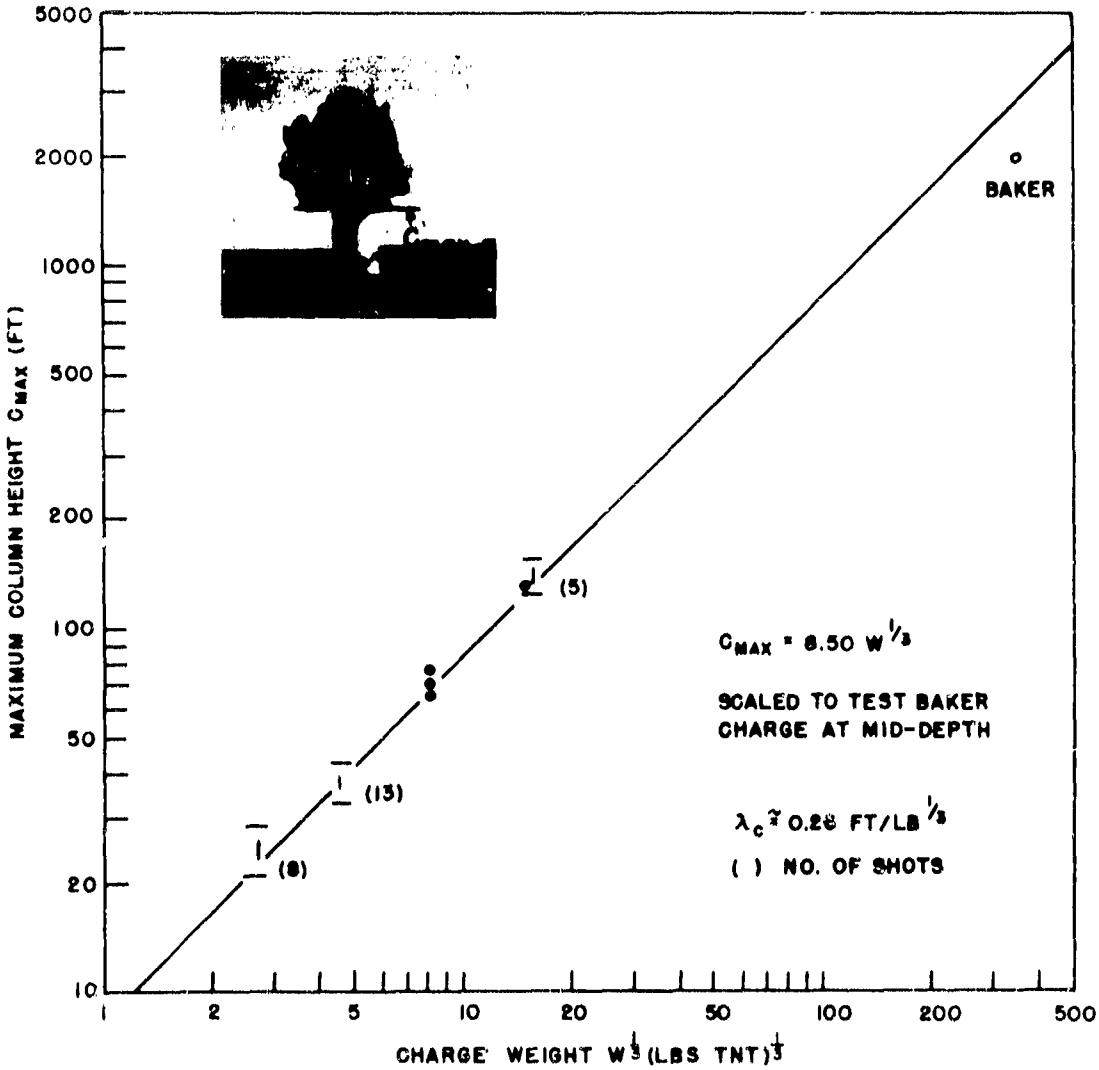

FIG. 2.14 MAXIMUM COLUMN HEIGHT
VS
CHARGE WEIGHT $^{\frac{1}{3}}$
(CHARGES SCALED TO TEST BAKER)

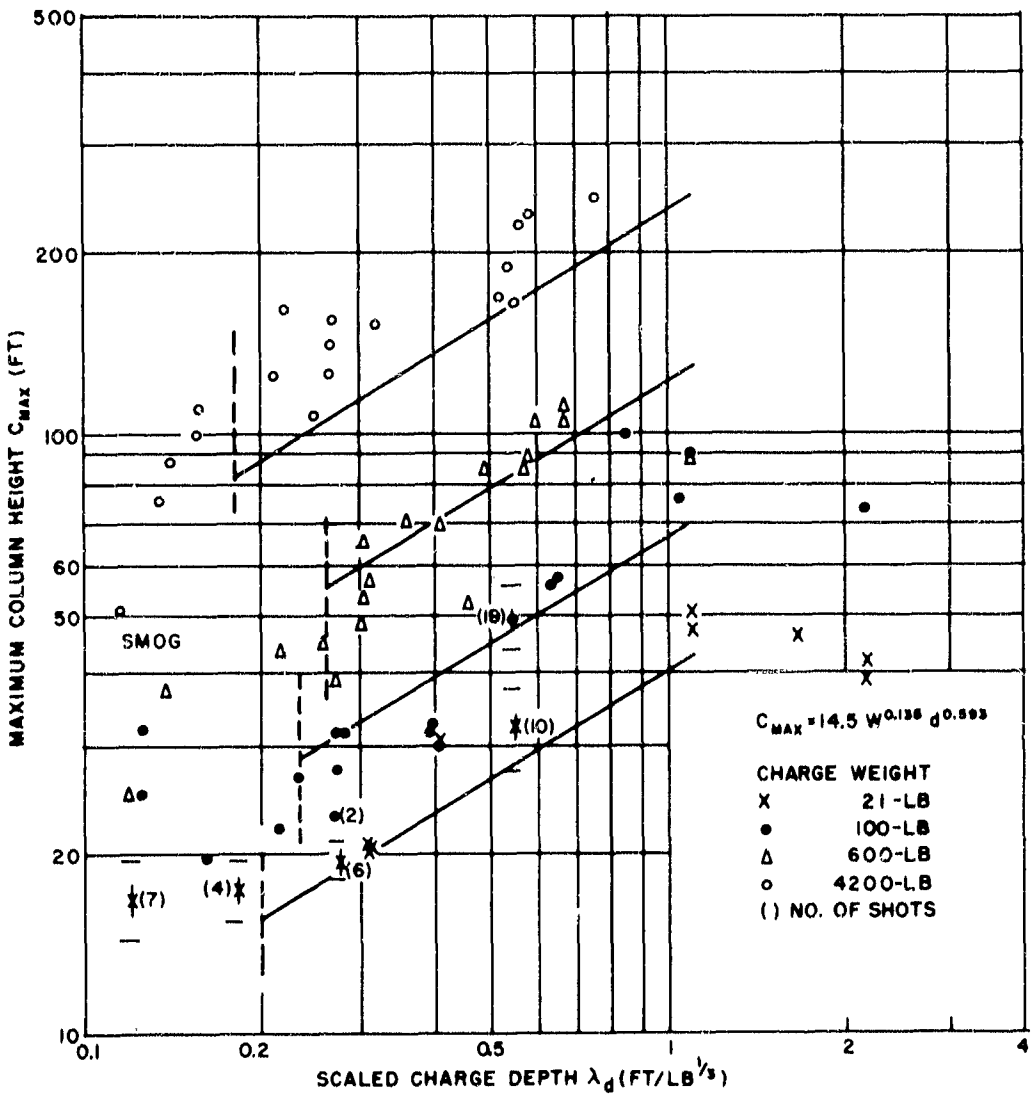

FIG. 2.15 MAXIMUM COLUMN HEIGHT
VS
SCALED CHARGE DEPTH
(CHARGES ON BOTTOM)

$$C_{max} = 7.15\ W^{1/3} \quad (0.24 < \lambda_d < 0.30) \quad \bar{\lambda}_d = 0.27\ ft/lb^{1/3} \qquad (15)$$

$$C_{max} = 10.0\ W^{1/3} \quad (0.48 < \lambda_d < 0.67) \quad \bar{\lambda}_d = 0.55\ ft/lb^{1/3} \qquad (16)$$

$$C_{max} = 17.0\ W^{1/3} \quad (0.74 < \lambda_d < 1.10) \quad \bar{\lambda}_d = 1.0\ ft/lb^{1/3} \qquad (17)$$

In Fig. 2.15 the range of shallow scaled charge depths which result in the formation of smog surges is delineated by vertical dashed lines for each charge weight. However, the column heights measured in the smog range fall in line with the data from explosions at greater depths fairly well. The formulas indicate an increase of column height with increasing depth of firing but should not be extended beyond a scaled depth of about 1.1 $ft/lb^{1/3}$ for bottom explosions. The surface phenomena from deeper explosions are markedly different in appearance, and column and base surge formation at greater values of λ_d have not been studied in detail.

The initial vertical column growth for four 4200-lb TNT charges on the bottom in water depths ranging from 2.52 ft to 8.25 ft is shown in Fig. 2.16a, and the column growth for two 4200-lb charges at mid-depth in 8.25 ft and 8.77 ft of water is shown in Fig. 2.16b. The curves indicate that bottom explosions in deeper water produce faster growing, higher columns than bottom explosions in shallow water within the given range. Bottom explosions scaled to the Baker water depth form higher columns than explosions at mid-depth in the same depth of water.

2.6 Jet. The jet produced by shallow underwater explosions appears above the rising and expanding smoke crown as a central spout of water and explosion products. It has an initial vertical velocity greater than that of the column, and rises well above it. Maximum jet height, J_{max}, is defined as the greatest height attained by the rising jet before its leading edge is distorted by upper winds and turbulence. Measurements

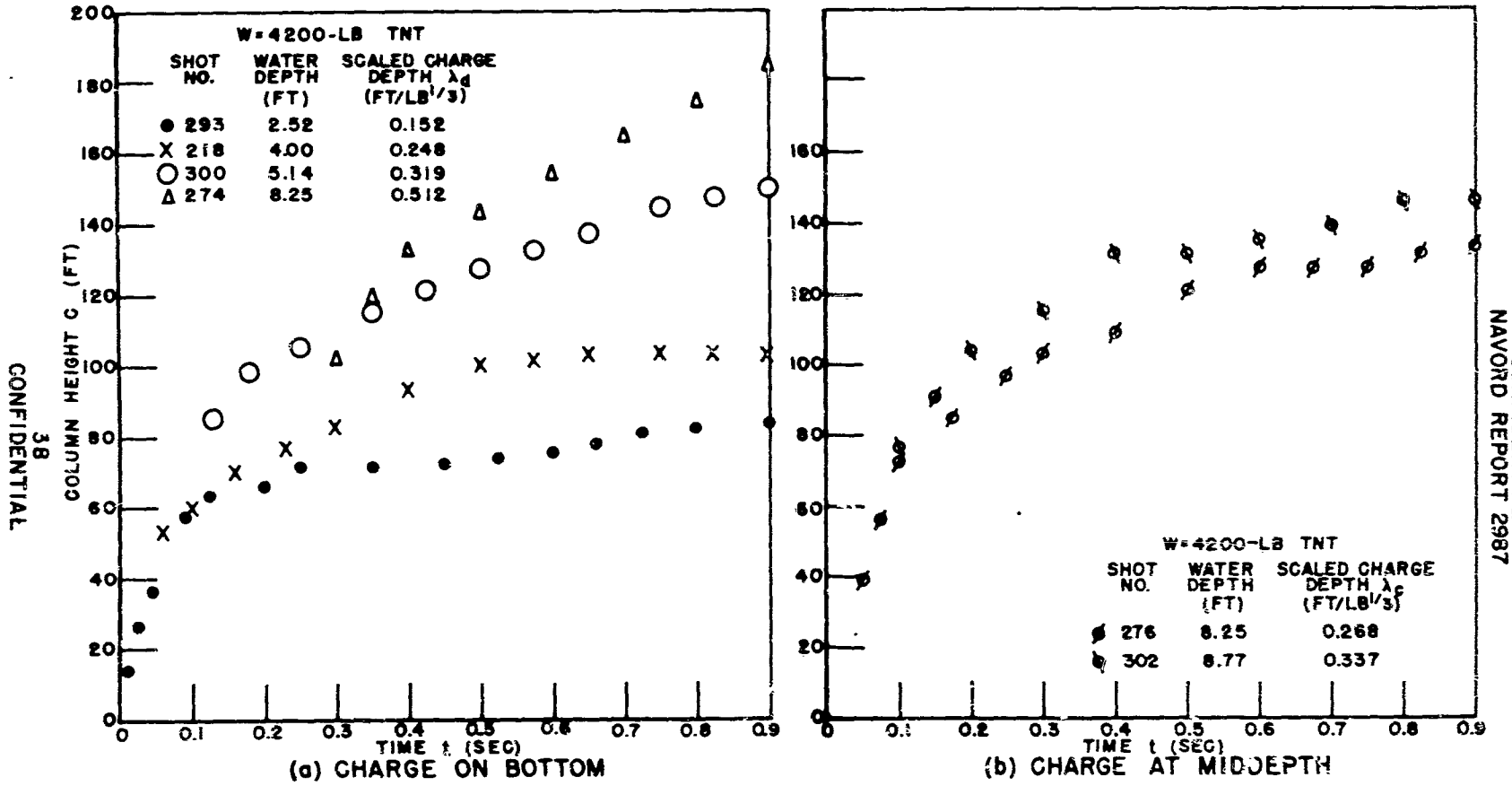

FIG. 2.16 COLUMN HEIGHT vs TIME (4200-LB CHARGES)

of the overall height, $\mathcal{Q}$, are made subsequent to the measurement of J_{max}.

The effects of charge depth and water depth on the jet are illustrated in Fig. 2.17. At scaled depths less than about 0.20 ft/lb$^{1/3}$, the leading edge of the jet, as it emerges above the smoke crown, is broad and bushy. The jet is almost black, indicating a high carbon content. As charge depth is increased, a faster, more clearly defined jet is observed. The leading edge is sharply outlined and a greater water content is apparent from the lighter color. As examples, the high, thin liquid jet produced by a 100-lb TNT charge fired on the bottom in 4.83 ft of water (scaled depth λ_d = 1.04 ft/lb$^{1/3}$) is shown in Fig. 2.17 and the jet resulting from a 4200-lb TNT charge fired on the bottom in 12 ft of water (λ_d = 0.745 ft/lb$^{1/3}$) is also illustrated.

Maximum jet height is plotted against the cube root of the charge weight for shots scaled to Test Baker in Fig. 2.18. On the basis of the NOL results, the relationship is expressed by the formula:

$$J_{max} = 65.8\ W^{1/3} \qquad (\lambda_c \cong 0.26\ \text{ft/lb}^{1/3}) \qquad (18)$$

Data reported by J. W. Johnson [10] for explosions scaled to Baker are shown in Fig. 2.18 for comparison with the NOL results. Johnson's formula for maximum plume height is:

$$Z_p = 109\ W^{1/3} \qquad (19)$$

where Z_p is in ft and W is in lbs.

Cube root relationships for maximum jet height obtained for bottom explosions at scaled depths equal to or greater than 0.25 ft/lb$^{1/3}$ are presented below:

J_{max} = 870 FT 10 SEC

SHOT NO. 280 WATER DEPTH = 1.83 FT
W = 4200 LB λ_d = 0.114 FT/LB$^{1/3}$

J_{max} = 1350 FT 8.5 SEC

SHOT NO. 220 WATER DEPTH = 12.0 FT
W = 4200 LB λ_d = 0.745 FT/LB$^{1/3}$

J_{max} = 1023 FT 8 SEC

SHOT NO. 276 WATER DEPTH = 8.25 FT
W = 4200 LB λ_c = 0.268 FT/LB$^{1/3}$

J_{max} = 370 FT 1.75 SEC

SHOT NO. 262 WATER DEPTH = 4.83 F
W = 100 LB λ_d = 1.04 FT/LB$^{1/3}$

FIG. 2.17 JET FORMATION BY EXPLOSIONS AT DIFFERENT FIRING CONDITIONS

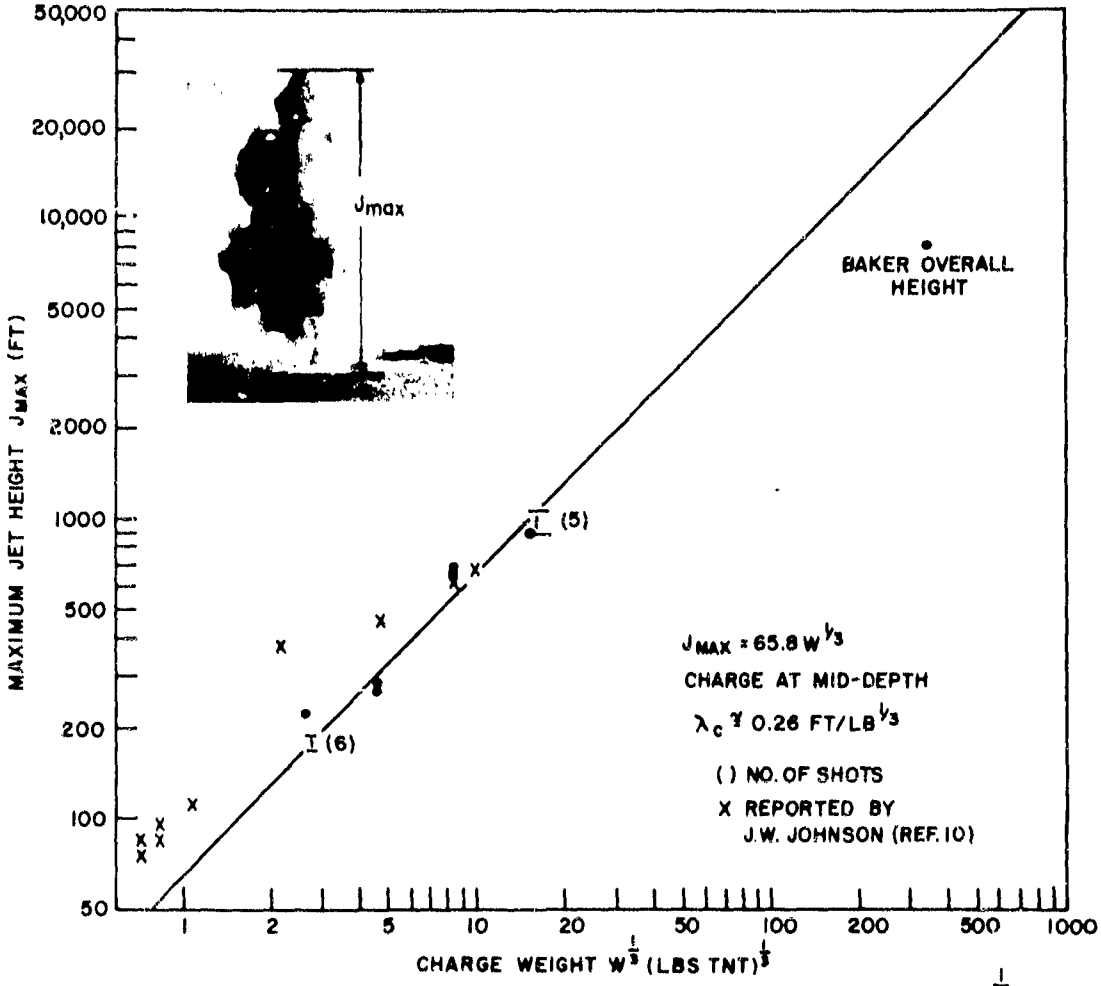

FIG. 2.18 MAXIMUM JET HEIGHT VS CHARGE WEIGHT $^{\frac{1}{3}}$
(CHARGES SCALED TO TEST BAKER)

$$J_{max} = 64.0\ W^{1/3} \quad (0.25 < \lambda_d < 0.31)\ \bar{\lambda}_d = 0.28\ \text{ft/lb}^{1/3} \qquad (20)$$

$$J_{max} = 72.0\ W^{1/3} \quad (0.48 < \lambda_d < 0.58)\ \bar{\lambda}_d = 0.54\ \text{ft/lb}^{1/3} \qquad (21)$$

$$J_{max} = 85.0\ W^{1/3} \quad (0.74 < \lambda_d < 1.1)\ \bar{\lambda}_d = 0.97\ \text{ft/lb}^{1/3} \qquad (22)$$

For charges on the bottom, the effects of charge weight and depth on maximum jet height are shown in Fig. 2.19, a plot of all available J_{max} data versus scaled charge depth, λ_d. The relationship in ft and lbs can be represented by the formula:

$$J_{max} = 84.8\ W^{0.256}\ d^{0.232} \quad (0.1 < \lambda_d < 1.1\ \text{ft/lb}^{1/3}) \qquad (23)$$

Very shallow scaled depths at which smog surges are observed are delineated in Fig. 2.19, but the data indicate that formula (23) is valid within the smog range. The scaled depth range of the data is $0.1 < \lambda_d < 1.1$ ft/lb$^{1/3}$ and the extension of the formula to shallower or deeper scaled charge positions may not be justified. In addition, it is not wise to apply formula (23) to TNT explosions considerably larger than 4200 lbs because the retardation of the jet by atmospheric friction may not scale to jet size in a simple manner. Also, Johnson's results indicate that small charges may not fall in line with formula (23).

Within the range of variables used it can be noted that J_{max} is approximately equal to 10 D_{max}.

Jet height as a function of time for 4200-lb and 600-lb TNT charges at scaled depths ranging from 0.114 ft/lb$^{1/3}$ to 1.08 ft/lb$^{1/3}$, and the maximum height attained, are shown in Fig. 2.20. Within the experimental range, the initial jet velocity and the maximum height increase with increasing charge depth. For a 4200-lb charge at a scaled depth, λ_d, of about 0.5 ft/lb$^{1/3}$, the jet is first observed above the

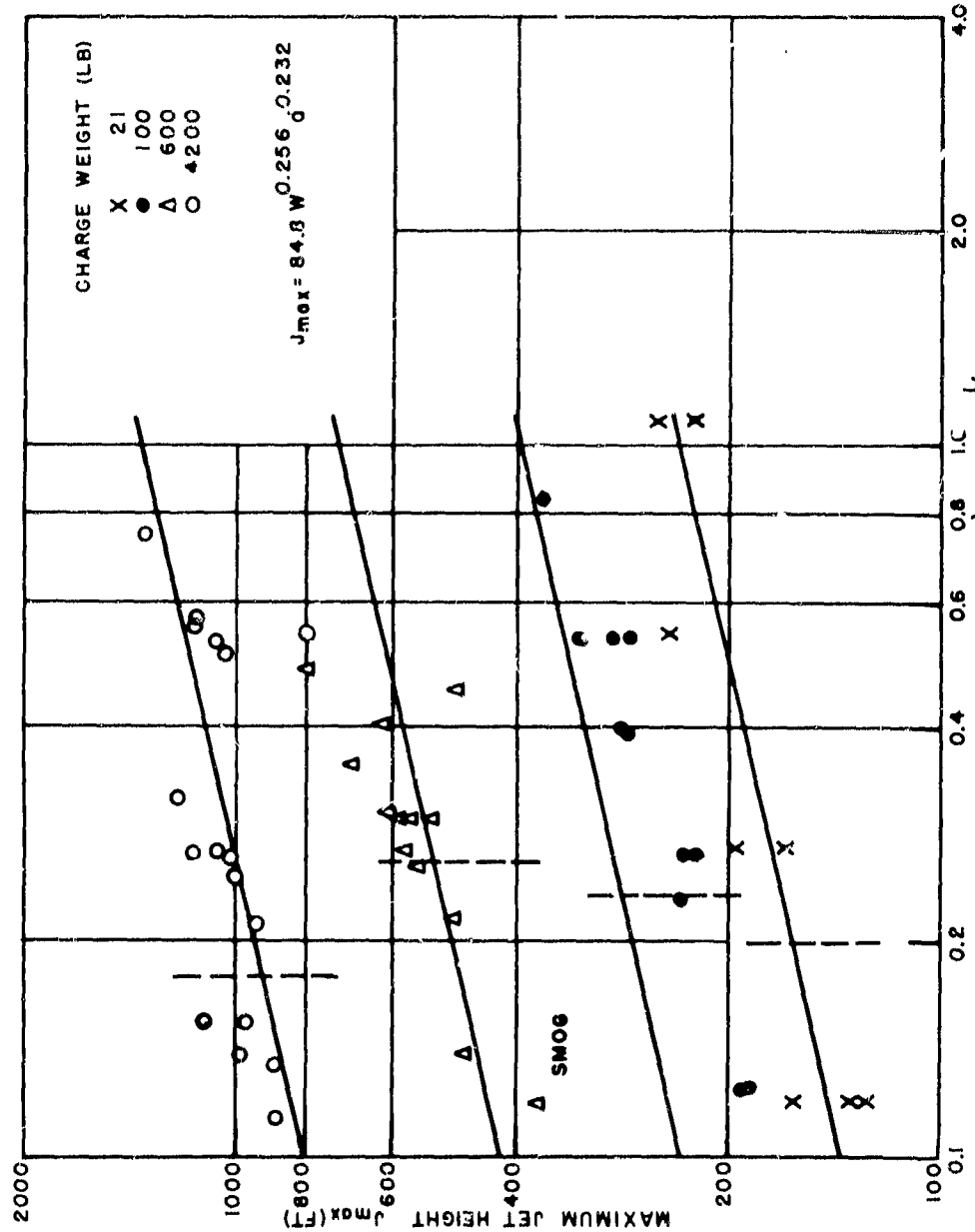

FIG. 2.19 MAXIMUM JET HEIGHT vs SCALED CHARGE DEPTH (CHARGES ON BOTTOM)

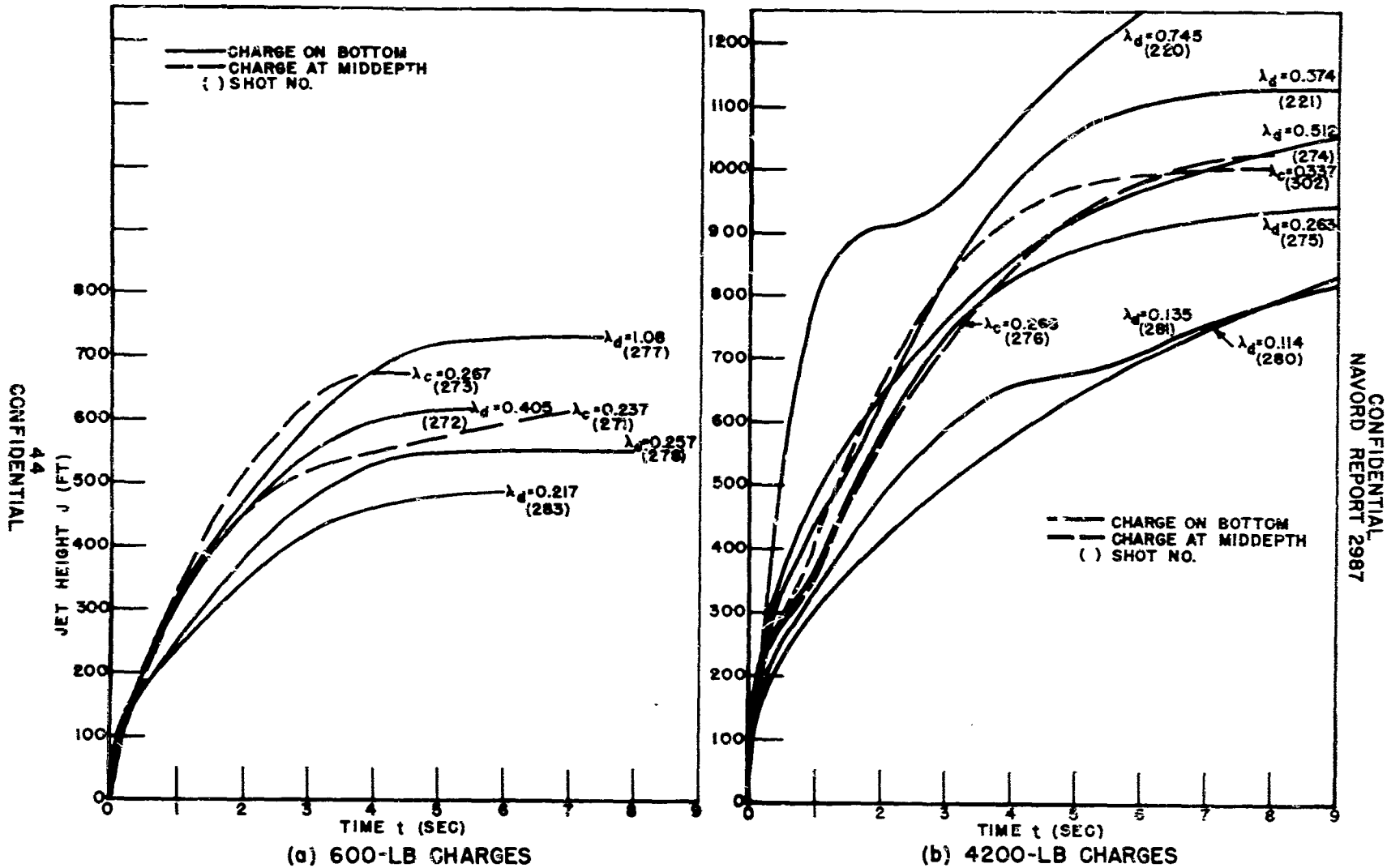

FIG. 2.20 JET HEIGHT vs TIME (600-LB AND 4200-LB CHARGES)

narrow smoke crown at about 0.15 seconds, the initial jet velocity being of the order of 1500 ft/sec. At a scaled depth λ_d of 0.135 ft/lb$^{1/3}$, the broad bushy leading edge of the jet is first observed above the wide bowl-shaped smoke crown at about 0.05 seconds. The initial jet velocity is of the order of 800 ft/sec, and decreases to about 150 ft/sec after 0.5 seconds.

Deeper charges may produce multiple-stage jets. A 4200-lb TNT charge fired on the bottom in 12 ft of water, scaled depth λ_d = 0.745 ft/lb$^{1/3}$ (Shot 220), produced a distinct two-stage jet. In this case the initial jet reached a maximum height of 920 ft at 2.3 seconds, and was overtaken by a second jet which reached a maximum height of 1350 ft. This effect is illustrated in Fig. 2.21, and by the jet height vs time curve (Fig. 2.20). A two-stage jet resulted from Shot 303, a 3600-lb charge fired at a depth of 5.29 ft in 8.42 ft of water (scaled depth λ_c = 0.346 ft/lb$^{1/3}$). In this case the secondary jet did not overtake the initial or primary jet.

Measurements of the minimum jet diameter, j_{min}, were obtained whenever possible, the measurement being made while the jet was well defined and at a minimum width. Subsequent to the time of measurement, the jet breaks up and collapses. The data (see Appendix A) show considerable scatter, due to obscuration of the early stages of jet development by the water column and the smoke crown. (The outline of the jet is most clearly visible when the charge is fired between the cameras and the sun.)

In view of the large amount of scatter and irregular nature of the available data, it is not possible to determine reliable formulas for the prediction of j_{min}. However, the results indicate that jet diameter decreases with increasing charge depth. The data also indicate that minimum jet

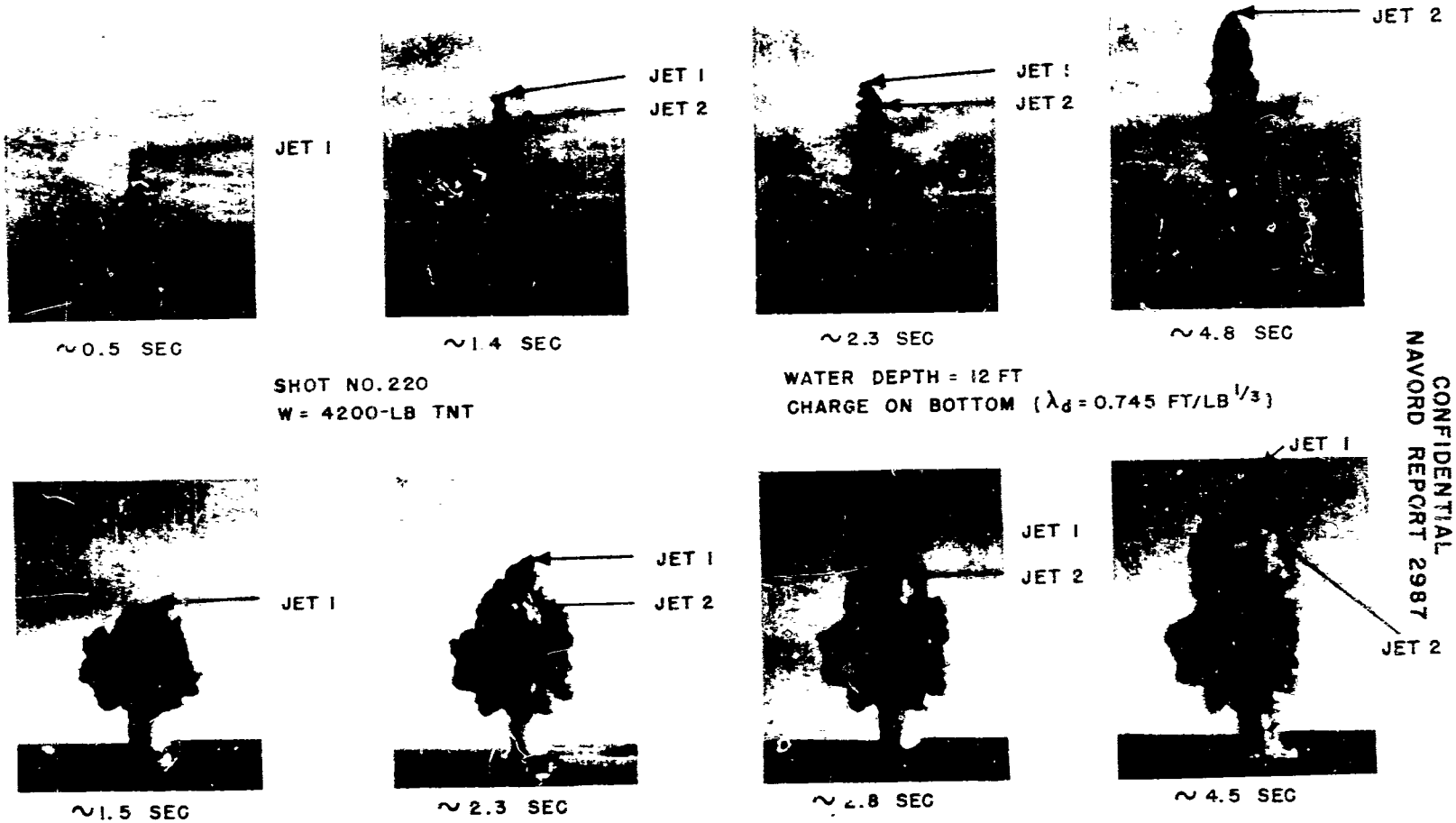

FIG. 2.21 MULTIPLE JET FORMATION

diameter is directly proportional to the cube root of the charge weight when charges are fired at the same scaled depth.

As the range of the data presented here is relatively limited, it would be of interest to obtain some information concerning jet formation by explosions at somewhat greater depths.

Measurements of maximum plume height have been reported by Johnson and Chinn [11] for 1-lb spherical charges of Composition C-3 exploded at various depths in water ranging from 0.1 to 4.0 ft in depth, and by Kolsky, Sampson, Snow, and Shearman [12] for 1-lb approximately spherical charges of Nobel's plastic explosive No. 808 fired in 11.0 ft of water. The data are presented in Fig. 2.22 in the form of J_{max} vs charge depth at different water depths. "Plumes" from 1-lb charges at the depths shown are similar to the "jets" reported here. At greater depths, plumes with different characteristics would be formed.

The data shown in Fig.2.22 all tend to indicate a maximum jet height at a 1 ft charge depth, which corresponds to a scaled depth, λ_c, of about 1 ft/lb$^{1/3}$. This is an interesting result, as the charges were fired in water depths ranging from 0.1 ft to 11.0 ft and include a few that were detonated above the surface and several that were buried in the bottom. The NOL data are not extensive enough to check the validity of the result for larger charges.

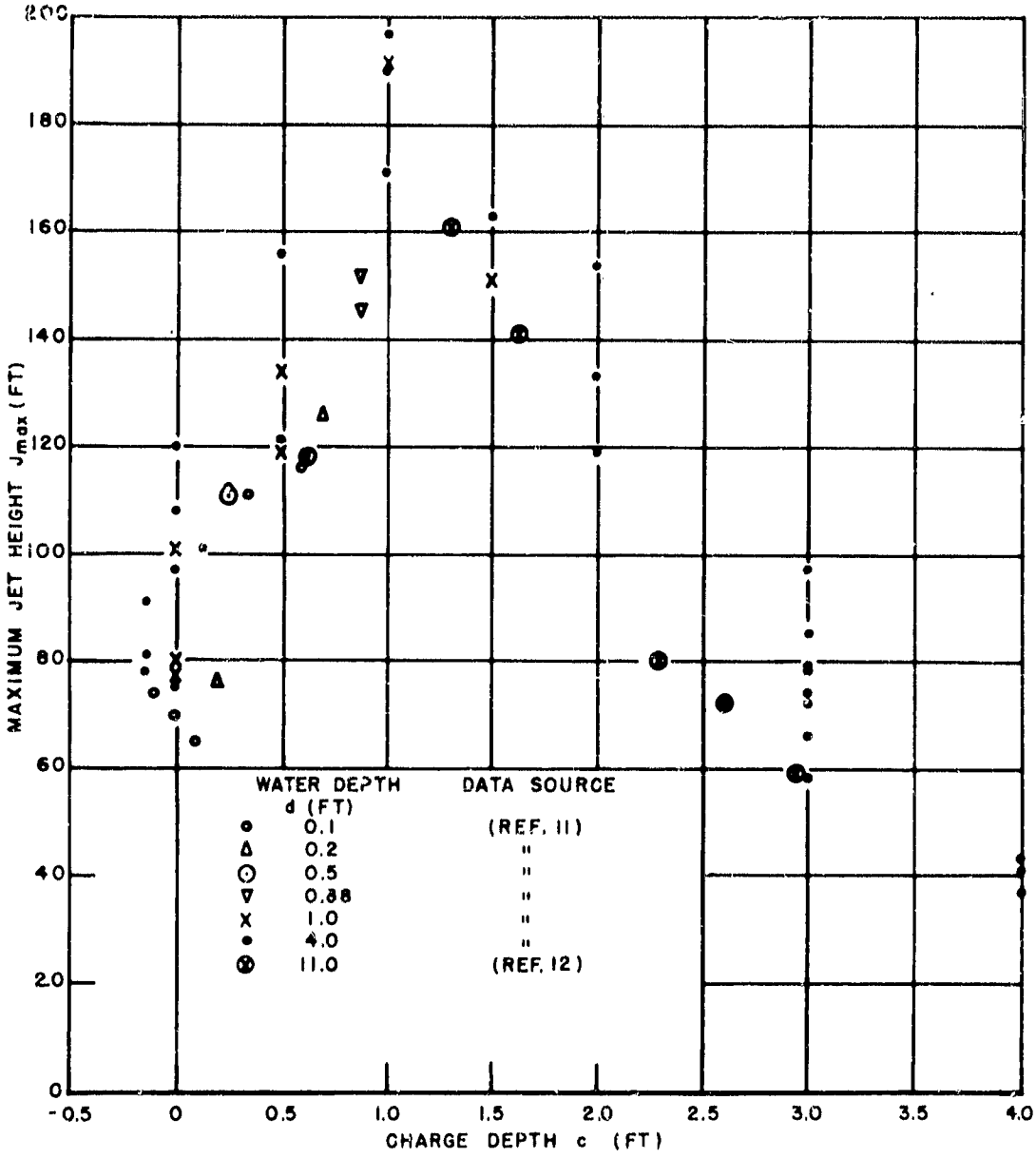

FIG. 2.22 MAXIMUM JET HEIGHT vs CHARGE DEPTH (1-LB CHARGES)

CHAPTER III
BASE SURGE

3.1 Description of the Base Surge. The base surge is formed by the descent of the water column thrown up by an underwater explosion and the subsequent radial outflow of the column material along the water surface. The surge consists of water droplets suspended in air and resembles a cloud or a fog. As it flows outward, it increases in height. During this process, the surge mixes with the surrounding air, becomes thin and tenuous at the outer parts, and gradually evaporates.

At extremely shallow charge positions, detonation products enter the base surge in considerable amounts. The surge is gray or black if appreciable quantities of carbon are present, and resembles a "smog" in appearance.

The high explosive charges fired underwater in the NOL programs have produced base surges that were initially similar in appearance to the base surge observed at Test Baker (see Fig. 3.1a). A later view of the Baker surge formation is shown in Fig. 3.1b; this was obtained from an altitude of 12,000 ft at 41 seconds after the detonation, when the surge had grown to a radius of 3600 ft and a height of 650 ft, and shows the torus-like form of the surge cloud.

Figure 3.2 illustrates base surge formation by 600-lb and 4200-lb charges scaled to the Baker charge and water depth. It should be noted that material falling from the jet and smoke crown enters the base surge after the column has disappeared.

In Fig. 3.3 the formation of base surges at two charge positions close to the extremes of the experimental range for 4200-lb bottom explosions is illustrated. The upper prints show the dark "smog" surge formed by an explosion in 1.83 ft

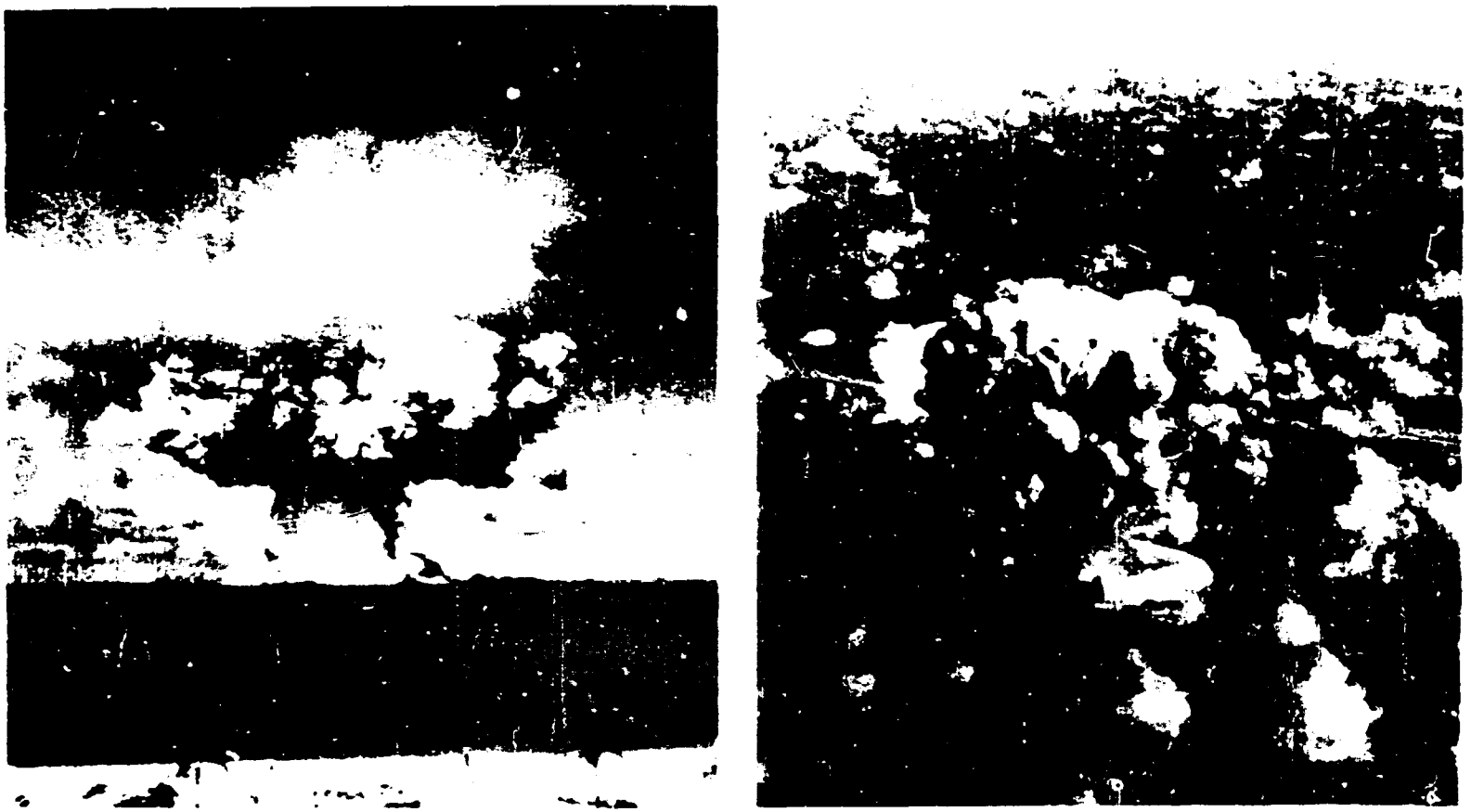

(a) 15 SEC

SURGE RADIUS = 1800 FT
SURGE HEIGHT = 400 FT

(b) 41 SEC

SURGE RADIUS = 3600 FT
SURGE HEIGHT = 650 FT

FIG. 3.1 BASE SURGE FORMATION (TEST BAKER)

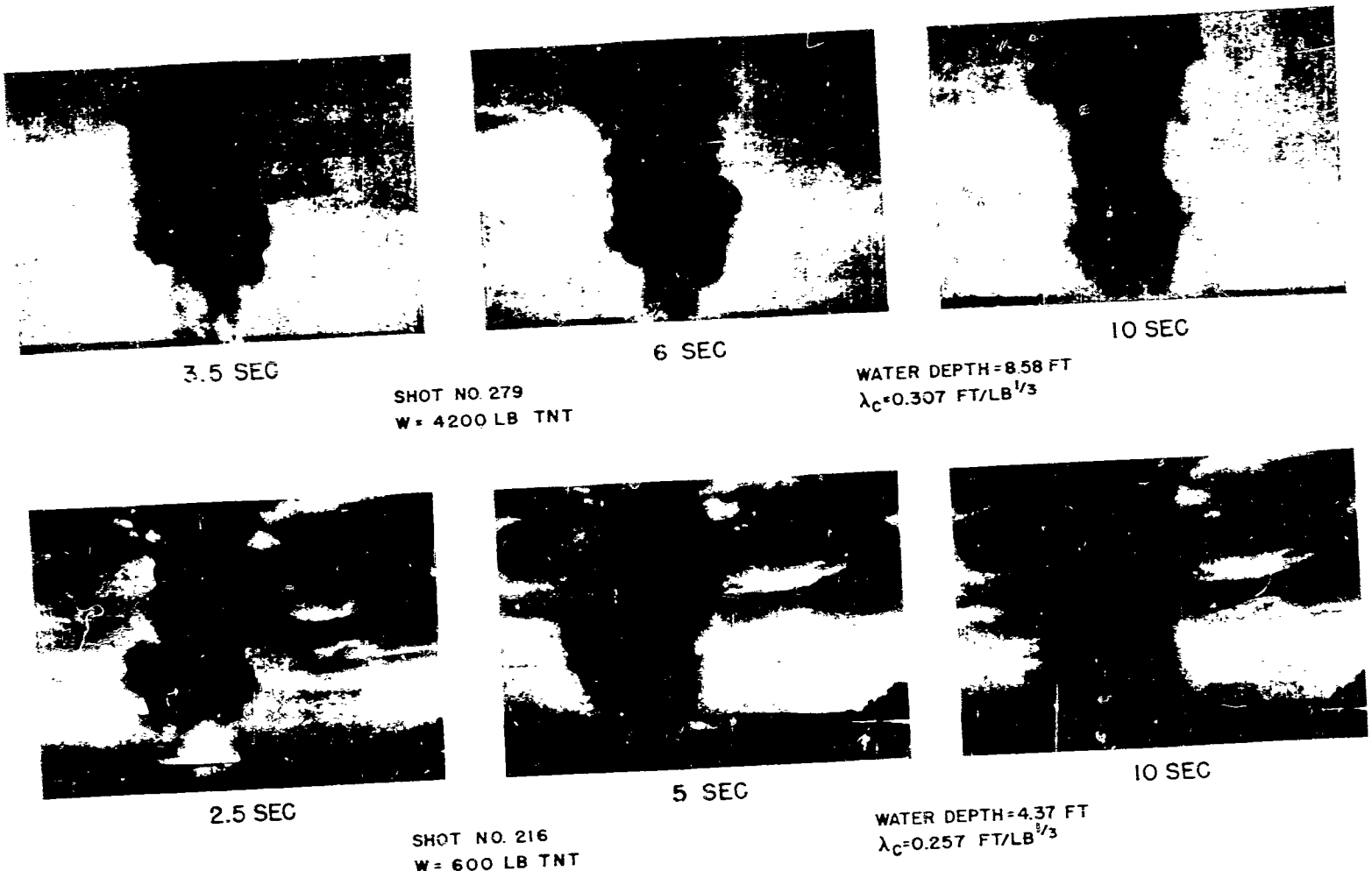

FIG. 3.2 BASE SURGE FORMATION (TESTS SCALED TO BAKER)

SHOT . 280
W = 42 LB TNT
WATER EPTH = 1.83 FT
λ_d = 0. FT/LB$^{1/3}$

SHOT NO. 22!
W = 4200 LB TNT
WATER DEPTH = 9.25 FT
λ_d = 0.574 FT/LB$^{1/3}$

FIG. 3.3 BASE SURGE FORMATION (CHARGES ON BOTTOM)

of water (λ_d = 0.114 ft/lb$^{1/3}$) and the lower show the white surge produced by an explosion in 9.25 ft of water (λ_d = 0.574 ft/lb$^{1/3}$). The contrast between the phenomena in Fig. 3.3 can be clearly seen and is indicated by the following table of data; for comparison, the data from the 4200-lb shot shown in Fig. 3.2 are included.

TABLE 3.1
COMPARISON OF SURFACE PHENOMENA FROM 4200-LB EXPLOSIONS AT DIFFERENT DEPTHS

Shot Number	Scaled Charge Depth (λ_d) (ft/lb$^{1/3}$)	D_{max} (ft)	C_{max} (ft)	J_{max} (ft)	P_{max} (ft)	H_{max} (ft)
280	0.114	85.4	51	870	345	184
221	0.574	114.0	231	1130	>469*	92
279	(Approx. scaled to Baker)	99.6	156	985	322	104

Table 3.1 indicates the increased size of column, jet and base surge when charges are fired at increasing depths within this range.

---

* When the "greater than" symbol is used with maximum surge radius, R_{max}, it means that the surge exceeded the photographic field of view while expanding, or was carried out of the field by winds, so that a final determination of surge size could not be made. In addition, it should be noted that the reported values of R_{max} and maximum surge height, H_{max}, represent the maximum visible extent of the surge cloud. There is evidence that the cooled air in the surge continues to propagate after the water droplets have evaporated [13].

The greatest scaled depth at which charges were fired in the NOL programs reported here was at a λ_d equal only to 2.17 ft/lb$^{1/3}$ (Shots 45, 46, and 65). Examples of surge formation at scaled depths of 1.09 ft/lb$^{1/3}$ and 2.15 ft/lb$^{1/3}$ are shown in Fig. 3.4. However, base surges have been observed at deeper charge positions.

3.2 Surge Radius. As the smaller TNT explosions usually formed base surges that were tenuous, brief in duration, and difficult to measure, most of the surge analysis in this report is based upon data from 600-lb and 4200-lb charges. A plot of base surge radius versus time for four 600-lb and four 4200-lb charges fired on the river bottom at shallow depths is presented in Fig. 3.5. Water depth and shot number are indicated at the end of each curve; data for mid-depth shots scaled to the Test Baker geometry are included for comparison. It can be seen that within this range of scaled depths ($0.114 < \lambda_d < 0.745$ ft/lb$^{1/3}$) base surge rate of growth and maximum extent increase with increasing depth of firing. This is consistent with the fact that maximum column diameter and maximum column height increase with increasing charge depth (see Sec. 2.5), since a higher and broader column produces a larger and faster base surge. It also appears that the Baker condition was probably not the optimum and that placing the atomic bomb on the bottom of the lagoon at Bikini might have produced a larger base surge.

Figure 3.6 illustrates that the same depth effect for base surges results from 100-lb TNT explosions.

A plot of all maximum surge radius data versus scaled charge depth for charges on the bottom is shown in Fig. 3.7. The limit of scaled depth in which smog surges were formed is delineated for each charge weight by a vertical dashed line. There is obviously a considerable degree of scatter in these measurements and there is only a slight indication

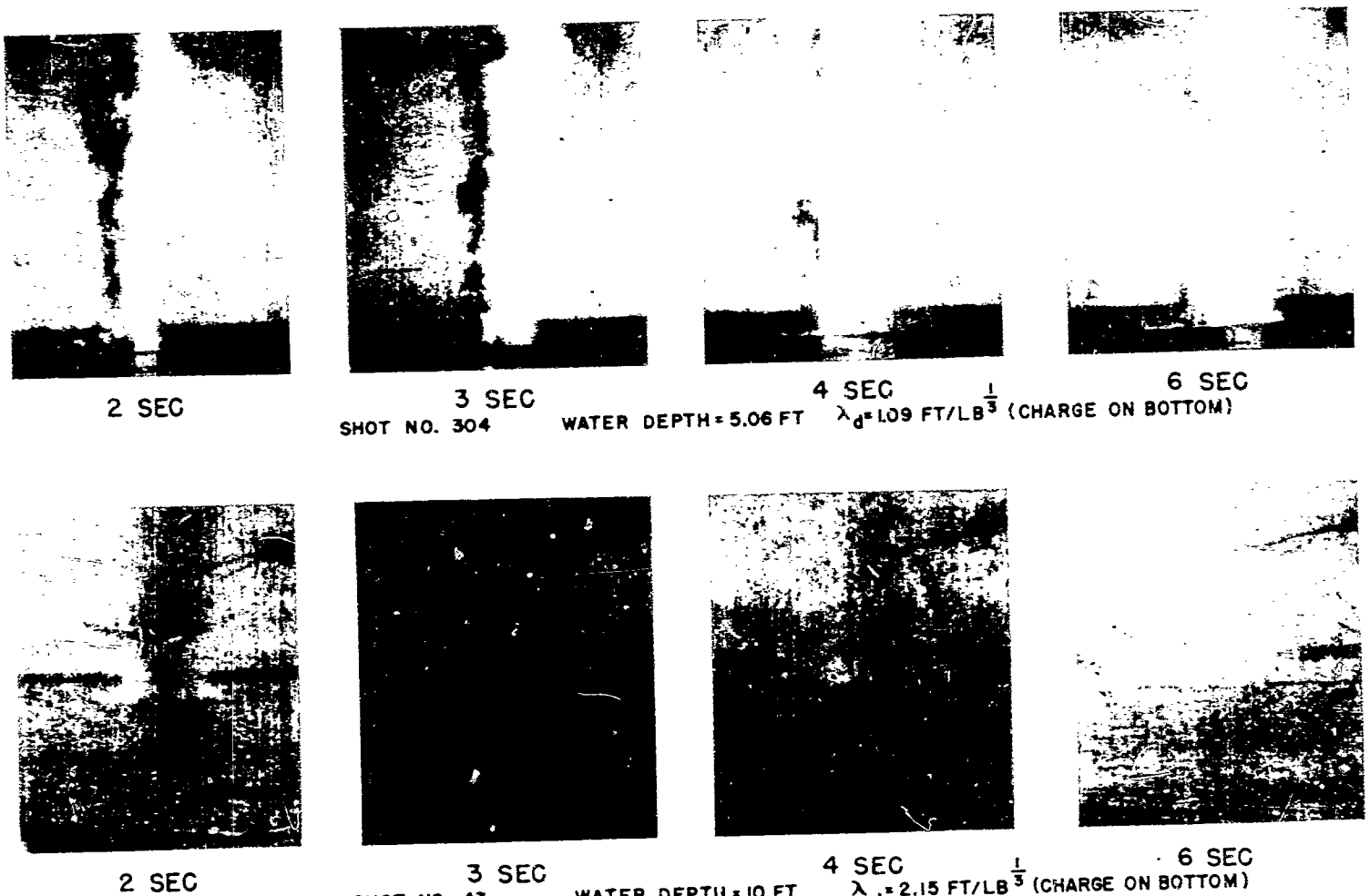

FIG. 3.4 BASE SURGE FORMATION BY 100 LB CHARGES
IN RELATIVELY DEEP WATER

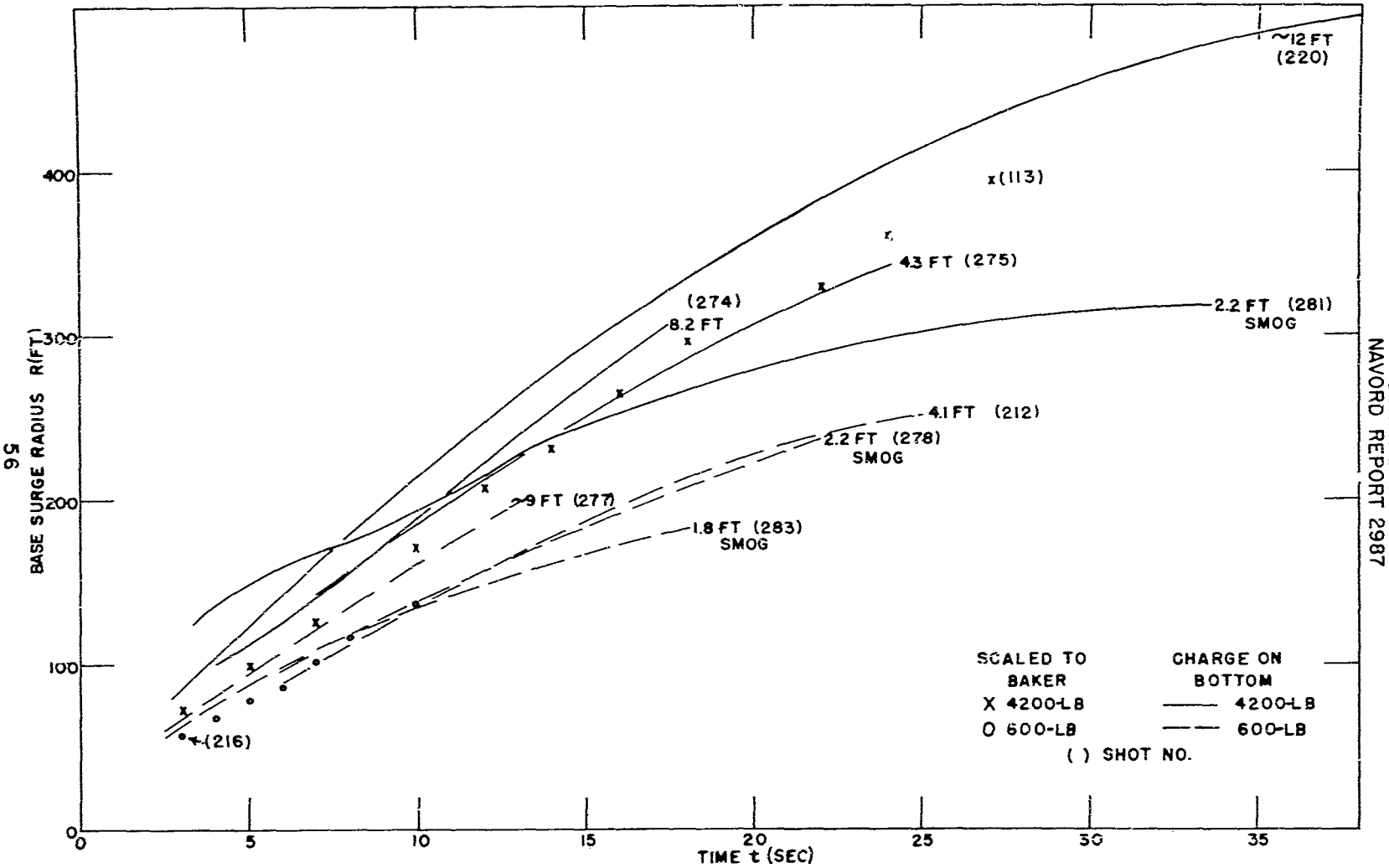

FIG. 3.5 BASE SURGE RADIUS vs TIME (600-LB AND 4200-LB CHARGES)

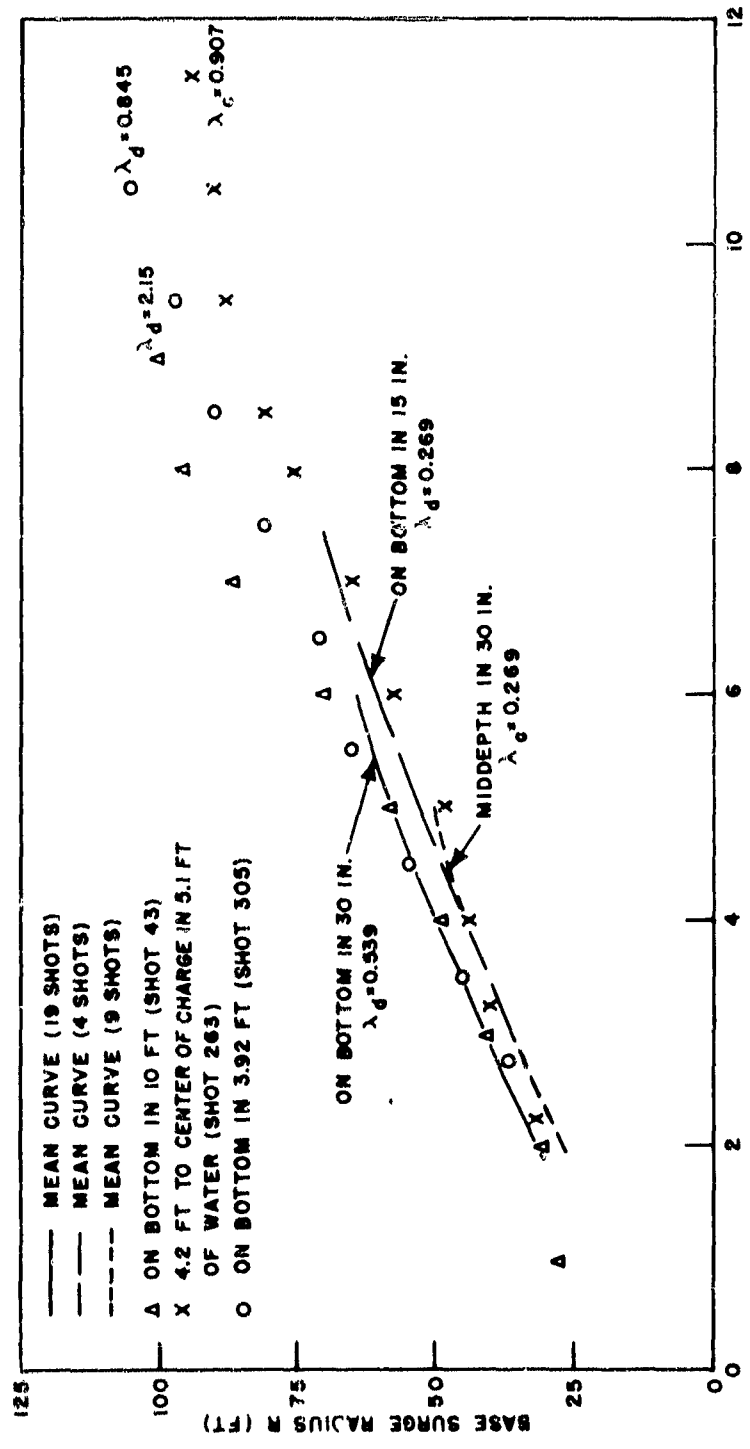

FIG. 3.6 BASE SURGE RADIUS vs TIME
(100-LB CHARGES)

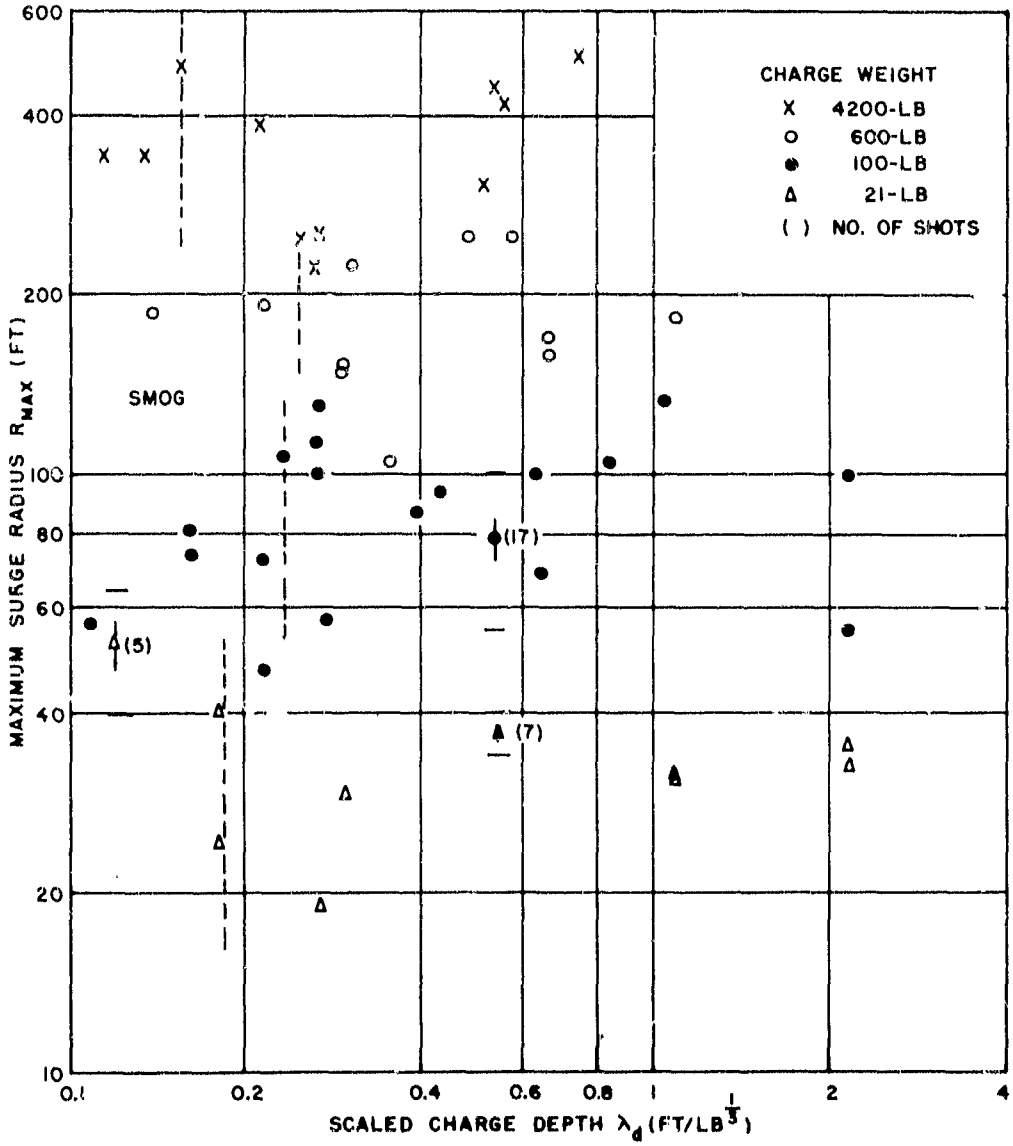

FIG. 3.7 MAXIMUM SURGE RADIUS vs SCALED CHARGE DEPTH
(CHARGES ON BOTTOM)

of an increase of maximum surge radius with increasing depth. However, since there is an increase in initial surge radial velocity with increasing depth, this increase of radius is probably real. (Wind is one of the major contributors to the scatter in base surge radial growth measurements.* Some effects of wind on the base surge are shown in Fig. 3.8. In addition, splashes due to throwout of mud and rocks frequently obscure and distort the tenuous leading edge of the surge.)

By grouping the data, it is possible to obtain the following empirical expressions for R_{max} which may be used for approximate predictions within the range of variables indicated:

$$R_{max} = 10\ W^{0.42} \qquad (\lambda_c = 0.26\ ft/lb^{1/3}) \qquad (24)$$

$$R_{max} = 20\ W^{1/3} \qquad (0.11 < \lambda_d < 0.26\ ft/lb^{1/3}) \qquad (25)$$

$$R_{max} = 8.2\ W^{0.49} \qquad (0.53 < \lambda_d < 2.2\ ft/lb^{1/3}) \qquad (26)$$

The total surge extent is greatly affected by atmospheric conditions which cannot be scaled. A weight effect must also be considered and it will be shown in Chapter VI that larger charges form surges which extend to a greater scaled maximum radius than smaller charges. The surge radius is therefore not simply a function of scaled charge depth.

3.3 Surge Height. The irregular but continuous increase in the height of the surge clouds from high explosive underwater detonations is initially similar to that of the Test Baker surge. This behavior is shown in Fig. 3.9, a plot of surge height versus time for 4200-lb and 600-lb TNT charges.

* It has been a general policy in field tests to fire only during periods of light wind or calm. However, this was not always possible, and in a few cases shots were fired on windy days to study the effects of wind.

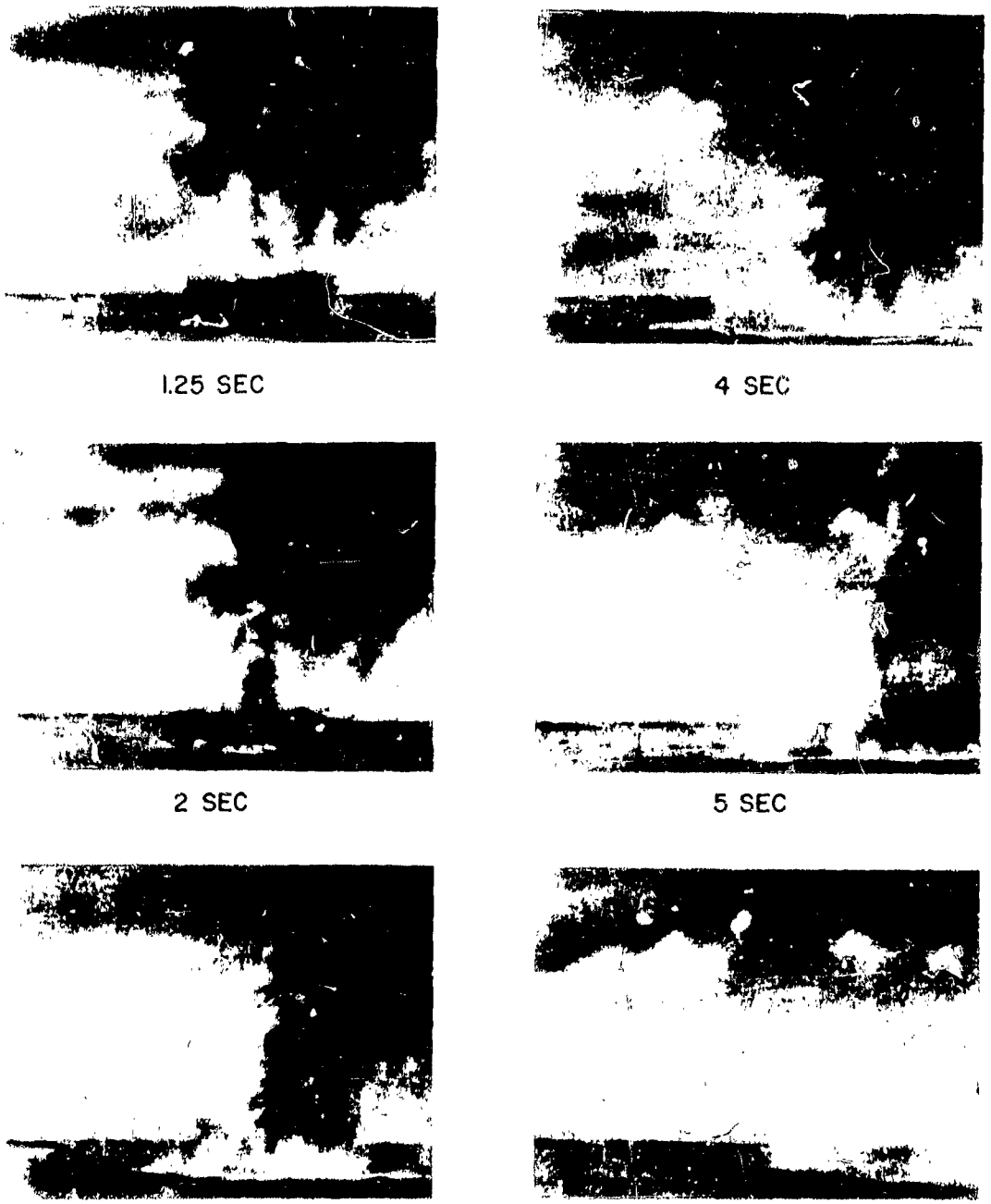

1.25 SEC

4 SEC

2 SEC

5 SEC

3 SEC

7 SEC

SHOT NO. 272
W=600 LB TNT
WATER DEPTH = 3.42 FT

$\lambda_d = 0.405$ FT/LB$^{\frac{1}{3}}$
WIND VELOCITY = 11 KNOTS

FIG. 38 EFFECT OF WIND ON BASE SURGE

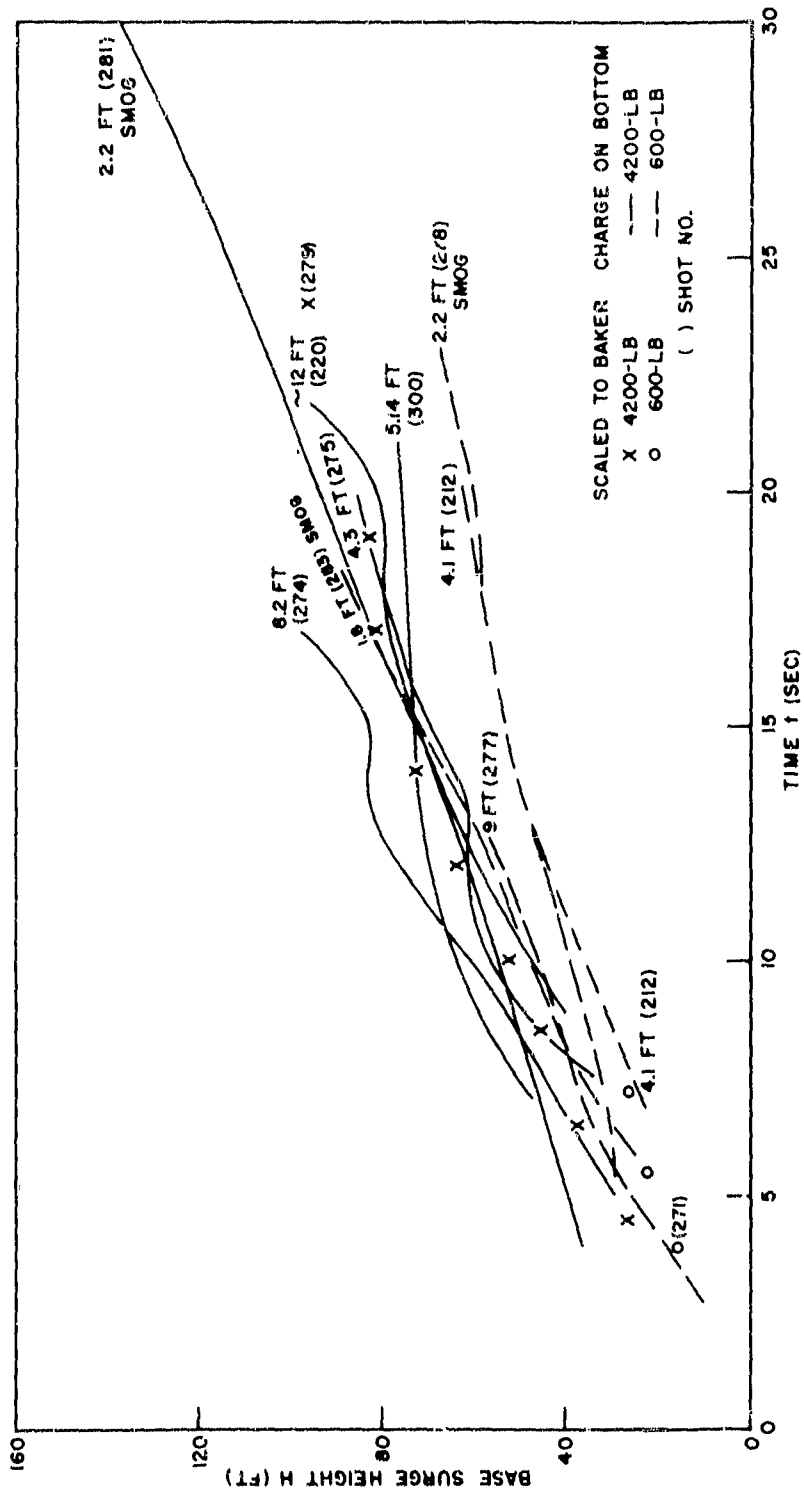

FIG. 3.9 BASE SURGE HEIGHT vs TIME
(600-LB AND 4200-LB CHARGES)

Values of H_{max} reported here represent the maximum average height of the surge cloud as visible on photographic prints. Due to the presence of carbon particles, smog surge heights are measurable for relatively long periods. The tops of the "clean" surges from small scale TNT explosions quickly become extremely tenuous due to mixing with the surrounding air and evaporation of the water droplets.

That there is any effect of charge depth upon the rate of growth of the surge height or the maximum height attained is not clearly apparent. This may be seen in Fig. 3.9 and also in Fig. 3.10, a plot of H_{max} in ft versus the scaled charge depth, λ_d in $ft/lb^{1/3}$, for charges on the bottom.

Plots of H_{max} in ft versus the cube root of the charge weight in lbs show the following relationships at the indicated scaled depths:

$$H_{max} = 1.9\ W^{0.45} \qquad (\lambda_c = 0.26\ ft/lb^{1/3}) \qquad (27)$$

$$H_{max} = 1.9\ W^{0.45} \qquad (\lambda_d = 0.26\ ft/lb^{1/3}) \qquad (28)$$

$$H_{max} = 2.4\ W^{0.45} \qquad (\lambda_d = 0.53\ ft/lb^{1/3}) \qquad (29)$$

$$H_{max} = 2.2\ W^{0.45} \qquad (0.75 < \lambda_d < 2.2\ ft/lb^{1/3}) \qquad (30)$$

These formulas indicate a slight increase in surge height with depth of firing to a λ_d of 0.53 $ft/lb^{1/3}$, and some decrease in height at greater depths; they are probably not valid if extended beyond the range of weights and depths used in this analysis.

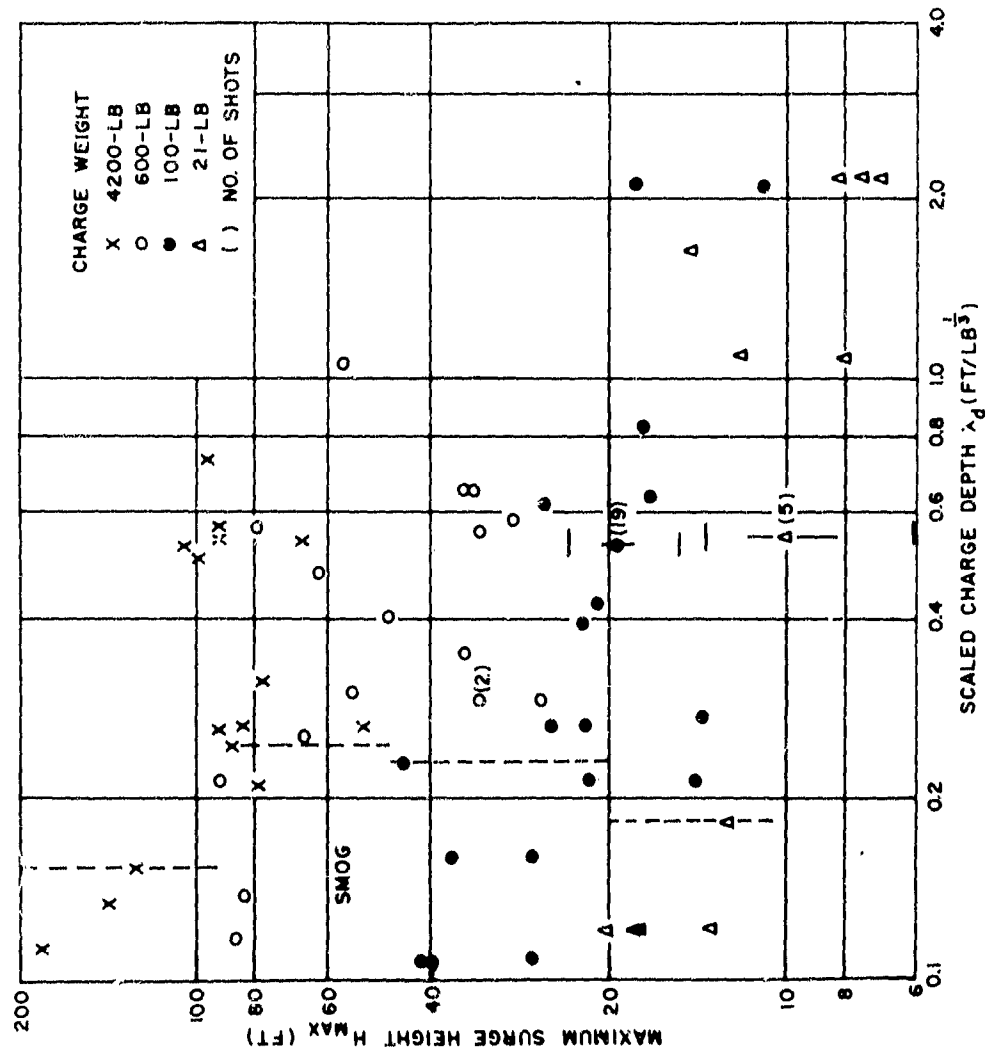

FIG. 3.10 MAXIMUM SURGE HEIGHT vs SCALED CHARGE DEPTH
(CHARGES ON BOTTOM)

CHAPTER IV

EFFECTS OF SHALLOW CHARGE POSITIONS

4.1 Characteristics of Smog Surges. When a charge is fired on or near the water surface, or is only partially submerged, the explosion products are vented directly to the atmosphere and solid smoke particles enter the surge cloud. If an appreciable amount of carbon is produced, the base surge is gray or black in appearance and resembles a smog. The proportion of solid contaminants in the surge increases with decreasing charge depth.

"Smog surges" remain visible after the water droplets they contain have evaporated. They can be measured for relatively long periods and their behavior studied after gravitational flow has ceased, and until they are dispersed by atmospheric turbulence. An example of a smog surge produced by a 4200-lb TNT charge on the bottom in 1.83 ft of water (λ_d = 0.114 ft/lb$^{1/3}$) was shown in Fig. 3.3.

Figure 4.1 shows smog surges produced by 100-lb TNT charges fired at zero depth (bottom of charge level with water surface) and with 10 inches of the charge submerged. At the shallower charge position a surface smoke cloud is blown radially along the water surface at detonation, and the surge which forms later at the base of the falling column propagates into the surface cloud, mixes with it and pushes it outward. This surface detonation cloud was not observed when 100-lb TNT charges were fired with more than 3 inches of the charge submerged.

In some blasting gelatin explosions, white surface clouds and base surges were formed at smog depths. The white color was due to chalk, which was used as a filler in the explosive. The surge behavior was similar to that

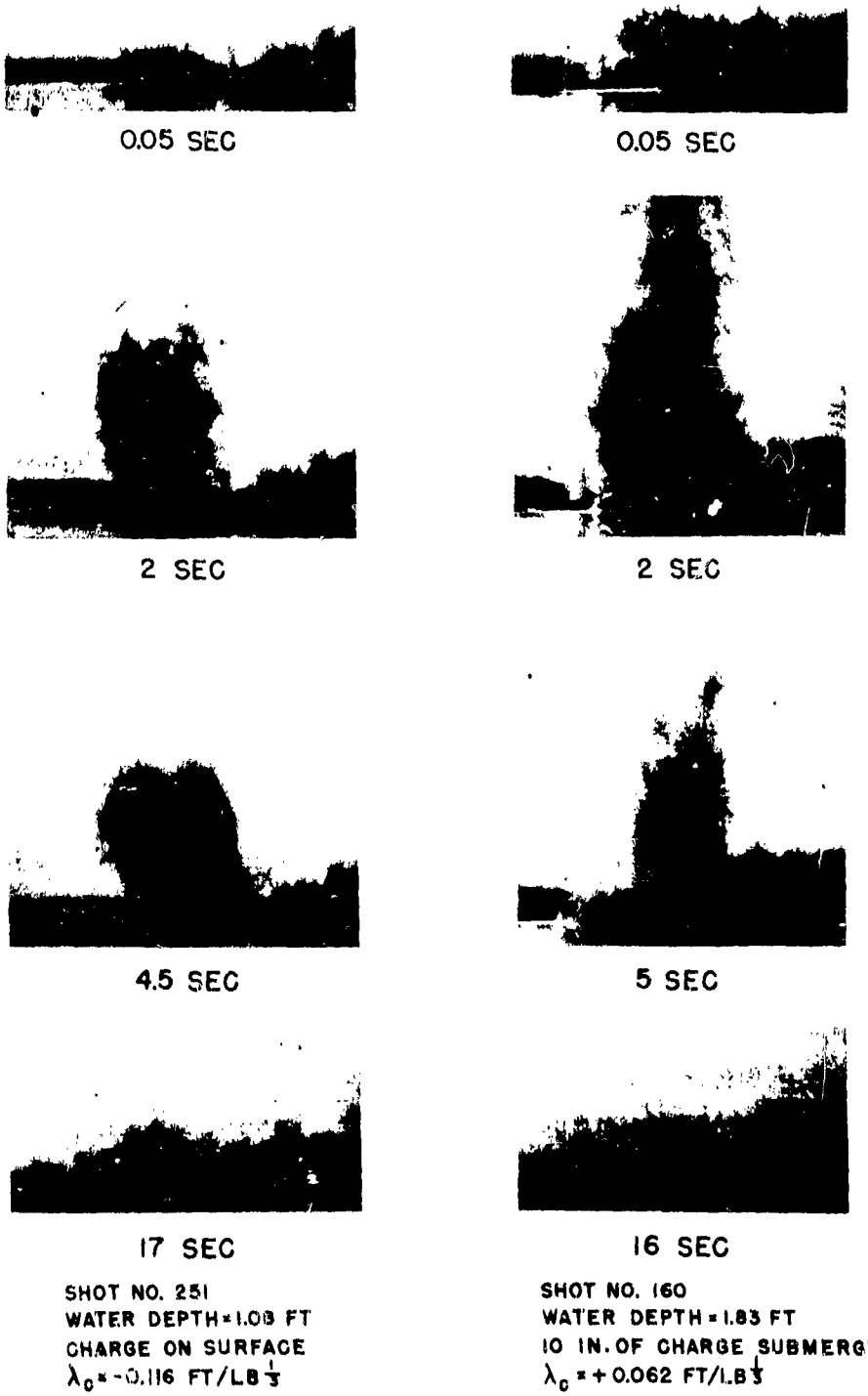

FIG. 4.1 SMOG SURGES FORMED BY 100-LB TNT CHARGES FIRED AT SHALLOW POSITIONS

of the dark, carbon-laden smog surges from very shallow TNT explosions.

4.2 Effects of Charge Depth and Water Depth. A series of 34 100-lb TNT charges was fired at shallow positions in shallow water (1.1 to 5.3 ft) and deeper water (15 to 16 ft) to study smog effects. Charge position was varied systematically from just above the water surface to complete submergence. In addition, photographic records of a group of 7 100-lb surface shots fired in water from 24 to 30 ft deep were obtained from another NOL program. A smog surge was observed in all cases in which part of the charge was above the water surface. With zero to 2 inches of water above the top of the charge, smog surges were observed from roughly 50 percent of the shots. With slightly more than 2 inches of water above the top of the charge, "clean" base surges composed of water droplets and containing no visible traces of smoke were observed.

Surge radius versus time curves for this shallow series are presented in Fig. 4.2 (water depth 1.1 ft to 5.3 ft) and Fig. 4.3 (water depth 15 ft to 30 ft). In general, the rate of growth and maximum extent of smog surges increase with increasing water depth beneath the charge. A similar effect is obtained when charge submergence is increased in the same depth of water.

The initially large surge radius indicated in Figs. 4.2 and 4.3 for Shots 251, 266, 172, 174, 175, 176, 170, 139 and 168 is due to the surface smoke cloud described in Sec. 4.1 above. Part of this cloud extended beyond the true base surge, thereby resulting in an apparently greater surge extent. Attempts to exclude this leading material in making surge measurements were not successful.

When 100-lb TNT charges were fired at shallow smog positions in deep water, an upheaval was observed at the base

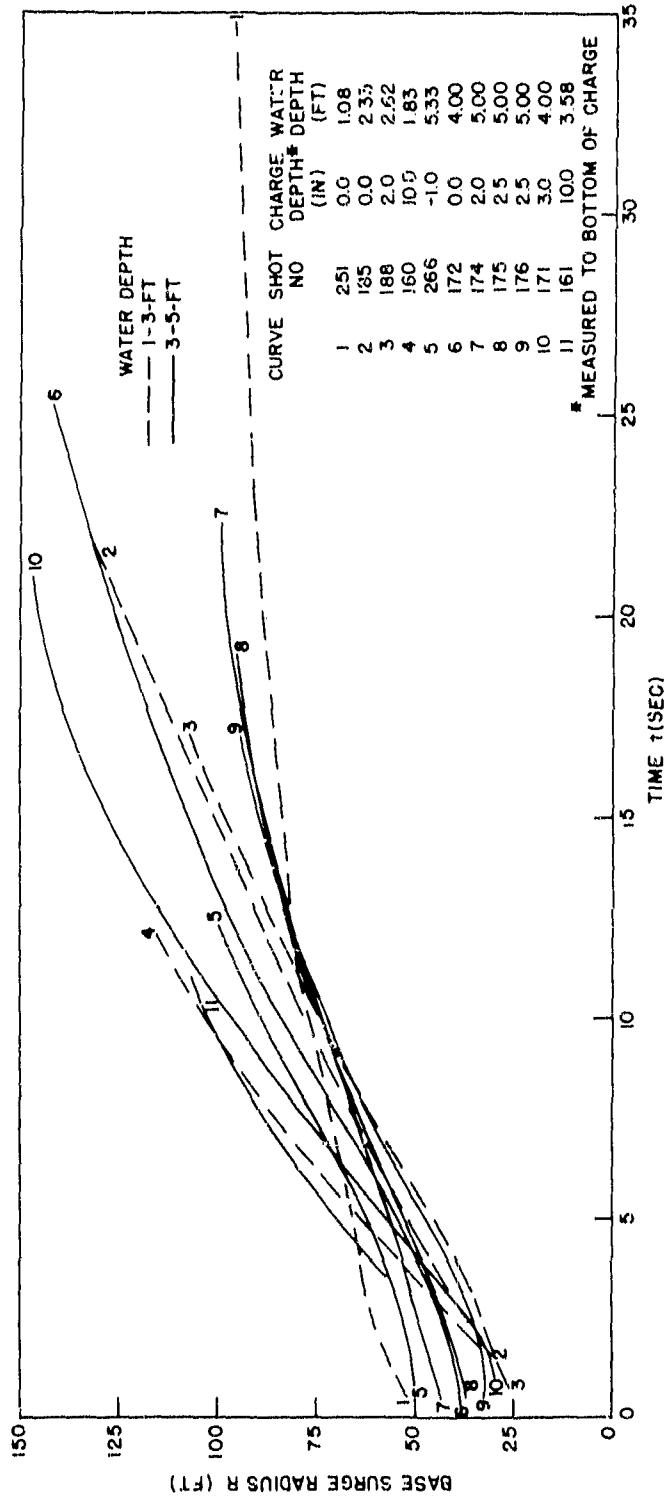

FIG. 4.2 SMOG SURGE RADIUS vs TIME
(SHALLOW 100-LB CHARGES IN SHALLOW WATER)

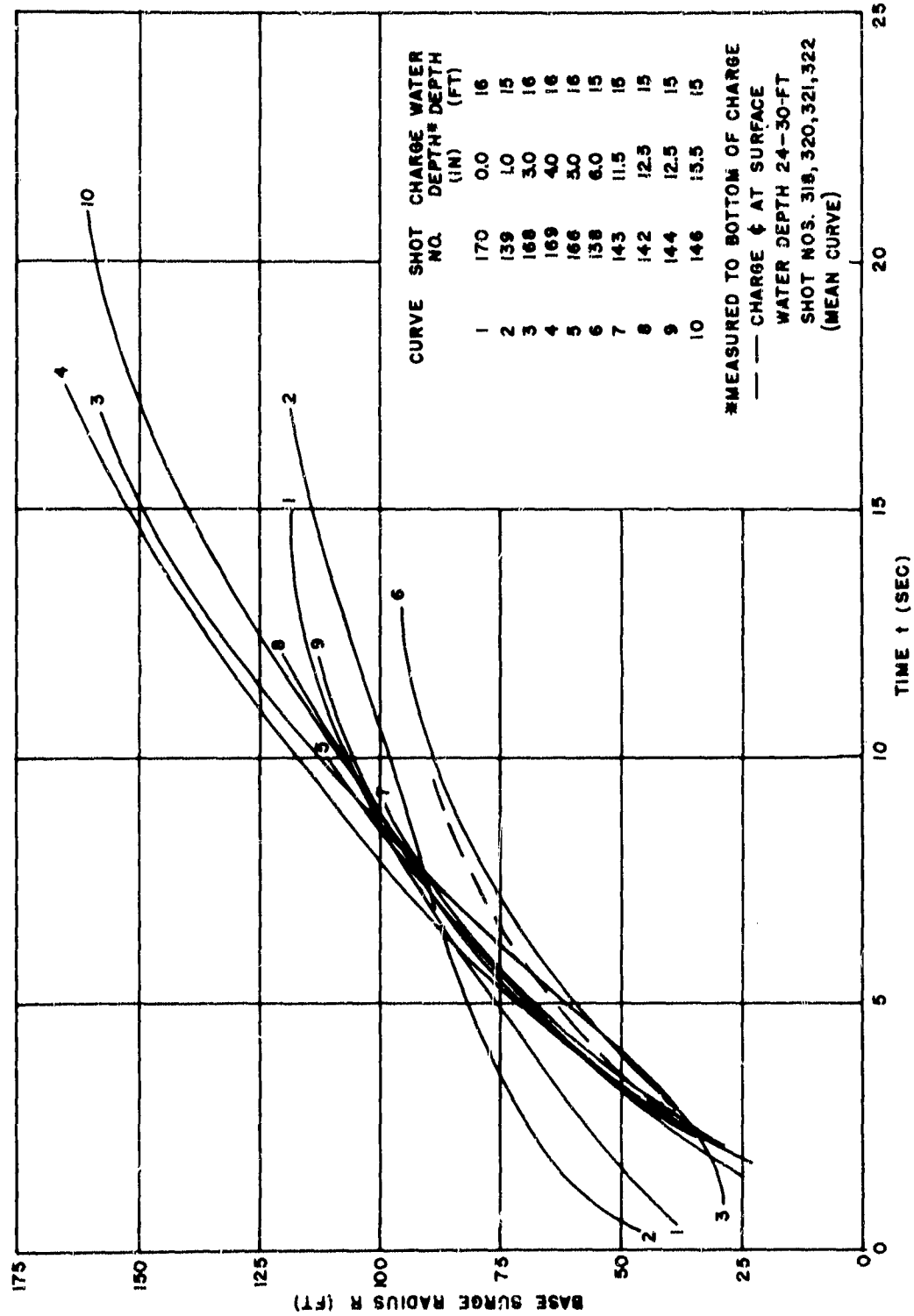

FIG. 4.3 SMOG SURGE RADIUS vs TIME
(SHALLOW 100-LB CHARGES IN DEEP WATER)

of the column between 1.5 and 2.0 seconds, indicating that not all the explosion products are vented directly to the atmosphere at detonation, as occurs in shallow water. The carbon-laden material in the secondary venting mixes with the falling column material during the initial stages of surge formation. This phenomenon is illustrated in Fig. 4.4. It was also observed in Britain in experiments with 1-lb and 10-lb charges [12].

The maximum column diameters formed by 21-lb and 100-lb explosions fired with the bottom of the charge level with the water surface over the range of scaled water depths from 0.50 ft/lb$^{1/3}$ to 3.45 ft/lb$^{1/3}$ can be related to charge weight in the following way:

$$D_{max} = 14.9\ W^{0.147} \tag{31}$$

where D_{max} is in ft and W is in lbs.

As formula (31) is based upon a limited amount of data, its validity over a wide range of charge weights is highly questionable. However, it is probably significant that D_{max} is not a function of the cube root of the charge weight for these surface shots.

Within the shallow water range of 1-4 ft, maximum jet height increases with increasing water depth, for 100-lb charges fired on the surface. Lower jets are observed, however, for 100-lb surface shots fired on deeper water (15-16 ft). This may be due to the incomplete initial venting of the bubble in deep water, as can be seen from the subsequent secondary venting of explosion products, described above.

Smog surge radius versus time curves for charges on the bottom in very shallow water ($0.11 < \lambda_d < 0.26$ ft/lb$^{1/3}$)

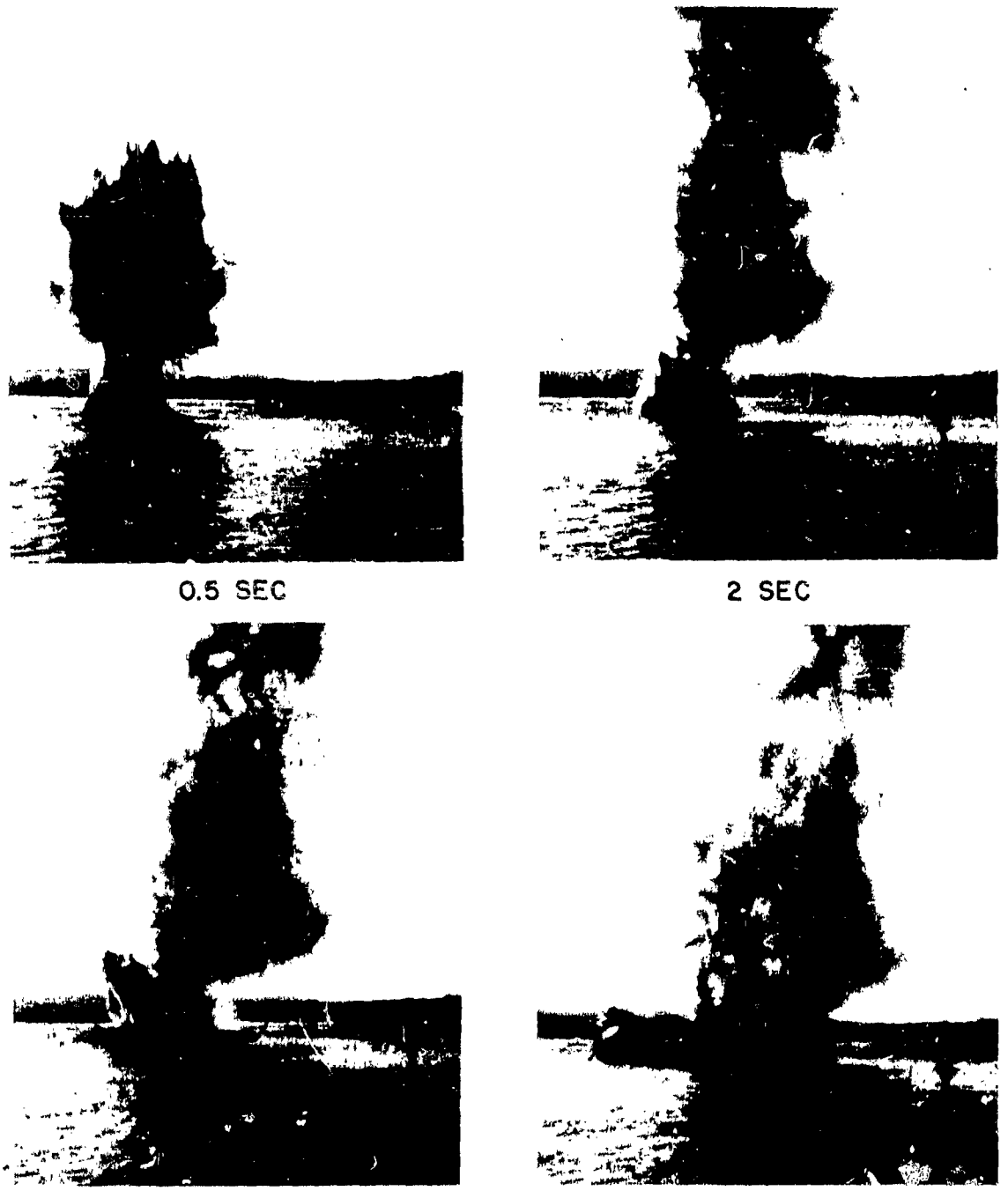

SHOT NO. 151
W = 100-LB TNT
WATER DEPTH = 15-FT

TOP OF CHARGE LEVEL
WITH WATER SURFACE
$\lambda_c = 0.125$ FT/LB$^{\frac{1}{3}}$

FIG. 4.4 SECONDARY VENTING OF GASES
(SHALLOW EXPLOSION IN DEEP WATER)

are shown in Fig. 4.5. In general, the same trend of steeper curves and greater maximum extent is observed as water depth is increased.

A study of smog surge height versus time curves showed no clearly defined effects of charge depth or water depth on this parameter, within the range of $0.11 < \lambda_d < 0.26$ ft/lb$^{1/3}$. The tops of the smog surges show a tendency to rise in irregular tufts after the surge radial growth has ceased. In general, the maximum visible heights of smog surges are greater than the maximum visible heights of "clean" surge clouds by a factor of about 2.

Maximum column diameter, maximum column height, maximum jet height and maximum surge height are plotted against the cube root of the charge weight in Fig. 4.6 for explosions on the bottom in shallow water in the range of $0.11 < \lambda_d < 0.26$ ft/lb$^{1/3}$*. The empirical formulas for the data are:

$$D_{max} = 6.7\ W^{1/3} \quad (0.11 < \lambda_d < 0.26) \quad \bar{\lambda}_d = 0.15 \text{ ft/lb}^{1/3} \qquad (32)$$

$$C_{max} = 5.5\ W^{1/3} \quad (0.11 < \lambda_d < 0.26) \quad \bar{\lambda}_d = 0.15 \text{ ft/lb}^{1/3} \qquad (33)$$

$$J_{max} = 54.0\ W^{1/3} \quad (0.11 < \lambda_d < 0.26) \quad \bar{\lambda}_d = 0.15 \text{ ft/lb}^{1/3} \qquad (34)$$

$$H_{max} = 3.8\ W^{0.46} \quad (0.11 < \lambda_d < 0.26) \quad \bar{\lambda}_d = 0.15 \text{ ft/lb}^{1/3} \qquad (35)$$

An indication of the differences between the surface phenomena in the smog range and the surface phenomena at slightly deeper charge positions where smog was not observed may be obtained by comparing the formulas listed above with those given in Chapters II and III. For example: for the

---

* It should be noted that the scaled depth limits within which smog surges were formed vary for different charge weights because of the differences in the shapes of the charges used in the experimental program (see Sec. 1.3).

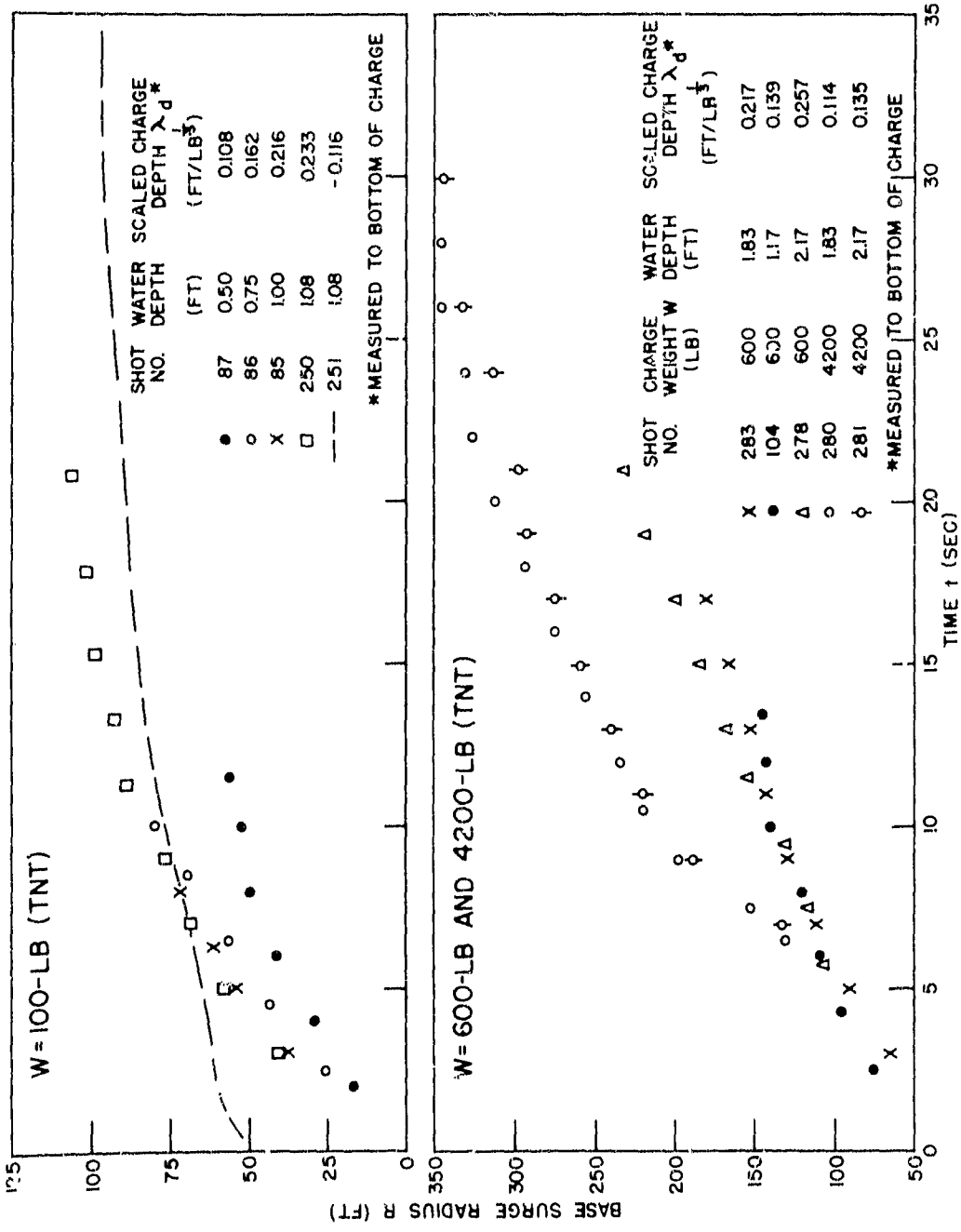

FIG. 4.5 SMOG SURGE RADIUS vs TIME
(CHARGES ON BOTTOM IN VERY SHALLOW WATER)

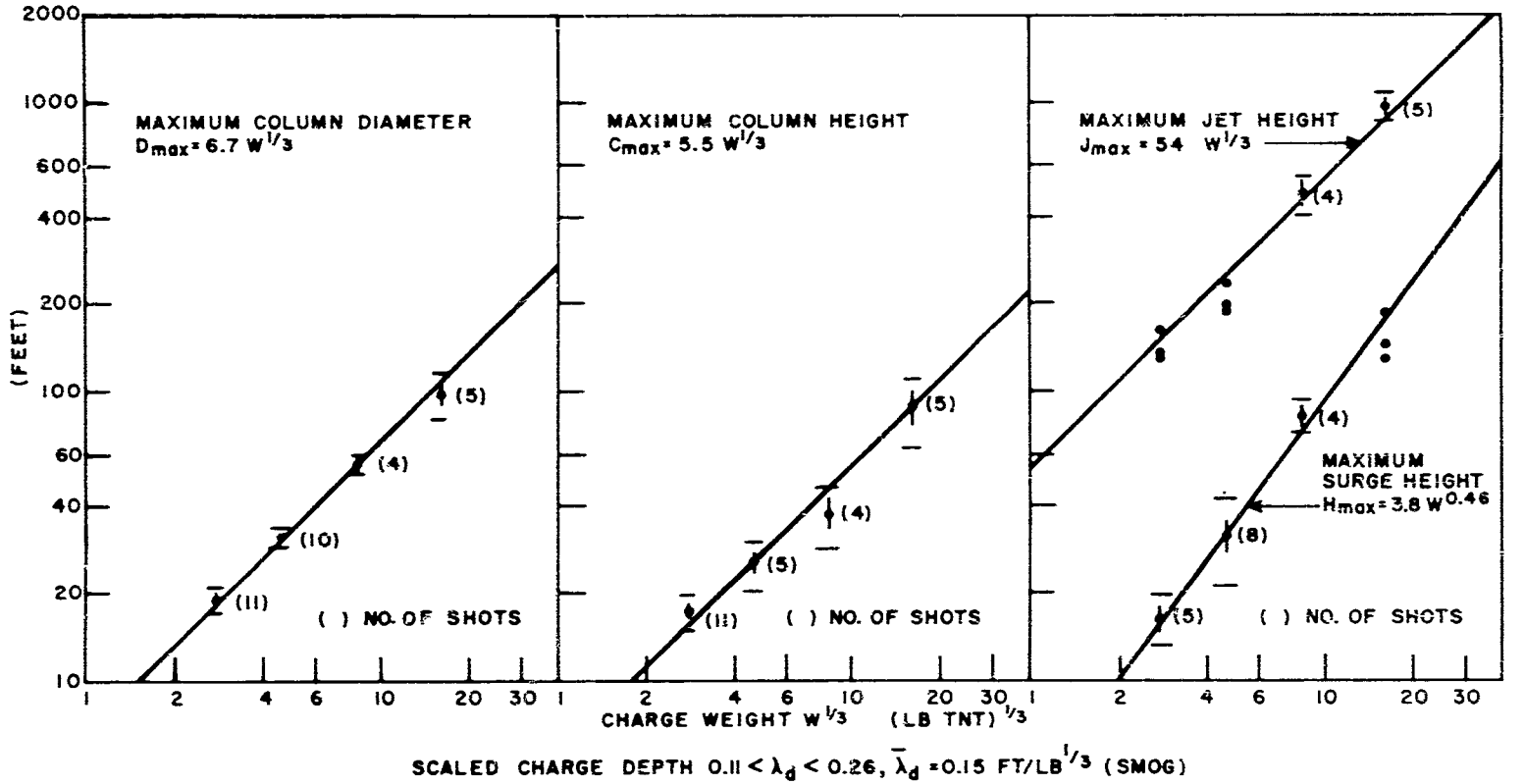

FIG. 4.6 MAXIMUM COLUMN DIAMETER, MAXIMUM COLUMN HEIGHT, MAXIMUM JET HEIGHT AND MAXIMUM SURGE HEIGHT vs CHARGE WEIGHT $^{1/3}$ (CHARGES ON BOTTOM IN VERY SHALLOW WATER)

same charge weight, D_{max} is larger in the smog range than at $\overline{\lambda}_d = 0.28$ ft/lb$^{1/3}$ (formula 8) and C_{max} is less in the smog range than at $\overline{\lambda}_d = 0.27$ ft/lb$^{1/3}$ (formula 15), indicating relatively broad "squatty" columns for explosions in very shallow water. J_{max} is less in the smog range than at $\overline{\lambda}_d = 0.28$ ft/lb$^{1/3}$ (formula 20) and both C_{max} and J_{max} follow the general trend toward lower values with decreasing water depth (see formulas 14 and 23). D_{max} data show a reversal of this trend (shown in formula 11) and increase when water depth decreases below the smog limit.

The magnitude of H_{max} indicated by formula (35) is roughly twice that observed at $\lambda_d = 0.26$ ft/lb$^{1/3}$ (formula 28) due to the presence of smoke particles, which remain visible until their concentration has been greatly reduced by turbulent diffusion.

Results from 100-lb TNT and blasting gelatin explosions at or near the surface of the water, indicated that the maximum radius, R_{max}, of the surge cloud is increased by a factor of 2 or more when part or all of the charge is exposed to the air and smog effects occur (see Fig. 11, Reference 3). However, this effect is not observed with shallow bottom shots, and smog surges formed by bottom explosions in the shallow depth range have about the same radial extent as the "clean" surges from slightly deeper bottom shots; formula (25) applies equally well to both these conditions. Explosions at the greater depths considered in this report form larger surges.

CHAPTER V
EFFECTS OF PARTIAL BURIAL OF CHARGE

5.1 Experimental Data. The scaling of atomic bursts in shallow water with high explosives is extremely difficult, if not impossible, due to the relative sizes of conventional and atomic weapons. For example: a nominal atomic bomb at the bottom of a 40 ft harbor would be completely submerged, whereas a cubical 100-lb TNT charge resting on the bottom at the same scaled water depth would be in 6.5 inches of water and would be half exposed to the atmosphere. Various methods of improving the geometrical scaling may be used in an attempt to achieve better similarity of the surface phenomena and other effects. These include lowering the center of gravity of the charge by changing the charge shape, increasing the water depth, or partial burial of the charge in the bottom.

In an attempt to apply the latter technique, four of the 4200-lb charges and one 600-lb charge fired in the NOL Dahlgren program in the fall of 1952 were partially buried in the river bottom. For additional data, photographic records of ten buried or partially buried charges fired in a Waterways Experiment Station program [9] were obtained for analysis. These charge weights ranged from 32 lbs to 2100 lbs (see Appendix A).

The Dahlgren results are listed in Table 5.1. Charges fired on the bottom in similar depths of water are included for comparison and data from three 256-lb W.E.S. tests are also shown. (The photographic fields of view of the W.E.S. cameras were not adequate for measurements of all of the surface phenomena.) All of the shots listed produced smog surges except Nos. 214, 215 and 298.

TABLE 5.1

EFFECTS OF CHARGE BURIAL

Shot No.	Chg.Wt. W (lb)	Water Depth d (ft)	Charge Depth* c (ft)	Charge Burial (%)	Soil Type	Max.Col. Diameter D_{max} (ft)	Max.Col. Height C_{max} (ft)	Max.Jet Height J_{max} (ft)	Max.Surge Radius R_{max} (ft)	Max.Throw-out Dia. T_{max} (ft)	Max.Smoke Crown Dia. S_{max} (ft)	Initial Venting Velocity (ft/sec)
280	4200	1.83	B	0	Sandy Clay	85.4	51.0	870	345	895	390	1000
295	4200	2.04	2.29	61.7	Sandy Clay	86.4	106	850	213	1300	313	1650
281	4200	2.17	B	0	Clay	87.7	77.0	872	339	938	372	1150
112	4200	2.50	B	0	Clay	127	112	1120	482	945	448	-
294	4200	2.65	2.51	43.5	Sandy Clay	81.9	88.2	950	217	1450	296	1700
297	4200	2.98	2.60	32.2	Sandy Clay	88.4	84.6	700	228	1680	368	1950
214	4200	4.33	B	0	Sand	91.0	140	1053	>236	325	400	-
215	4200	4.33	B	0	Clay	95.2	154	1150	253	478	448	1430
298	4200	4.37	3.81	23.8	Sandy Clay	91.5	132	1000	287	1024	370	1500
299	600	2.12	1.79	34.6	Sandy Clay	59.2	67	533	-	960	260	1600
278	600	2.17	B	0	Clay	51.0	44	548	>236	300	244	-
V-1 427	256	0.56	1.40	100	Sand	41.0	41	-	123	-	135	-
V-1 428	256	0.56	2.24	100	Sand	42.6	71	-	112	-	188	-
V-1 429	256	0.56	2.24	100	Sand	40.4	69	-	96	-	200	-

* Charge depth is to mid-point of charge unless the charge is on the bottom, as indicated by the letter "B".

1 Film records obtained from Waterways Experiment Station, Vicksburg, Miss.

5.2 Discussion of Results. It is difficult to isolate the effects of charge burial with the limited data available. One of the more obvious results is the increase in the amount and extent of radial throwout, which is illustrated in Fig. 5.1. Cratering tests at W.E.S. [9] have shown that crater dimensions increase when a charge is buried in the bottom, which indicates an increased throwout of bottom material.

The initial velocity of rise of the smoke crown (venting velocity) appears to increase with increasing burial of 4200-lb charges, and narrower smoke crowns are formed by buried 4200-lb charges than by bottom shots. However, the 256-lb charges showed the opposite trend when the explosions occurred below the bottom.

No significant effects on maximum column diameters can be observed, but the data show an increase in column height with increasing burial of the charge.

The jets formed by partially buried charges are broad and bushy, and generally similar in appearance to the jets produced by bottom shots in the same depths of water. Maximum jet heights show considerable scatter but are not significantly different. The development of the jets formed by a 4200-lb and a 600-lb partly buried charge is shown in Fig. 5.2.

The base surges formed by partially buried charges in the shallow depth range considered here are more tenuous and less clearly defined than the surges formed by charges placed on the bottom. Surge radial growth data for two on-bottom and three partially buried 4200-lb charges are presented in Fig. 5.3 and tend to show that smaller surge clouds are formed by the buried charges. This reduction in size is due to a reduced carbon content and also to the heavy radial throwout of rocks and bottom material, which disrupts the column and tends to interfere with base surge formation and

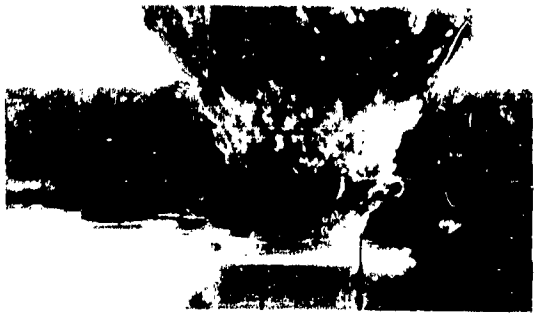

MITCHELL CAMERA 0.1 SEC

1.5 SEC

0.25 SEC

3.0 SEC

0.5 SEC

K-25 CAMERA 10.5 SEC

1.0 SEC

SHOT NO. 294
W = 4200 LB TNT
WATER DEPTH = 2.65 FT
CHARGE DEPTH = 2.51 FT
$\lambda_c = 0.156$ FT/LB$^{\frac{1}{3}}$

FIG. 5.1 COLUMN FORMATION AND RADIAL THROWOUT BY PARTIALLY BURIED CHARGE

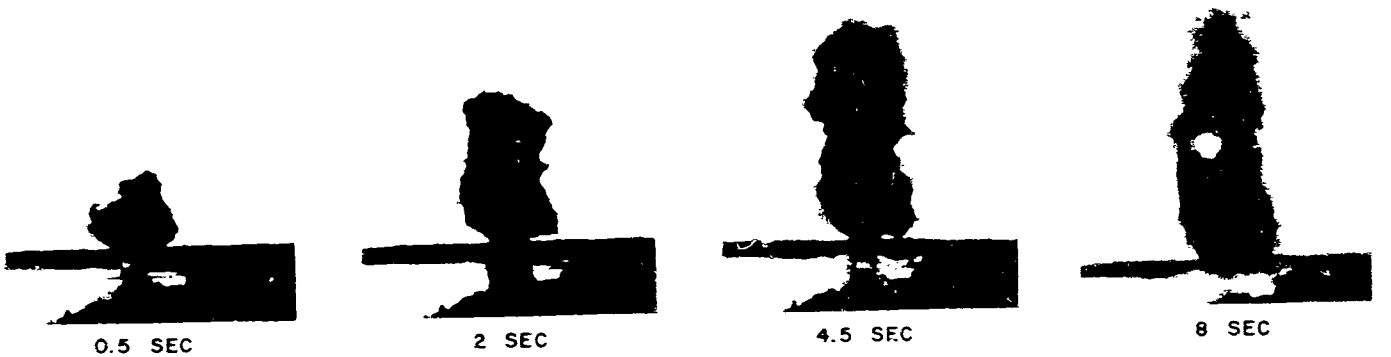

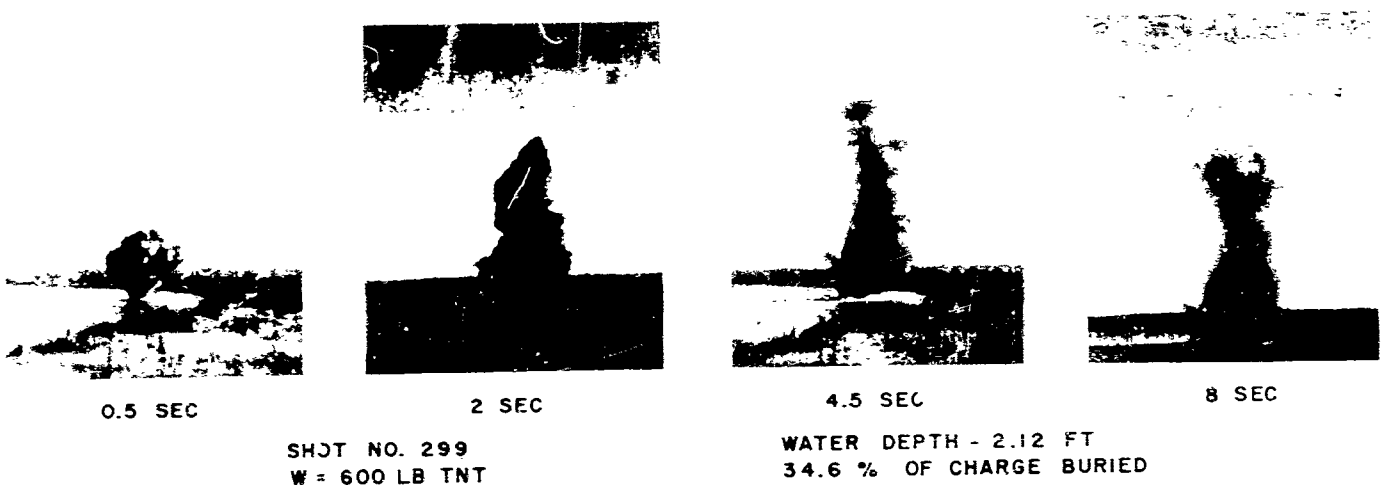

FIG. 5.2 JET FORMATION BY PARTIALLY BURIED CHARGES

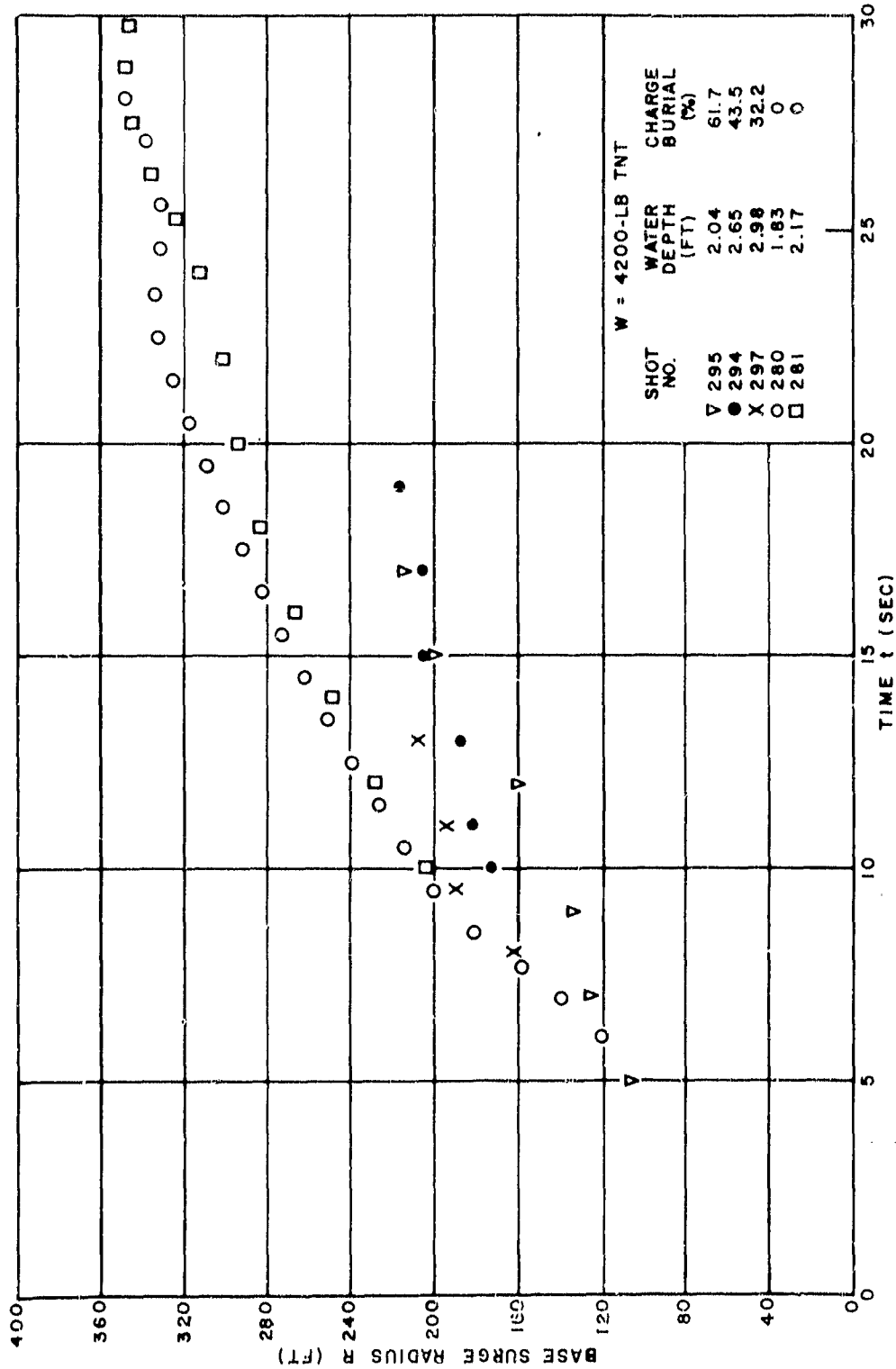

FIG. 5.3 SMOG SURGE RADIUS vs TIME
FOR ON-BOTTOM AND PARTIALLY BURIED CHARGES

growth. The tenuous nature and small extent of the smog surges resulting from Shots 295 and 297 (61.7 and 32.2 percent of charge buried, respectively) may be seen in Fig. 5.4.

Although the data in Chapter III show a tendency for base surges to decrease in size when charge depth is decreased, the trend does not continue into the smog range, due to the presence of smoke or other solids in the surge cloud. As large quantities of smoke would not be present in the surge formed by a shallow nuclear detonation, a base surge of relatively small extent would be expected.

The smaller surges formed by the partially buried TNT charges apparently contain little carbon, and probably constitute a better scaling of nuclear bursts than the smog surges formed by shallow bottom explosions. In this respect, scaling has been improved by charge burial. A quantitative check on this cannot be made until shallow water nuclear explosion data become available.

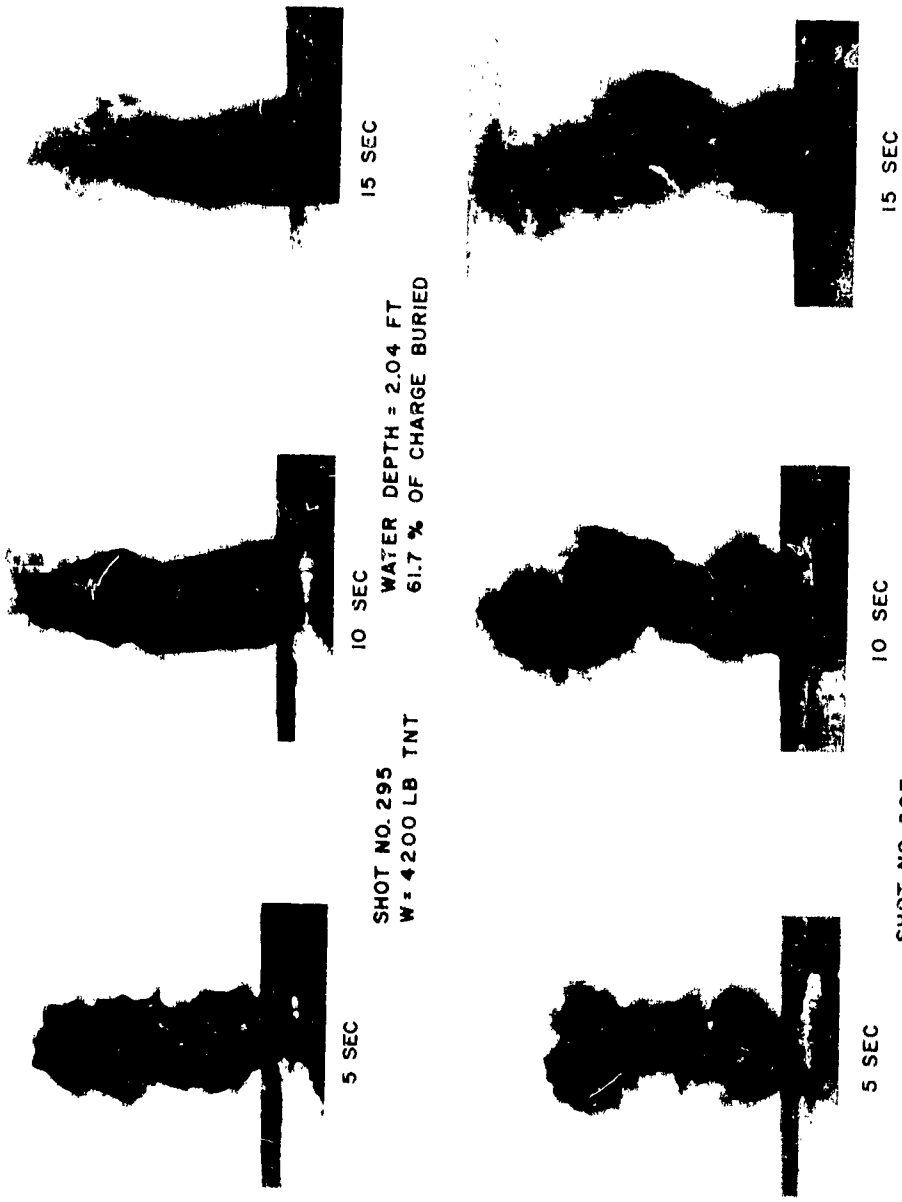

FIG. 5.4 BASE SURGE FORMATION BY PARTIALLY BURIED CHARGES

CHAPTER VI
THE GENERAL SCALING PROBLEM

6.1 Scatter of Data. The measurements of the surface phenomena presented here show considerable scatter, due to the impossibility of controlling all conditions in field experimentation and also to the difficulties of measuring the phenomena. The base surge in particular may be somewhat tenuous and irregular in shape and is easily distorted by winds and atmospheric turbulence. Fallout material from the smoke crown and jet and splashing due to the radial throwout of soil and rocks also tend to disrupt and obscure the base surge.

Although some subjective judgment enters into the measurement of records, all of the NOL data analysis was completed by one person, in order to maintain internal consistency. The criteria to be followed in obtaining the critical measurements were agreed upon in conferences among the project personnel and consultants, and intermittent checks by others were made.

An indication of the degree of dispersion of data is given in Table 6.1 which presents the results of two groups of 100-lb explosions, one group scaled geometrically to Test Baker and the other fired on the bottom in the Baker scaled water depth. The number of shots in each group is large enough so that the results may be treated with confidence.

TABLE 6.1

STATISTICAL DATA FOR 100-LB TNT CHARGES

	No. of Values (N)	Range	Arith. Mean ($\bar{X}$)	Standard Deviation (σ)	Coefficient of Variation (V)
A. Charge at Mid-depth in 2.5 ft of Water (λ_c = 0.26 ft/lb$^{1/3}$)					
D_{max} (ft)	13	27.3-37.0	30.9	2.93	9.5%
C_{max} (ft)	13	30.0-47.0	38.2	4.87	12.7%
R_{max} (ft)	7	50.0-113	70.5	20.9	29.6%
H_{max} (ft)	5	8.8-18.6	15.1	4.0	26.5%
B. Charge on Bottom in 2.5 ft of Water (λ_d = 0.54 ft/lb$^{1/3}$)					
D_{max} (ft)	24	27.8-40.4	33.4	3.50	10.5%
C_{max} (ft)	19	32.7-59.0	48.9	6.15	12.6%
R_{max} (ft)	17	35.2-120	77.8	23.1	29.7%
H_{max} (ft)	19	12.0-27.5	19.4	4.29	22.1%

Column diameters and heights are fairly reproducible but the base surge measurements show a high degree of scatter, for the reasons noted previously.

In many figures in this report, the arithmetic mean, the standard deviation of a single observation, and the standard deviation of the mean are indicated. The coefficients of variation obtained from the data used in the preparations of Figures 2.12, 2.14, and 2.18, which represent the Baker scaling, are presented in Table 6.2 to indicate the effect of charge weight on the degree of scatter. No value is given when fewer than 4 observations are available.

TABLE 6.2
COEFFICIENTS OF VARIATION OF DATA
FOR CHARGES SCALED TO TEST BAKER
($\lambda_c \cong 0.26$ ft/lb$^{1/3}$)

W	D_{max}	C_{max}	J_{max}
21-lb	(9) 11.1%	(8) 16.3%	(6) 5.08%
100-lb	(13) 9.5%	(13) 12.7%	-
4200-lb	(5) 2.59%	(5) 11.9%	(5) 9.82%
Mean	7.73%	13.6%	7.45%

( ) No. of shots

The degree of scatter of data for bottom shots is shown in Table 6.3. No value is given when fewer than 4 observations are available.

TABLE 6.3
COEFFICIENTS OF VARIATION OF DATA FOR BOTTOM EXPLOSIONS

W	D_{max}	$\bar{\lambda}_d$	C_{max}	$\bar{\lambda}_d$	J_{max}	$\bar{\lambda}_d$
21-lb	(11) 12.6%	0.28	(6) 7.20%	0.27	---	--
	(12) 8.51%	0.54	(10) 15.8%	0.54	---	--
	(9) 10.5%	1.59	----	--	---	--
100-lb	(7) 5.91%	0.27	(5) 15.3%	0.27	---	--
	(24) 10.5%	0.54	(19) 12.6%	0.54	---	--
	(5) 8.72%	1.46	----	--	---	--
600-lb	(5) 5.10%	0.29	(4) 21.4%	0.29	(5) 5.09%	0.29
	(6) 6.23%	0.59	(6) 11.0%	0.59	---	--
4200-lb	(5) 4.47%	0.27	(4) 15.6%	0.26	(4) 6.23%	0.26
	(4) 2.92%	0.54	(4) 14.2%	0.54	(4) 4.70%	0.54

( ) No. of shots

Tables 6.2 and 6.3 indicate a decreasing dispersion of data with increasing charge weight. This is due in part to the smaller number of tests with large charges, but probably indicates that a greater degree of confidence in the large charge results is in order. This is to be expected, because of the more extensive photographic coverage and the better definition and longer duration of the phenomena in the 600-lb and 4200-lb shots.

6.2 Scaling of Column and Jet. As the behavior of the base surge is related to the size and structure of the column and jet, it is important to consider the usefulness of D_{max}, C_{max}, and J_{max} as scaling parameters. In particular, the column diameter seems to be the most important indication of similarity between explosions of different charge weights fired at the same scaled depth*.

For charge weights ranging from 21 to 4200 lbs, the maximum column heights, column diameters and jet heights are all proportional to the cube root of the charge weight when shots are fired at the same scaled depth. However, the data show varying degrees of scatter. D_{max} is the most reproducible dimension, with a mean coefficient of variation of about 7.7% at the Baker geometry. Extrapolation of the high explosive results to a 20 kiloton charge yields a D_{max} value of 2310 ft. The observed value at Test Baker was 2030 ft, which is 12% less than this. However, 12% is less than twice the standard deviation, and the value falls within the range of scatter of the high explosive data.

Thus, the available evidence indicates that column diameters are a reliable scaling index for atomic weapons at mid-depth in shallow water. This is probably also true for bottom explosions in the shallow range of water depths. The usefulness of D_{max} for the scaling of surface bursts is somewhat uncertain.

---

* High speed motion pictures of the explosion of charges weighing 0.1 gram, fired in a tank at a depth scaled to Test Baker and similar depths, have shown that the inner wall of the column is continuous with the expanding gas bubble beneath it [2]. Thus, for shallow underwater explosions, scaling of maximum column diameter may indicate that maximum bubble size is also being scaled.

The Baker measurement of C_{max} (2000 ft) was 31% lower than would be predicted by extrapolation of high explosive data (2910 ft) and the observed overall height of the surface phenomena at Bikini (8000 ft) was 64% less than 22,500 ft, the value scaled from the TNT data. These are far beyond the observed range of scatter.

These heights do not scale from the high explosive tests in a simple manner, as the maximum column diameter does. That the Baker maximum column height is lower than would be predicted may well be due to a difference in behavior of the smoke crown, which could have obscured a greater proportion of the top of the Baker column. Since there was no central jet at the Baker test, it is not surprising that the over-all height was lower than would be predicted. In addition, the heights of the column and jet would not be expected to scale as a function of charge weight over a wide range of weights because the retarding effect of gravity becomes increasingly important when charge weight is increased. In addition, the effect of air resistance would not scale to charge weight simply.

A more detailed discussion of column and jet formation and the mechanisms involved will be presented in Reference [13].

6.3 Scaling of Base Surge. The base surge is formed by the collapse of the water column formed by underwater explosions. Consequently the rate of growth and maximum extent of the surge are dependent upon the maximum height and diameter attained by the column, as shown in Chapter III.

It has been assumed [1] that the base surge is simply a gravity dominated flow, in which the potential energy of the column is converted to the kinetic energy of the surge. If this is correct, the scaling of the surge can be characterized by the Froude number.

In a gravity flow of a fluid beneath an ambient fluid

of lesser density, such as the flow of the base surge through the atmosphere, the Froude number is defined as:

$$F = \frac{V^2}{g\left(\frac{\rho-\rho_o}{\rho}\right) L} \tag{36}$$

where V = radial velocity of surge
g = acceleration due to gravity
ρ = density of surge
ρ_o = density of atmosphere
L = a characteristic length

In base surge studies, the maximum column diameter, D_{max}, is used as the characteristic length for scaling purposes and equation (36) becomes:

$$F = \frac{V^2}{g\,\sigma\,D_{max}} \tag{37}$$

where

$$\sigma = \frac{\rho-\rho_o}{\rho} \tag{38}$$

In order to plot a dimensionless radius-time curve for base surge propagation with Froude parameters, the instantaneous radius, R, is reduced by the characteristic length, D_{max}, giving:

$$r = R/D_{max} \tag{39}$$

Since g is unchanged in the experiments, it can be omitted. If the assumption is made that σ also remains unchanged, a simple expression for scaled time, τ, can be derived:

$$\tau = t/D^{1/2} \qquad (40)$$

The derivation of these terms and others used in the scaling of the base surges from high explosives and liquid models has been presented in Reference [3] and is shown in a different form in Appendix C.

It was shown in Chapter III that increasing the depth of firing of high explosives results in the formation of larger and faster growing surges. Plotting the data from a group of 4200-lb and 600-lb shots fired at different depths in the form of r vs τ, as shown in Fig. 6.1, gives a group of curves with the same general slope, indicating that the scaling technique is valid for reducing the data from explosions of different charge weights and depths.

The reduced radius-time data from explosions of different weights scaled to Test Baker is presented in Fig. 6.2. The effectiveness of the scaling procedure is demonstrated here also and it should be noted that the mean trend of the data points is the same as in Fig. 6.1, where various charge depths were used.

It is evident that the base surges from high explosives fired underwater at greater than smog depths can be scaled effectively by the use of simple Froude parameters. In both figures, the Test Baker measurements are indicated in the form of a smooth curve, reduced in the same manner. The Baker data were obtained from measurements reported by Isaacs, Wiegel and Chinn [14] and by Roger Revelle [15] and are presented in Appendix D.

The TNT data show good agreement with the Baker result to a τ of about 1.5 sec/ft$^{1/2}$ but indicate a continued growth at about the same rate while the Baker curve tends to level off.

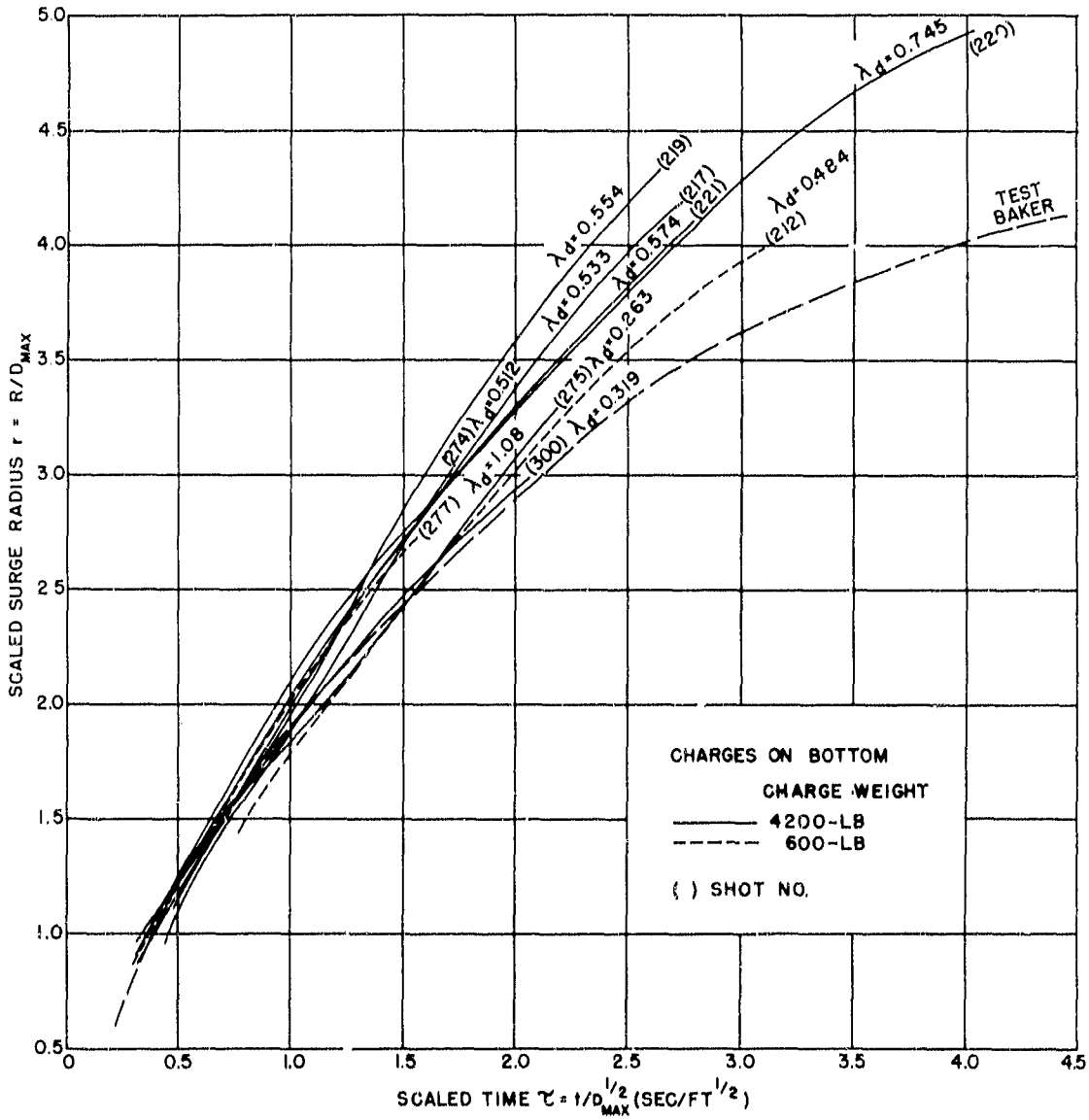

FIG. 6.1 SCALED SURGE RADIUS vs SCALED TIME (CHARGES ON BOTTOM)

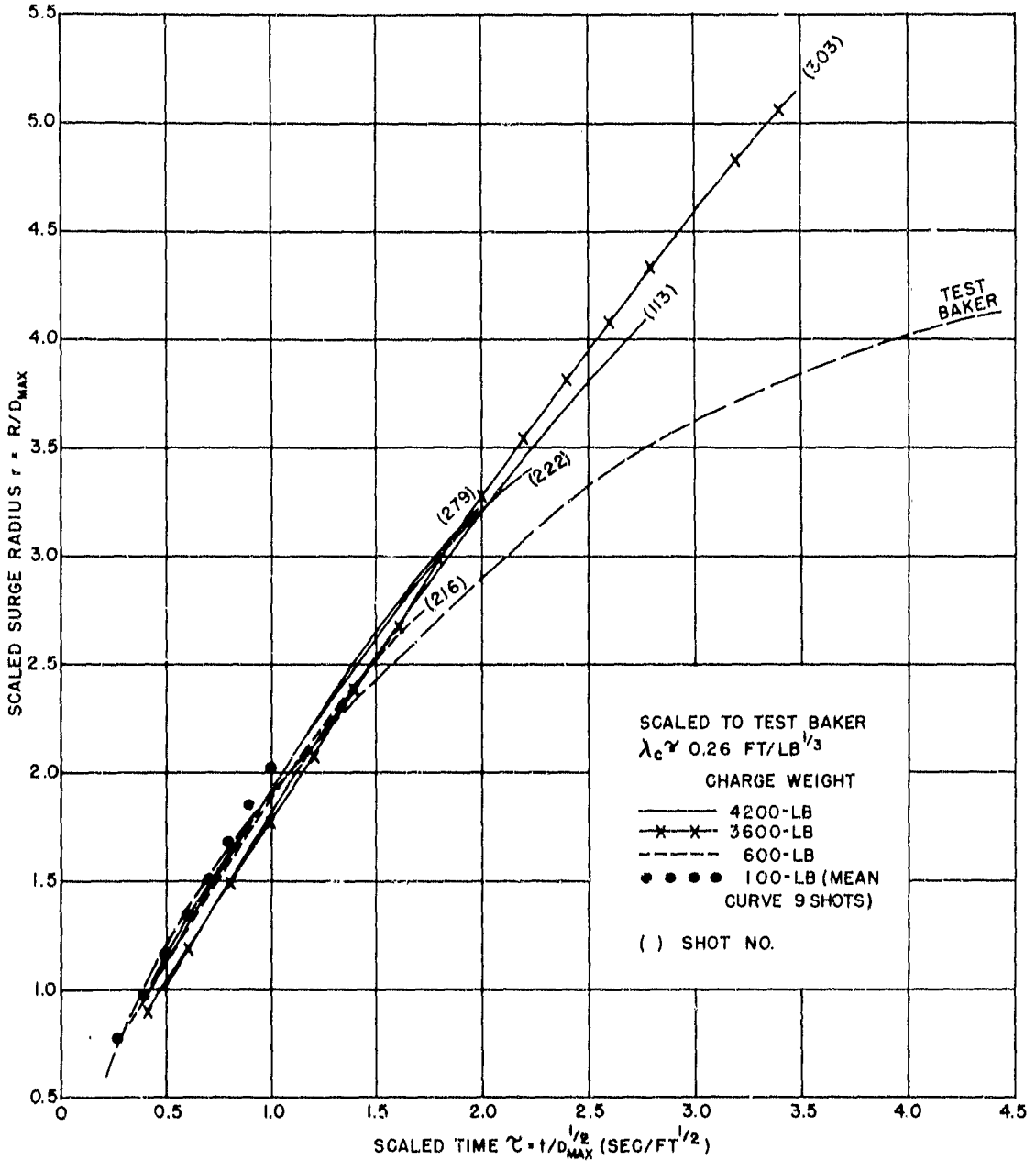

FIG. 6.2 SCALED SURGE RADIUS vs SCALED TIME (CHARGES SCALED TO TEST BAKER)

Figure 6.2 indicates the increasing length of the r vs τ curves when charge weight is increased. The relatively short curves for the 100-lb explosions are within the area of good agreement with the nuclear test and the experimenter is misled into believing that the Test Baker base surge can be scaled effectively with high explosive models. The 600-lb and 4200-lb results indicate a major deviation of surge behavior from the Test Baker curve, which was not shown by smaller charges. This example serves to indicate the possible danger of attempting to duplicate large-scale tests with small explosions, or attempting to extrapolate all of the effects of charges of a limited weight range to large-scale experiments.

The implication of this result is that the initial driving effects are similar in the high explosive shots and in Test Baker. Physically, this means that the water columns formed by the two types of explosions can be considered to be geometrically similar. However, the central jet formed by high explosives was not observed at Baker and the overall height of Baker was only about 1/3 as great as would be expected from an extrapolation of TNT results.

At Bikini, the water column subsided to form the base surge, which flowed outward radially to a maximum extent of about 8400 ft. No further growth was recorded, though it is possible that a very slow expansion continued. Large masses of material fell into the surge from the cauliflower cloud, mostly within a ring extending from about 1500 ft to 4500 ft from the zero point.

In the high explosive experiments it has been observed that the water column collapses to form the primary base surge. This initial flow is similar to the Baker surge and is represented in scaled form by the r vs τ curves to a τ of about 1.5 sec/ft$^{1/2}$. However, the jet and part of the smoke

crown then fall into the center. The heavier water masses drop back into the underlying water surface but material which has been broken into fine droplets and particles flows outward along the surface, similarly to the primary surge. This aerosol provides additional impetus to the surge flow, causing it to continue at a fast rate well beyond $\tau = 1.5$ until the cloud has dissipated.

The vertical growth of the base surge from high explosives can also be scaled effectively by the use of Froude scaling methods. As the upper surface of the surge is irregular and the growth is not continuous, there is considerable scatter in the results. In addition, the upper surface is more subject to atmospheric mixing than the leading edge of the surge.

Surge height can be reduced in the same manner as surge radius, thus:

$$h = H/D_{max} \tag{41}$$

and the data plotted as a function of τ, as shown in Fig. 6.3.

The high explosive data scatter widely and do not show any systematic weight or depth effects. They do not show good agreement with the Baker result, but scaling can be improved by introducing column height into the Froude parameters in the following manner:

$$h' = H/(C_{max} D_{max})^{1/2} \tag{42}$$

$$\tau' = t C_{max}^{1/2}/D_{max} \tag{43}$$

Presenting the data in this fashion (Fig. 6.4) yields fairly good agreement between TNT and nuclear results. However, the physical behavior of the model and prototype surges is considerably different. The high explosive surges

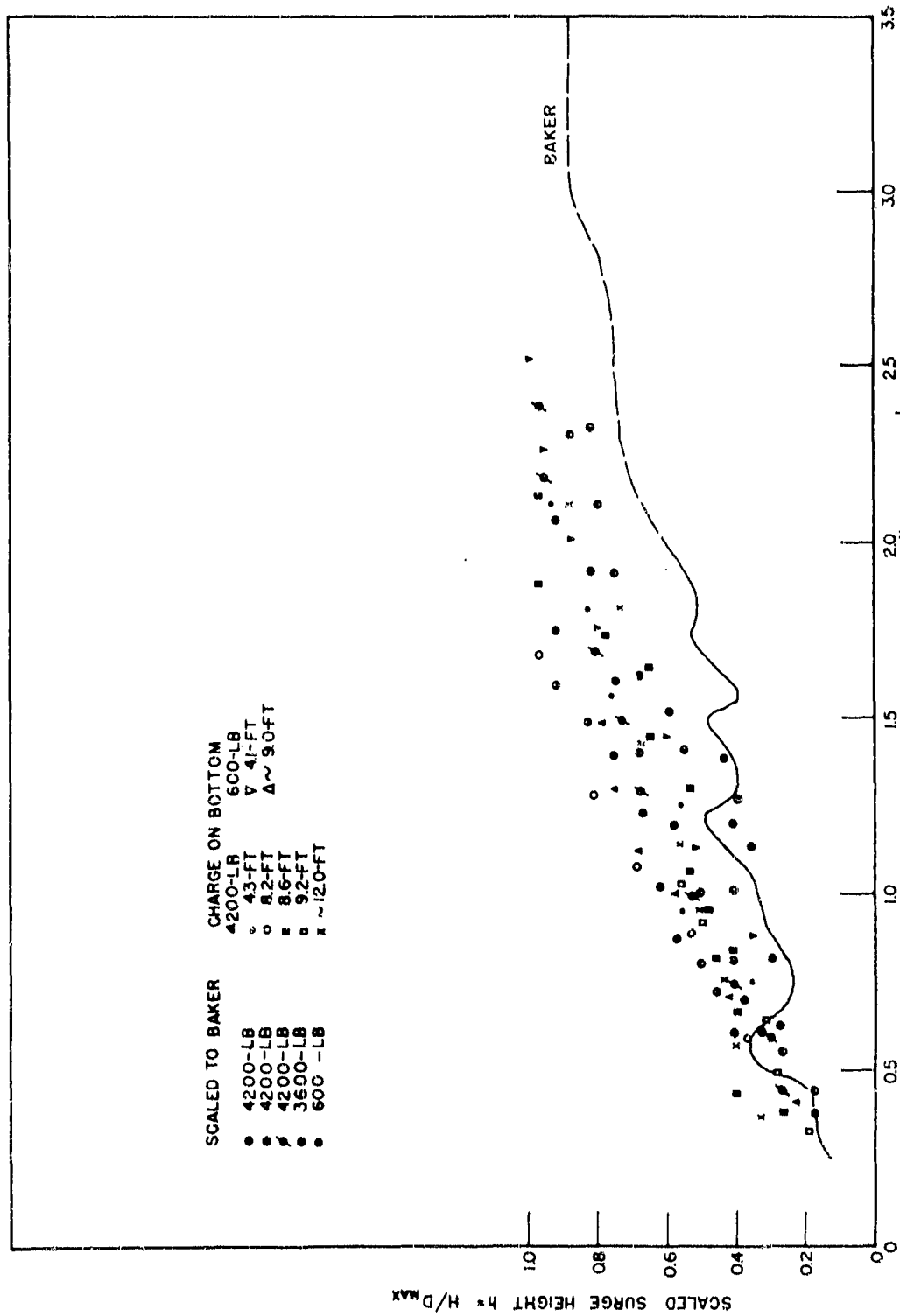

FIG. 6.3 SCALED SURGE HEIGHT vs SCALED TIME

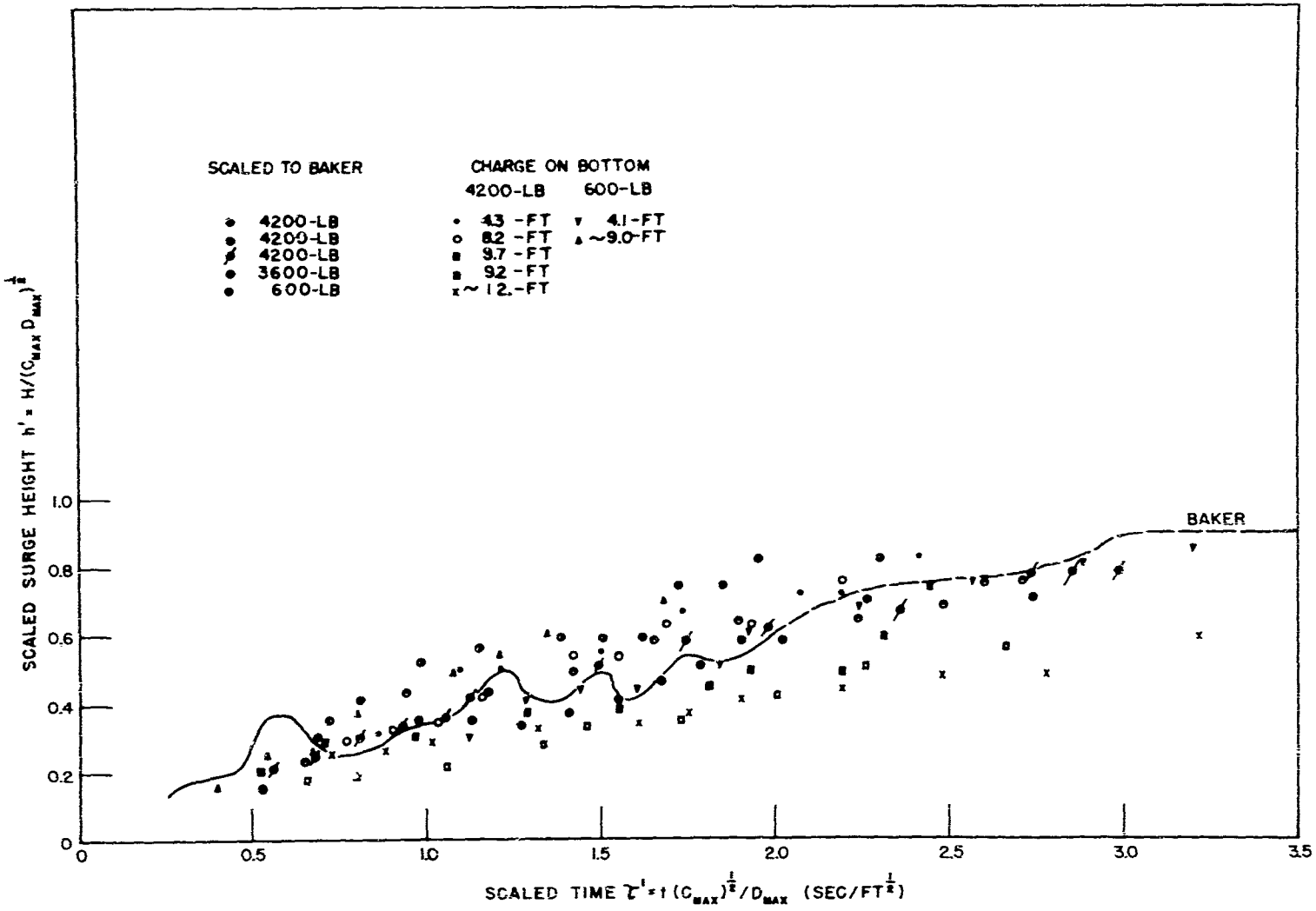

FIG. 6.4 SCALED SURGE HEIGHT vs SCALED TIME
(EFFECT OF COLUMN HEIGHT INCLUDED)

rise and become increasingly tenuous until mixing and evaporation are complete. The Baker surge did not appear to evaporate at its upper surface, but showed evidence of the condensation of water vapor within the surge cloud as the surge top rose above 1200 ft. When the upper surface rose above 1500 ft, a new cloud deck formed above the surge in the ambient air that had been lifted from the surface. Thus, any measurements of the height of the Test Baker surge made above the 1200 ft level were affected by the ambient meteorological conditions and comparison of these with high explosive results is not valid.

Smog surges formed by bottom explosions in very shallow water can also be scaled in the form of r vs τ, as shown in Fig. 6.5. These data show a greater degree of scatter than the data from shots fired in deeper water but have the same general slope. The scaled height vs scaled time data (Fig. 6.6) show the exceptional vertical growth of smog surges due to the carbon content, which remains visible after the water droplets in the surge have evaporated.

The scaled radial growth of the surges from four partially buried charges are compared with the Baker scaled growth in Fig. 6.7. The data show a tendency toward slower surge growth with increased charge burial, which is probably due in part to a decreased smoke content, as indicated in Sec. 5.2.

6.4 Scaling of Surface Shots. Measurements of the radial growth of the base surges formed by 100-lb charges fired at shallow positions on or near the water surface are shown in Fig. 6.8, reduced in the form of r vs τ. The records are exceptionally long for charges of this size, due to the smog nature of the surge clouds. When scaled in this manner, the growth curves for explosions in water from 2 to 5 ft deep show a similarity in slope to the Test Baker curve. The

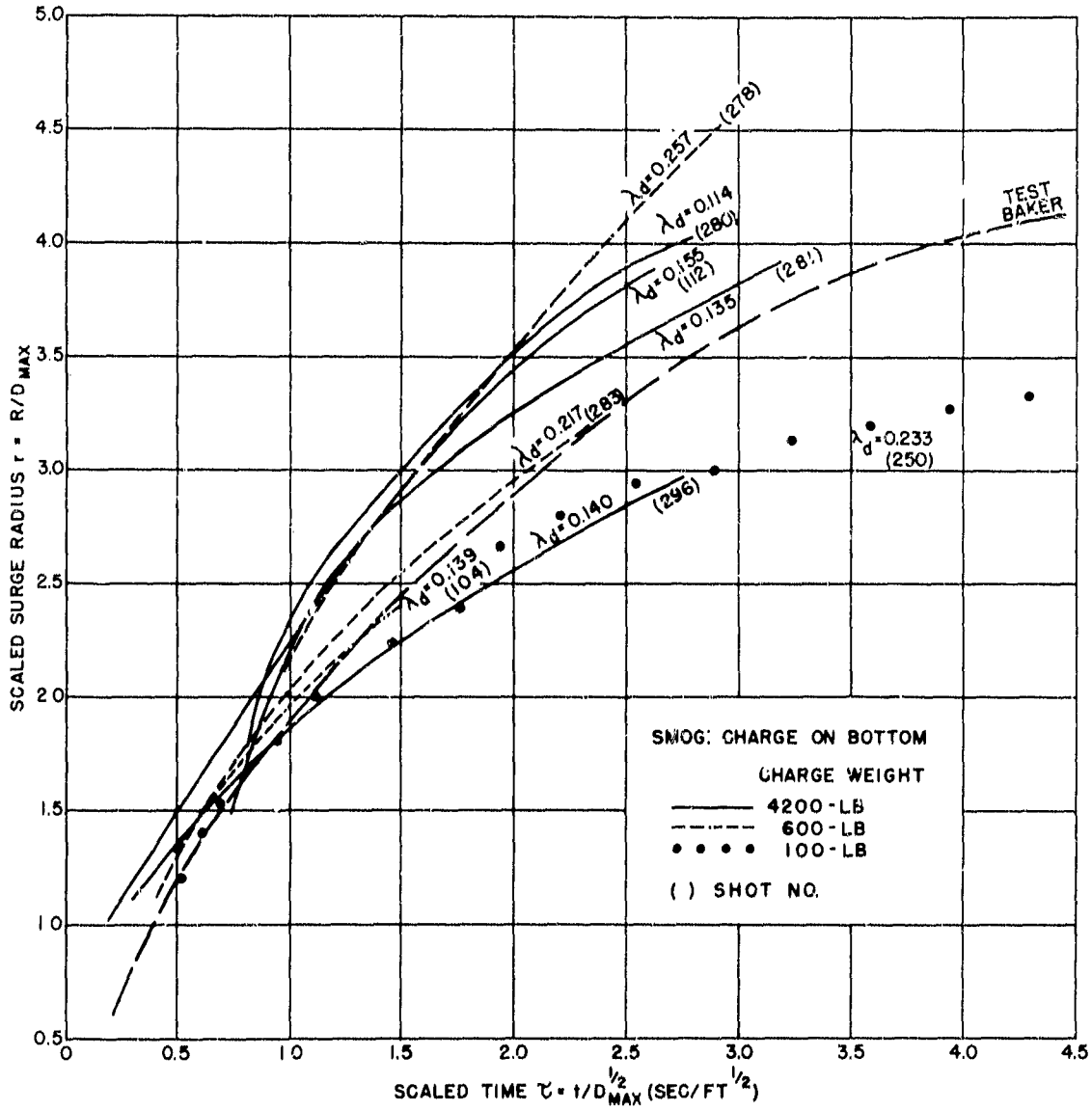

FIG. 6.5 SCALED SMOG SURGE RADIUS vs SCALED TIME
(CHARGES ON BOTTOM IN VERY SHALLOW WATER)

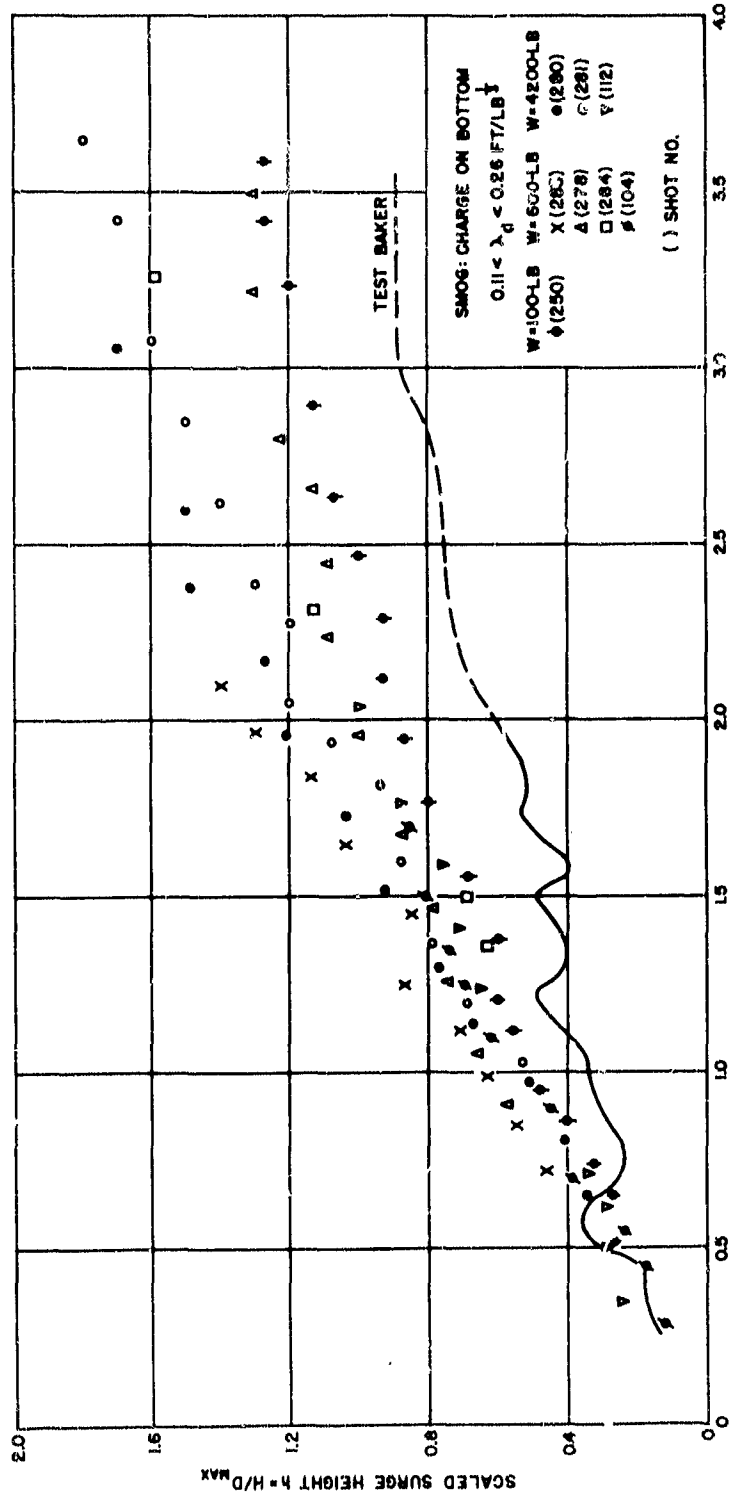

FIG. 6.6 SCALED SMOG SURGE HEIGHT
VS
SCALED TIME
(CHARGES ON BOTTOM IN VERY SHALLOW WATER)

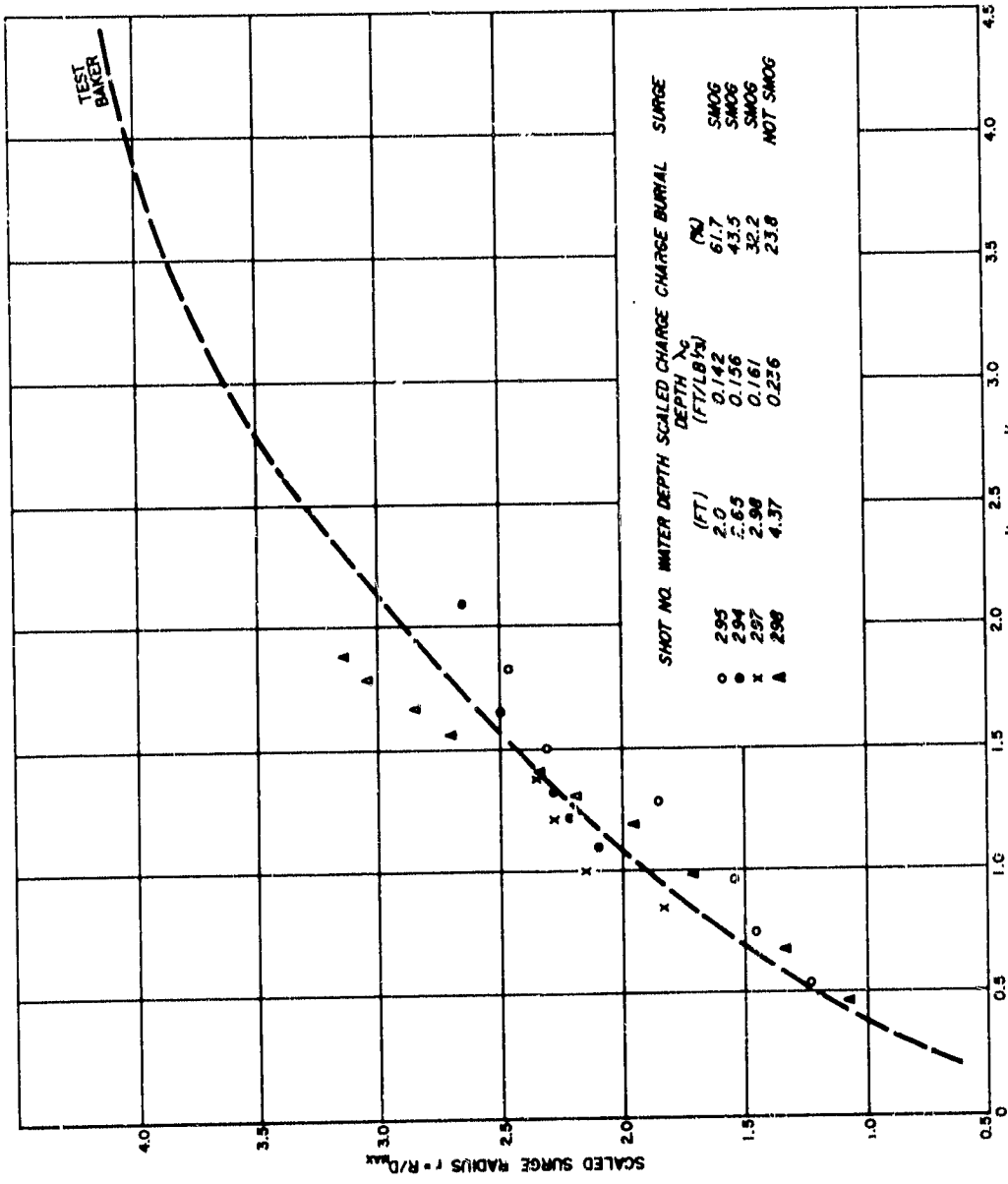

FIG. 6.7 SCALED SURGE RADIUS vs SCALED TIME
(PARTIALLY BURIED 4200-LB CHARGES)

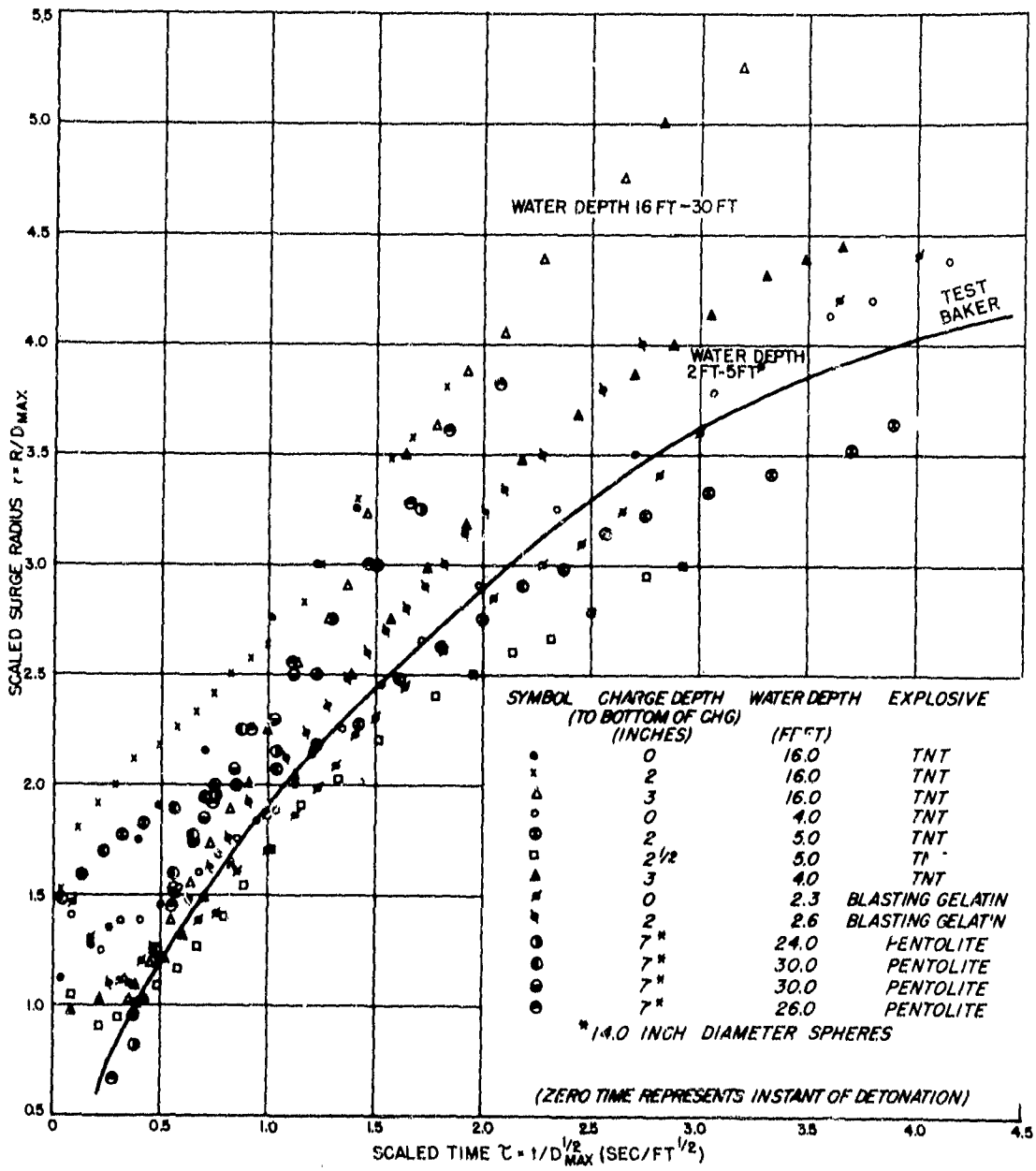

FIG. 6.8 SCALED SMOG SURGE RADIUS vs SCALED TIME (100-LB SURFACE SHOTS)

scaled surge growth curves for smog explosions in water 16 to 30 ft deep indicate a more rapid radial expansion, similar to that shown by deeper explosions that are not smog-forming.

The agreement between the data for explosions in shallower water and the scaled Baker curve does not imply a satisfactory scaling of the Baker condition, since there are many physical differences between both the initial conditions and the surface phenomena at the different scales. The scaling of surface bursts will be discussed in Sec. 7.2.

CHAPTER VII
THE PREDICTION OF LARGE SCALE EFFECTS

7.1 The Underwater Burst. The data presented in this report have been obtained from explosions in relatively shallow water. Scale-wise, the firing conditions would correspond to the employment of atomic weapons in harbors and in coastal areas over the continental shelf.

Before an extrapolation of high explosive results to nuclear weapons can be made, further consideration of the scaling of explosions in general is necessary. It is known that an explosion in deep water forms a spherical bubble of gases which expands to a maximum size and then contracts to a minimum. The bubble continues to oscillate radially while rising to the surface where the explosion gases are vented to the atmosphere. (At great firing depths, the bubble loses its identity before reaching the surface.) The plume phenomena appearing at the surface depend upon the phase of oscillation of the bubble at the time of break-through [16].

The maximum radius attained by an underwater TNT explosion bubble depends upon charge weight and total hydrostatic pressure in the following way:

$$A_{max} = 12.6 \left(\frac{W}{c + 33} \right)^{1/3} \qquad (44)$$

Venting depth may be defined as the depth at which the gas globe would just break the surface at its maximum size. It is therefore convenient to define shallow underwater explosions as those occurring at less than the venting depth ($c < A_{max}$). In these cases, the globe of gaseous explosion products vents during its initial expansion and no further oscillation occurs.

Venting depth is not a simple function of λ_c. For very small charges it is roughly proportional to $W^{1/3}$, but for large-scale explosions venting depth is approximately proportional to $W^{1/4}$. Therefore venting during the first bubble expansion occurs at decreasing values of λ_c as charge weight is increased. For example: a 100-lb charge will vent during the initial bubble expansion at a scaled depth as great as 3.48 ft/lb$^{1/3}$, but venting depth for a 20 kiloton charge is reached at a λ_c of 1.55 ft/lb$^{1/3}$.

The size and behavior of the column, jet, and base surge are dependent upon the dynamics of the expanding gases and, generally speaking, may be classed as bubble phenomena. These surface phenomena may be scaled in terms of charge depth and the cube root of the charge weight only within the shallow depth range considered in this report.

For explosions in deep water, geometrical scaling (in terms of λ_c) is not valid for the study of bubble phenomena and the resulting surface effects.

In the tests reported here the water columns formed by high explosives fired within the scaled depth range of $0.2 < \lambda_d < 2.2$ ft/lb$^{1/3}$ appear during the initial expansion of the explosion gases. As it is not reasonable to expect that the formulas obtained are applicable beyond venting depth, the range of applicability will be relatively smaller for atomic weapons than for high explosives. This range is shown as a function of charge weight in Fig. 7.1. The assumption has been made that the shallow depth limit of $\lambda_d = 0.2$ ft/lb$^{1/3}$ obtained with high explosives fired on the bottom is valid for the prediction of column diameters formed by atomic weapons.

It has been noted in Sec. 6.2 that the observed Baker maximum column diameter (2030 ft) falls within the range of scatter of high explosive results. However, this is based

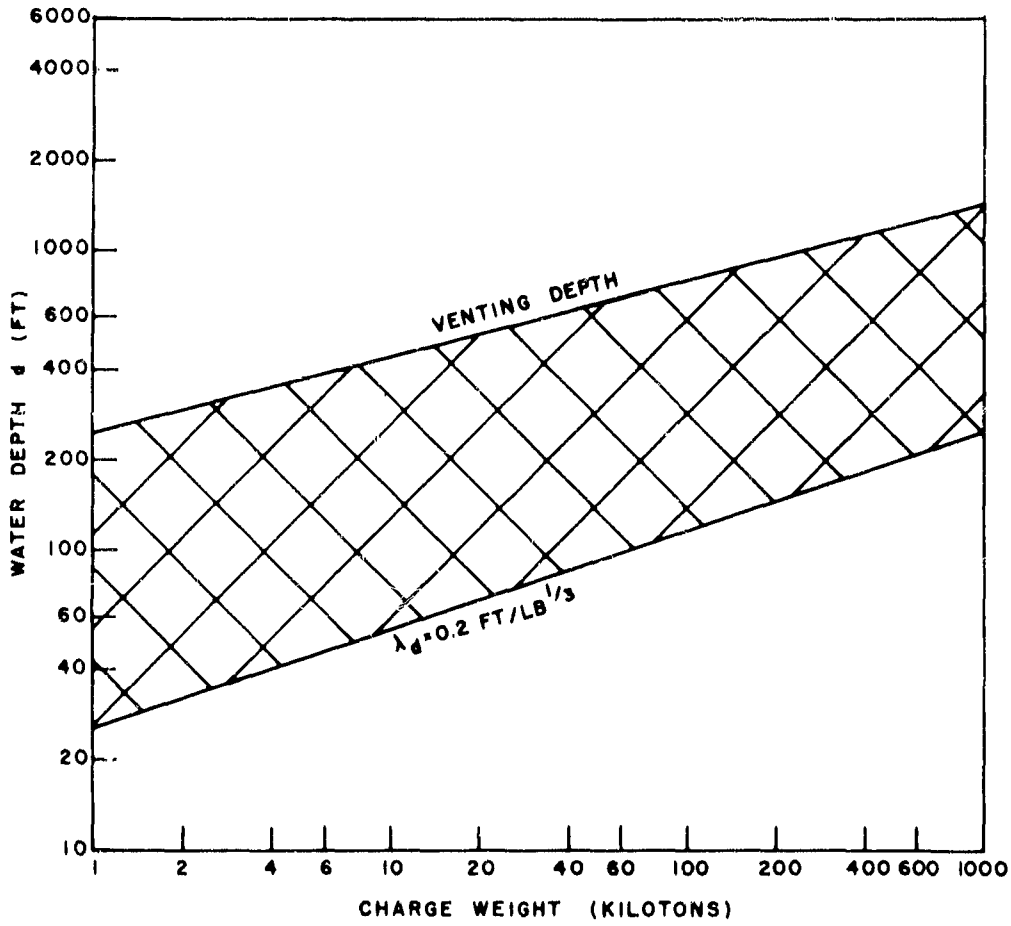

FIG. 7.1 RANGE OF APPLICABILITY OF HIGH EXPLOSIVE FORMULAS USED FOR THE PREDICTION OF ATOMIC WEAPON EFFECTS

on a nominal yield of 20 kilotons. As the estimates of the Baker yield are not irrefutable, a corrected yield might place the column diameter beyond the range of scatter. Therefore, it seems more realistic to attribute the apparently low value of the Baker column diameter to a difference in the energy partition of high explosives and atomic weapons.

Formula (7) indicates that a TNT charge weighing about 13.6 kilotons would produce a column 2030 ft in diameter when fired at a depth scaled linearly to the Test Baker condition. The cube root of this charge weight in pounds is 301. In order to predict column diameters for underwater nuclear explosions as accurately as possible it is necessary to multiply formulas (7) and (11) by a correction factor of $\frac{301}{W_B^{1/3}}$, where W_B is equal to the total energy release of the Baker weapon, expressed as the equivalent weight of TNT in lbs. The resulting equations are:

$$D_{max} = 6.75\ W^{1/3} \left(\frac{301}{W_B^{1/3}} \right) \tag{45}$$

and

$$D_{max} = 8.01\ W^{1/3}\ \lambda_d^{0.166} \left(\frac{301}{W_B^{1/3}} \right) \tag{46}$$

Equation (45) can also be expressed as:

$$D_{max} = 2030 \left(\frac{W}{W_B} \right)^{1/3} \tag{47}$$

where D_{max} is in ft and W is in lbs (TNT).

By observing the limitations in Fig. 7.1 it is possible to predict maximum column diameters for explosions scaled to Test Baker and for bottom explosions over a considerable range of depths through the use of formulas (45) and (46). Explosions off the bottom would be expected to form somewhat smaller columns than bottom shots, though the exact relationship is not known. For practical purposes, it is probably sufficiently accurate to use formula (46) for explosions off the bottom, but deeper than $\lambda_c = 0.2$ ft/lb$^{1/3}$.

When the predicted D_{max} has been obtained, the values of D_{max} and $D_{max}^{1/2}$ can be inserted into the Froude parameters (r and τ) used in the scaling of the flow of the base surge and a predicted radius-time curve for surge growth will be obtained.

It was shown in Section 6.3 that Froude scaling is effective for comparing the radial growth of the base surges from high explosives and the Baker test to a τ of about 1.5 sec/ft$^{1/2}$. Subsequently, the surges formed in the high explosive tests grow at a greater rate. However, as the scaling method is effective for reducing all of the TNT results to a single curve, it is probably also reasonable to assume that the Baker scaled curve is typical of nuclear results in relatively shallow water and can be used to predict surge growth for underwater bursts over the range of depths given in Fig. 7.1.

The smoothed values of r and τ obtained from the Test Baker scaled curve are given in Table 7.1. Formulas (39) and (40) can be expressed in the following way:

$$R = r D_{max} \tag{48}$$

$$t = \tau D_{max}^{1/2} \tag{49}$$

TABLE 7.1
SCALED BASE SURGE DATA FOR TEST BAKER - SMOOTHED VALUES

Scaled Radius r (dimensionless)	Scaled Time τ (sec/ft$^{1/2}$)
0.60	0.22
0.80	0.30
1.00	0.40
1.25	0.53
1.50	0.70
1.75	0.89
2.00	1.09
2.25	1.31
2.50	1.57
2.75	1.84
3.00	2.14
3.25	2.44
3.50	2.80
3.75	3.24
4.00	3.90
4.13	4.43

To predict the radial growth and maximum extent of a nuclear base surge the predicted values of D_{max} and $D_{max}^{1/2}$ are inserted into formulas (48) and (49) and then multiplied by the individual values of r and τ listed in Table 7.1. The result is a list of data points in ft and seconds. Examples of predicted curves obtained in this manner are given in Fig. 7.2.

The Baker data indicate that the following relation between maximum surge radius and maximum column diameter is applicable to underwater nuclear bursts scaled to the Baker

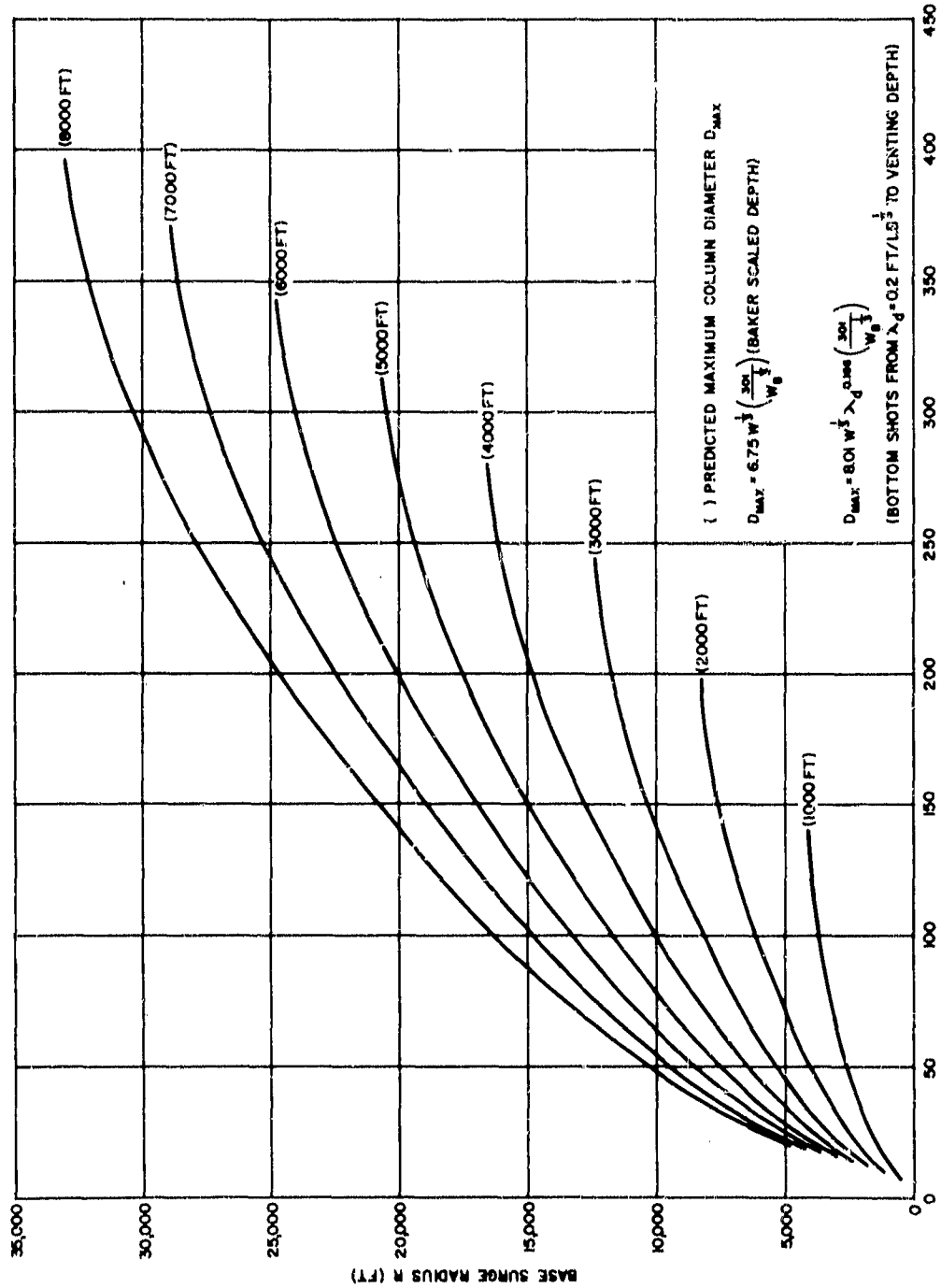

FIG. 7.2 PREDICTED RADIAL GROWTH OF BASE SURGES FROM ATOMIC WEAPONS

geometry:

$$R_{max} = 4.13\ D_{max} \qquad (50)$$

The base surge behavior subsequent to the time of R_{max} is dependent upon ambient meteorological conditions. An analysis of these effects will be given in Reference [13].

It was shown in Sections 6.3 and 6.4 that a base surge that propagates similarly to the Test Baker surge on the basis of Froude scaling, is formed by some smog shots on the bottom or surface of the water when the water depth is shallow. The reasons for this are not clear, but the result is probably due to the formation of a wide jet by these explosions. The column evidently does not converge rapidly to form a narrow liquid jet, and thus behaves somewhat similarly to the hollow Baker column. Another reason for the relatively slow surge growth is the smaller amount of material ejected into the air by the shallow explosions. However, there are many physical differences between the smog surface phenomena and the Baker phenomena and the agreement of the scaled surge propagation curves does not indicate successful scaling of Test Baker.

7.2 The Surface Burst. The scaling with high explosives of the surface phenomena of nuclear bursts at the surface of the water is questionable, because the thermal effects of the fireball can not be reproduced. However, there may be qualitative similarities in effects, though the horizontal and vertical extent of the clouds from nuclear surface shots are not predictable by a simple extrapolation of high explosive results.

Small scale experiments indicate that the expanding gases from a surface explosion form a hemispherical depression in the water, and that a column of water is ejected into the air

from the edge of the water cavity. This column tends to be smaller than the column formed by an underwater burst in the same depth of water. It was shown in Chapter IV that surface TNT explosions form base surges that contain large percentages of carbon. Due to the carbon content, the surge growth can be measured for a long period of time.

By analogy with high explosive results it might be expected that an atomic bomb exploded at the water surface would produce a relatively small but highly contaminated base surge. It also seems probable that the rate of growth and maximum extent of the surge would increase with increasing depth of water beneath the charge.

At present, the only known example of a burst close to the surface is the British atomic test in the Monte Bello islands on 3 October 1952. The object of the test was to investigate the effects of an atomic explosion in a harbor (17) and the bomb was detonated inside a frigate. The water depth is not known at this time, but the water in the Monte Bello area is generally shallow [18].

Photographs released to the press are reproduced in Fig. 7.3 and show a small surge formation. A small surge development was also observed on the film "Operation Hurricane", which was released for public showing.

It was stated that the cloud at Monte Bello reached a height greater than 2 miles. It is highly significant that the base of the cloud remained at the water surface and the entire cloud did not rise to high altitudes. In this respect the phenomena differ in behavior from the clouds formed by atomic bursts on dry land.

7.3 Conclusions. The results obtained with high explosive charges weighing up to 4200 lbs indicate that the formation and initial propagation of the Test Baker base surge can be scaled adequately with such relatively small charges. However,

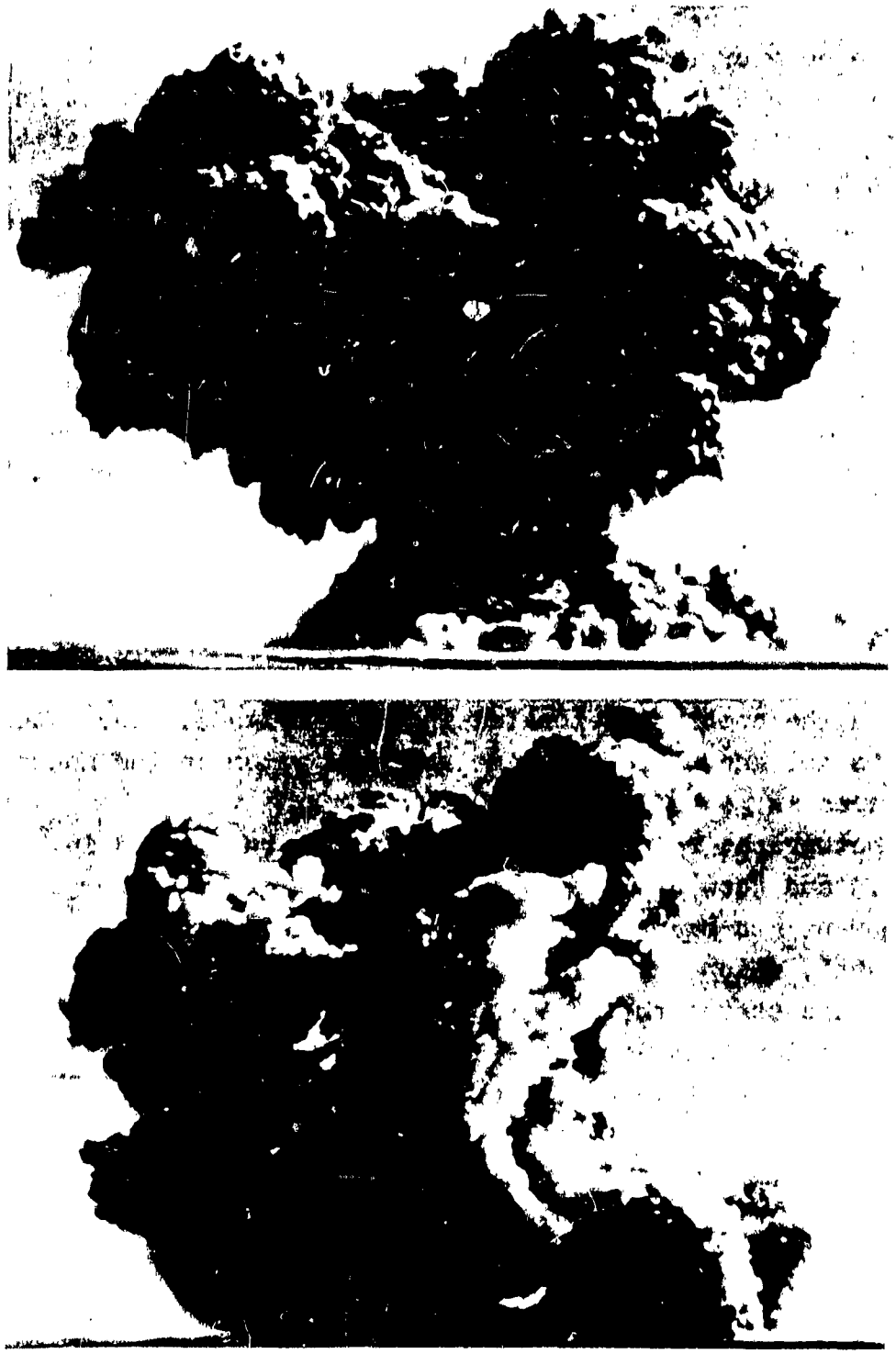

FIG. 7.3 PHOTOGRAPHS OF BRITISH ATOMIC TEST IN MONTE BELLO ISLANDS
(OCTOBER, 1952)

the subsequent growth and dissipation of the Baker surge cloud can not be reproduced on a small scale. This is due in part to the formation by high explosives of a central jet, which collapses and feeds additional material into the surge, and also to large scale meteorological factors which were important at Bikini, but which do not influence the surface phenomena from small charges.

The study of the surface effects of high explosives has resulted in the accumulation of considerable information about the dynamics of column development and base surge formation and growth, and has made possible the prediction of the surface phenomena from full-scale weapons in relatively shallow water. However, because of the inherent differences between the nuclear and high explosive phenomena, there is some uncertainty in the scaling method. In particular, the value of high explosive models for the scaling of contamination patterns is questionable because of differences in base surge behavior.

Test Baker is the only underwater nuclear test that has been conducted and all predictions of the effects of underwater bursts are based upon the Baker data, combined with theory and the results of high explosive tests. Although the photographic coverage at Operation CROSSROADS was excellent, the data concerning contamination by radioactivity in the Baker base surge are inadequate and controversial.

It is considered highly desirable to obtain more information from shallow underwater nuclear bursts in order to fully understand the role of the base surge as a carrier of contamination and to extend the range of conditions so that predictions of the surface phenomena of atomic weapons may be more firmly established.

BIBLIOGRAPHY

[1] A. B. Arons: "Experimental Investigations of Base Surge Phenomena". Interim Report No. 1 of NOL Project 152, NAVORD Report 1501, 13 July 1950, Confidential.

[2] J. S. Coles and G. A. Young: "Investigations of Base Surge Phenomena by Means of High Explosives and a Liquid Model". Interim Report No. 2 of NOL Project 152, NAVORD Report 1744, 1 Sept. 1950, Confidential.

[3] A. B. Arons, G. A. Young and Mary L. Milligan: "Further Investigation of the Base Surge". Interim Report No. 3 of NOL Project 152, NAVORD Report 2144, 1 June 1951, Confidential.

[4] G. A. Young: "Base Surge Analysis - HE Tests". Operation JANGLE Project 1(9)-4, NOLR 1169, May 1952, Confidential.

[5] G. A. Young and M. L. Milligan: "Base Surge Analysis for Nuclear Tests". Operation JANGLE Project 1(9)b, NOLR 1170, June 1952, Secret.

[6] C. R. Niffenegger: "Airblast Peak Pressures Along the Water Surface from Shallow Underwater Explosions". Interim Report No. 7 of NOL Project 152, NAVORD Report 2571, AFSWP-262, 1 August 1952, Confidential.

[7] G. A. Young: "Crater Formation by Shallow Underwater Explosions at Dahlgren, Virginia". Interim Report No. 8 of NOL Project 152, NAVORD Report 2891, AFSWP-263, 1 July 1953, Confidential.

[8] J. H. Rosenbaum and H. G. Snay: "The Formation of a Water Column by an Explosion in Very Shallow Water". Interim Report No. 4 of NOL Project 152, NAVORD Report 2436, 1 July 1952, Unclassified.

[9] "Effects of Explosions in Shallow Water", Report Nos. 1 to 9, Corps of Engineers, U. S. Army, Waterways Experiment Station, Vicksburg, Miss.. Dec. 1951 to Sept. 1953, Confidential.

[10] J. W. Johnson: "Model Studies of Explosions in Shallow Water". Joint Task Force One, Oceanographic Section, 15 June 1946, Confidential.

BIBLIOGRAPHY

[11] J. W. Johnson and A. J. Chinn: "Summary Report on Experiments on Underwater Explosion under Controlled Conditions, Part II - Plume Characteristics". University of California, Institute of Engineering Research, Dec. 1951, Confidential.

[12] H. Kolsky, M. T. Sampson, C. I. Snow and A. C. Shearman: "Splashes from Underwater Explosions, Part I Shallow Charges". Imperial Chemical Industries Limited, Undex 118, 1 Dec. 1944, Confidential.

[13] G. A. Young: "The Physics of the Base Surge". Interim Report No. 1 of NOL Project 152, NAVORD Report 2988, in preparation, Confidential.

[14] J. D. Isaacs, R. L. Wiegal, A. J. Chinn: "Photogrammetry of Test Baker. Report No. 3. Measurements of the Explosion". Dept. of Engineering, University of California. Waves Investigation Project. BuShips Contract Nobs 2490, 2 Aug. 1948, Confidential.

[15] Roger Revelle: "Characteristics of the Base Surge". Typescript, AFSWP File, Confidential.

[16] Robert H. Cole: "Underwater Explosions". Princeton University Press, 1948, Unclassified.

[17] "The Royal Navy's Part in British Atomic Test". U. S. Naval Institute Proceedings, Feb. 1953, pp 194-199, Unclassified.

[18] U. S. Navy Hydrographic Office, Chart No. 3490, Mary Anne Passage and Approaches, 2nd Edition, May 1947, Unclassified.

APPENDIX A: TABLE OF DATA FOR SCALED CHARGES

Shot No.	Chg.Wt. W (lb)	Water Depth d (ft)	Chg. Depth* c (ft)	Max.Col. Diameter D_{max} (ft)	Max.Col. Height C_{max} (ft)	Max.Jet Height J_{max} (ft)	Max.Surge Radius R_{max} (ft)	Max.Surge Height H_{max} (ft)	Max.Throw-out Dia. T_{max} (ft)	Max.Smoke Crown Dia. S_{max} (ft)	Min.Jet Dia. j_{min} (ft)	Scaled Depth λ_d (ft/lb$^{1/3}$)	Scaled Depth λ_c (ft/lb$^{1/3}$)
280**	4200	1.83	B	85.4	51	870	345	184	895	390	–	0.114	0.047
281**	4200	2.17	B	87.7	77	372	339	142	938	372	–	0.135	0.068
296**	4200	2.25	B	90.0	90	986	–	–	1388	312	75	0.140	0.073
293**	4200	2.52	B	91.6	100	965	–	–	956	496	78	0 156	0.090
112**	4200	2.50	B	127	112	1120	482	127	945	448	75	0.155	0.089
114	4200	3.42	B	93.1	124	931	388	78	–	352	57	0.212	0.146
301	4200	3.58	B	101	162	–	–	–	729	375	50	0.222	0.156
218	4200	4.00	B	86.7	107	1000	250	87	656	360	60	0.248	0.182
275	4200	4.29	B	97.5	125	1024	322	92	487	534	38	0.263	0.200
214	4200	4.33	B	91.0	140	1053	>236	52	325	400	28	0.269	0.202
215	4200	4.33	B	95.2	154	1150	253	83	478	448	50	0.269	0.202
300	4200	5.14	B	93.5	153	1213	>270	77	508	308	–	0.319	0.253
274	4200	8.25	B	101	169	1031	306	99	300	290	37	0.512	0.446
217	4200	8.58	B	107	190	1073	449	104	314	307	50	0.533	0.466
287	4143	8.75	B	98.8	164	790	>280	66	288	464	43	0.545	0.477
219	4200	8.92	B	98.2	223	1142	421	92	182	215	34	0.554	0.488
221	4200	9.25	B	114	231	1123	>459	92	209	284	35	0.574	0.508
220	4200	12.5	B	108	250	1350	504	96	172	167	50	0.745	0.679
111	4200	7.83	4.00	93.6	117	1120	507	86	–	351	31	0.486	0.248
113	4200	8.00	4.00	96.6	132	856	461	79	241	307	40	0.497	0.248
276	4200	8.25	4.33	95.3	139	1023	>242	61	182	338	55	0.512	0.268
222	4200	8.50	4.67	99.0	156	950	369	76	183	380	37	0.528	0.289
279	4200	8.58	4.96	99.6	156	985	322	104	193	280	26	0.533	0.307
302	4200	8.77	5.42	97.0	142	1001	>258	77	202	292	28	0.545	0.337
303	3600	8.42	5.29	98.2	134	896	>516	86	166	357	41	0.524	0.346

* Charge depth is to mid-point of charge unless the charge is on the bottom, as indicated by the letter "B".
** Smcg.

APPENDIX A: TABLE OF DATA FOR SCALED CHARGES (Cont.)

Shot No.	Chg.Wt. W (lb)	Water Depth d (ft)	Chg. Depth* c (ft)	Max.Col. Diameter D_{max} (ft)	Max.Col. Height C_{max} (ft)	Max.Jet Height J_{max} (ft)	Max.Surge Radius R_{max} (ft)	Max.Surge Height H_{max} (ft)	Max.Throw-out Dia. T_{max} (ft)	Max.Smoke Crown Dia. S_{max} (ft)	Min.Jet Dia. J_{min} (ft)	Scaled Depth λ_d (ft/lb$^{1/3}$)	Scaled Depth λ_c (ft/lb$^{1/3}$)
295**	4200	2.04	2.29	86.4	106	850	213	84	1300	313	66	0.127	0.142
294**	4200	2.65	2.51	81.9	88.2	950	217	93	1450	296	–	0.165	0.156
297**	4200	2.98	2.60	88.4	84.6	700	228	83	1680	368	–	0.185	0.161
298	4200	4.37	3.81	91.5	132	1000	287	83	1024	370	–	0.271	0.236
V[1] 420	2048	7.41	7.41	82.3	122	—	—	—	—	—	–	0.583	0.583
284**	600	1.00	B	54.1	25	369	—	85	1000	204	–	0.119	-0.008
104**	600	1.17	B	61.0	37	471	185	83	950	213	–	0.139	0.012
283**	600	1.83	B	57.4	43	488	189	91	400	249	43	0.217	0.090
278**	600	2.17	B	51.0	44	548	>236	66	300	244	–	0.257	0.130
285	600	2.27	B	48.3	39	568	–	–	288	254	–	0.270	0.142
101	600	2.50	B	52.1	65	566	156	33	391	260	33	0.297	0.170
105	600	2.50	B	54.4	53	526	149	2[illegible]	421	184	42	0.297	0.170
282	600	2.50	B	48.5	48	575	–	33	>265	238	22	0.297	0.170
102	600	2.58	B	51.8	56	607	225	54	337	225	34	0.306	0.179
100	600	3.0	B	54.8	71	676	105	35	274	223	29	0.356	0.229
272	600	3.42	B	55.9	70	614	–	47	150	190	19	0.405	0.279
286	600	3.83	B	52.1	52	484	–	30	–	234	–	0.454	0.328
212	600	4.08	B	62.5	87	790	250	62	146	225	22	0.484	0.357
26	600	4.75	B	62.9	87	–	>144	33	168	224	22	0.563	0.436
213	600	4.83	B	58.5	91	–	250	79	139	195	17	0.573	0.446
9	600	5.00	B	68.9	105	–	–	29	114	209	21	0.593	0.466
51	600	5.58	B	66.6	112	–	159	34	103	240	17	0.662	0.535
52	600	5.58	B	64.7	105	–	171	35	–	175	17	0.662	0.535
277	600	9.12	B	70.7	90	725	186	56	80	154	14	1.08	0.955
103**	600	2.50	1.0	58.7	43	480	256	96	–	235	–	0.296	0.119
271	600	4.25	2.0	54.9	66	610	–	–	100	170	14	0.504	0.237

* Charge depth is to mid-point of charge unless the charge is on the bottom, as indicated by the letter "B".

** Smog.

1 Film records obtained from Waterways Experiment Station, Vicksburg, Miss.

APPENDIX A: TABLE OF DATA FOR SCALED CHARGES (Cont.)

Shot No.	Chg.Wt. W (lb)	Water Depth d (ft)	Chg. Depth* c (ft)	Max.Col. Diameter D_{max} (ft)	Max.Col Height C_{max} (ft)	Max.Jet Height J_{max} (ft)	Max.Surge Radius R_{max} (ft)	Max.Surge Height H_{max} (ft)	Max.Throw-out Dia. T_{max} (ft)	Max.Smoke Crown Dia. S_{max} (ft)	Min.Jet Dia J_{min} (ft)	Scaled Depth λ_d (ft/lb$^{1/3}$)	Scaled Depth λ_c (ft/lb$^{1/3}$)
216	600	4.37	2.17	62.8	71	666	220	39	130	187	20	0.518	0.257
273	600	4.5	2.25	58.7	78	670	—	—	144	206	14	0.534	0.267
66	600	27.0	4.58	52.0	100	—	184	31	0	130	28	3.20	0.543
299**	600	2.12	1.79	59.2	67	533	—	—	960	260	—	0.251	0.212
v[1] 430**	600	0.85	0.85	50.0	42	—	198	62	413	242	—	0.101	0.101
v[1] 427**	256	0.56	1.40	41.0	41	—	123	29	—	135	—	0.088	0.220
v[1] 428**	256	0.56	2.24	42.6	71	—	112	27	—	188	—	0.088	0.353
v[1] 429**	256	0.56	2.24	40.4	69	—	96	23	—	200	—	0.088	0.353
v[1] 415	256	3.71	3.71	42.1	109	—	—	—	153	156	—	0.584	0.584
v[1] 416	256	3.71	3.71	41.4	123	—	—	—	—	—	—	0.584	0.584
87**	100	0.50	B	33.2	—	>120	56.5	26.6	270	96	9.3	0.108	-0.009
108**	100	0.50	B	27.2	—	—	—	41.4	—	—	—	0.108	-0.009
109**	100	0.50	B	29.7	—	—	—	40.0	—	—	—	0.108	-0.009
228**	100	0.58	B	32.3	32	185	—	—	—	—	—	0.125	0.009
253**	100	0.58	B	—	25	192	—	—	270	96	—	0.125	0.009
254**	100	0.58	B	—	—	—	—	—	—	—	—	0.125	0.009
86**	100	0.75	B	29.2	19.5	>117	79.6	27.3	325	104	9.1	0.162	0.045
88**	100	0.75	B	30.3	—	>131	—	—	324	78	—	0.162	0.045
110**	100	0.75	B	31.1	—	—	73.0	37.4	—	—	—	0.162	0.045
255	100	0.83	B	—	—	—	—	—	—	—	—	0.179	0.062
85**	100	1.0	B	30.6	22.0	>127	72.0	14.4	—	—	—	0.216	0.099
105**	100	1.0	B	—	—	—	—	—	—	—	—	0.216	0.099
107**	100	1.0	B	35.9	—	—	47.2	21.5	—	—	—	0.216	0.099
250**	100	1.08	B	33.4	26.7	231	107	44.5	—	111	20	0.233	0.116

* Charge depth is to mid-point of charge unless the charge is on the bottom, as indicated by the letter "B".
** Smog.

1 Film records obtained from Waterways Experiment Station, Vicksburg, Miss.

APPENDIX A: TABLE OF DATA FOR SCALED CHARGES (Cont.)

Shot No.	Chg.Wt. W (lb)	Water Depth d (ft)	Chg. Depth* c (ft)	Max.Col. Diameter D_{max} (ft)	Max.Col. Height C_{max} (ft)	Max.Jet Height J_{max} (ft)	Max.Surge Radius R_{max} (ft)	Max.Surge Height H_{max} (ft)	Max.Throw-out Dia. T_{max} (ft)	Max.Smoke Crown Dia. S_{max} (ft)	Min.Jet Dia. j_{min} (ft)	Scaled Depth λ_d (ft/lb$^{1/3}$)	Scaled Depth λ_c (ft/lb$^{1/3}$)
49	100	1.25	B	31.1	–	–	>78.3	>18.9	190	101	12.6	0.269	0.153
50	100	1.25	B	33.5	–	–	129	21.9	245	97	–	0.269	0.153
209	100	1.25	B	31.5	27.7	>210	113	–	190	100	–	0.269	0.153
211	100	1.25	B	30.2	31.5	>213	101	25.2	170	88	10.0	0.269	0.153
229	100	1.25	B	27.7	23.1	231	–	–	–	–	–	0.269	0.153
232	100	1.25	B	32.3	23.1	222	–	–	–	120	13.8	0.269	0.153
210	100	1.29	B	29.0	31.5	>205	56.7	13.9	95	95	7.6	0.278	0.162
163	100	1.83	B	26.6	33.3	–	86.0	22.2	–	–	–	0.395	0.278
252	100	1.83	B	32.2	32.2	276	–	–	–	–	–	0.395	0.278
243	100	1.87	B	30.0	30.0	283	–	–	–	–	17.0	0.403	0.286
47	100	2.0	B	–	–	–	–	–	–	–	–	0.431	0.314
48	100	2.0	B	31.0	–	–	93.0	21.1	74	81	12.0	0.431	0.314
3	100	2.5	B	34.1	59.0	–	62.2	16.5	–	88	10.0	0.539	0.422
4	100	2.5	B	40.4	56.3	–	61.0	14.1	–	–	7.5	0.539	0.422
5	100	2.5	B	39.0	46.9	–	64.9	17.2	–	133	–	0.539	0.422
7	100	2.5	B	40.1	48.2	–	35.2	18.6	–	126	–	0.539	0.422
126	100	2.5	B	36.8	48.8	>130	103	18.6	91	98	16.0	0.539	0.422
127	100	2.5	B	35.3	50.4	>130	113	20.2	63	95	19.0	0.539	0.422
128	100	2.5	B	35.8	50.4	>133	120	23.0	69	126	16.0	0.539	0.422
129	100	2.5	B	34.0	56.7	>134	95.8	22.7	63	88	11.0	0.539	0.422
130	100	2.5	B	34.0	44.1	>131	107	16.4	126	115	19.0	0.539	0.422
131	100	2.5	B	36.0	48.4	>118	71.3	18.6	99	99	–	0.539	0.422
132	100	2.5	B	33.2	–	–	–	25.5	–	–	–	0.539	0.422
133	100	2.5	B	–	–	–	–	–	–	–	–	0.539	0.422
134	100	2.5	B	32.2	53.2	>128	>73.2	21.3	60	126	13.0	0.539	0.422

* Charge depth is to mid-point of charge unless the charge is on the bottom, as indicated by the letter "B".

APPENDIX A: TABLE OF DATA FOR SCALED CHARGES (Cont.)

Shot No.	Chg.Wt. W (lb)	Water Depth d (ft)	Chg. Depth* c (ft)	Max.Col. Diameter D_{max} (ft)	Max.Col. Height C_{max} (ft)	Max.Jet Height J_{max} (ft)	Max.Surge Radius R_{max} (ft)	Max.Surge Height H_{max} (ft)	Max.Throw-out Dia. T_{max} (ft)	Max.Smoke Crown Dia. S_{max} (ft)	Min.Jet Dia. j_{min} (ft)	Scaled Depth λ_d (ft/lb$^{1/3}$)	Scaled Depth λ_c (ft/lb$^{1/3}$)
135	100	2.5	B	35.1	48.4	>103	64.1	14.6	91	127	12.0	0.539	0.422
155	100	2.5	B	30.6	–	>172	51.0	25.5	–	–	–	0.539	0.422
156	100	2.5	B	30.6	–	>176	74.5	23.0	–	–	–	0.539	0.422
157	100	2.5	B	30.0	–	>170	>93.0	27.5	–	–	–	0.539	0.422
158	100	2.5	B	30.0	48.0	>162	63.0	12.0	54	108	11.0	0.539	0.422
159	100	2.5	B	27.8	32.7	>134	81.8	16.4	48	120	14.2	0.539	0.422
173	100	2.5	B	33.2	53.2	>201	73.2	16.0	53	113	13.0	0.539	0.422
198	100	2.5	B	33.6	48.0	>198	–	–	162	108	18.0	0.539	0.422
230	100	2.5	B	30.5	50.8	291	–	–	220	87	–	0.539	0.422
235	100	2.5	B	30.0	38.6	274	–	–	320	104	–	0.539	0.422
245	100	2.5	B	28.3	47.0	326	81.0	–	–	–	–	0.539	0.422
197	100	2.62	B	30.5	–	–	–	–	–	–	–	0.565	0.448
164	100	2.92	B	31.1	55.5	>179	99.9	25.5	40	78	10.0	0.630	0.513
165	100	3.0	B	33.1	57.0	>111	68.4	17.1	0	63	11.4	0.647	0.530
305	100	3.92	B	42.5	100	367	105	17.5	–	120	–	0.845	0.728
262	100	4.83	B	36.4	77.1	370	133	>26.0	67	54	10.7	1.04	0.924
304	100	5.06	B	43.3	92.7	–	–	–	–	–	14.9	1.09	0.974
43	100	10.0	B	36.0	75.0	–	100	18.0	0	–	–	2.15	2.04
44	100	10.0	B	41.5	–	–	54.6	10.9	0	–	–	2.15	2.04
266**	100	5.33	-0.08[b]	33.2	–	132	>98	36.0	–	–	–	1.15	-0.134
251**	100	1.08	0[b]	29.0	22.8	116	98.0	49.7	–	–	–	0.233	-0.116
BG185**	100	2.33	0[b]	30.0	24.0	139	132	30.0	–	–	–	0.502	-0.116
172**	100	4.0	0[b]	30.8	18.0	193	162	46.2	–	–	–	0.862	-0.116
BG188**	100	2.62	0.17[b]	30.0	26.4	>194	>121	36.0	–	–	–	0.565	-0.080
174**	100	5.0	0.17[b]	27.5	25.0	173	100	48.8	–	–	–	1.08	-0.080
175**	100	5.0	0.21[b]	31.5	25.0	180	94.5	31.5	–	–	–	1.08	-0.071

* Charge depth is to mid-point of charge unless the charge is on the bottom, as indicated by the letter "B".
** Smog.

b Measured to bottom of charge.

BG Blasting Gelatin.

APPENDIX A: TABLE OF DATA FOR SCALED CHARGES (Cont.)

Shot No.	Chg.Wt. W (lb)	Water Depth d (ft)	Chg. Depth* c (ft)	Max.Col. Diameter D_{max} (ft)	Max.Col. Height C_{max} (ft)	Max.Jet Height J_{max} (ft)	Max.Surge Radius R_{max} (ft)	Max.Surge Height H_{max} (ft)	Max.Throw-out Dia. T_{max} (ft)	Max.Smoke Crown Dia. S_{max} (ft)	Min.Jet Dia. j_{min} (ft)	Scaled Depth λ_d (ft/lb$^{1/3}$)	Scaled Depth λ_c (ft/lb$^{1/3}$)
176**	100	5.0	0.21[b]	31.5	31.5	195	94.5	31.5	–	–	13.0	1.08	-0.071
171**	100	4.0	0.25[b]	33.0	22.5	>195	147	42.0	–	–	15.0	0.862	-0.062
BG189**	100	2.62	0.33[b]	28.8	30.0	>205	120	30.0	–	–	9.6	0.565	-0.045
BG183**	100	2.75	0.71[b]	29.4	28.3	>181	> 53.7	17.0	–	–	11.3	0.593	0.037
160**	100	1.83	0.83[b]	34.9	24.0	>179	>114	38.2	–	–	10.9	0.395	0.062
161**	100	3.58	0.83[b]	36.0	27.0	>144	>106	30.5	–	–	10.9	0.771	0.062
201	100	2.58	0.50	34.6	33.0	>226	–	–	239	120	17.0	0.556	0.108
207	100	2.50	0.75	31.5	37.8	>210	–	–	–	100	–	0.539	0.162
200	100	2.54	0.75	30.2	31.0	>208	–	31.5	139	113	12.6	0.548	0.162
246	100	2.50	1.0	25.7	25.7	257	–	–	–	–	–	0.539	0.215
206	100	2.33	1.25	32.8	37.8	>214	113	–	–	95	8.8	0.502	0.269
199	100	2.46	1.25	30.0	36.0	>188	63	18.0	–	96	10.8	0.530	0.269
208	100	2.50	1.25	31.3	37.5	>200	87.5	–	–	100	10.0	0.539	0.269
6	100	2.50	1.25	37.0	44.0	–	55.0	16.7	–	132	11.0	0.539	0.269
8	100	2.50	1.25	33.5	47.0	–	50.0	8.8	–	94	–	0.539	0.269
35	100	2.50	1.25	29.4	35.0	–	>54.2	>11.6	96	88	12.0	0.539	0.269
36	100	2.50	1.25	28.7	34.0	–	>51.0	> 9.8	123	85	–	0.539	0.269
180	100	2.50	1.25	30.0	36.0	>194	–	–	–	96	9.6	0.539	0.269
181	100	2.50	1.25	29.1	32.5	>181	50.4	13.4	–	90	8.9	0.539	0.269
BG184	100	2.50	1.25	27.3	37.2	>195	74.4	18.6	–	105	12.4	0.539	0.269
202	100	2.50	1.25	–	–	–	–	–	–	–	–	0.539	0.269
256	100	2.50	1.25	–	–	–	–	–	108	120	–	0.539	0.269
242	100	2.54	1.25	27.4	30.0	266	–	–	–	–	–	0.548	0.269
205	100	2.58	1.25	29.9	32.5	>213	–	–	–	98	13.0	0.556	0.269

* Charge depth is to mid-point of charge unless the charge is on the bottom, as indicated by the letter "B".
** Smog.

b Measured to bottom of charge.

BG Blasting Gelatin.

APPENDIX A: TABLE OF DATA FOR SCALED CHARGES (Cont.)

Shot No.	Chg.Wt. W (lb)	Water Depth d (ft)	Chg. Depth* c (ft)	Max.Col. Diameter D_{max} (ft)	Max.Col. Height C_{max} (ft)	Max.Jet Height J_{max} (ft)	Max.Surge Radius R_{max} (ft)	Max.Surge Height H_{max} (ft)	Max.Throw-out T_{max} (ft)	Max.Smoke Crown Dia. S_{max} (ft)	Min.Jet Dia. J_{min} (ft)	Scaled Depth λ_d (ft/lb$^{1/3}$)	Scaled Depth λ_c (ft/lb$^{1/3}$)
257	100	2.67	1.25	35.0	40.0	280	—	—	160	140	—	0.575	0.269
34	100	2.50	1.92	31.6	48.0	—	> 60.0	11.1	152	80	—	0.539	0.276
265	100	5.06	4.21	38.0	95.0	>356	95.0	26.0	67	—	10.0	1.09	0.907
150**	100	15.0	0[b]	25.3	—	162	58.8	12.6	—	—	7.6	3.23	-0.116
170**	100	15.0	0[b]	32.0	15.0	138	112	40.0	—	—	12.8	3.45	-0.116
139**	100	15.0	0.08[b]	36.0	22.5	>191	131	45.0	—	—	15.0	3.23	-0.099
167**	100	16.0	0.17[b]	35.9	—	203	>137	35.9	—	—	15.6	3.45	-0.080
168**	100	16.0	0.25[b]	30.0	30.0	>213	>158	52.5	—	—	12.0	3.45	-0.062
169**	100	16.0	0.33[b]	33.0	37.0	>207	>165	67.5	—	—	15.0	3.45	-0.045
166**	100	16.0	0.42[b]	33.0	37.0	>210	120	33.0	—	—	15.0	3.45	-0.026
136**	100	15.0	0.50[b]	26.4	36.0	>174	73.2	16.8	—	—	7.2	3.23	-0.009
138**	100	15.0	0.50[b]	32.8	31.5	>179	94.5	31.5	>292	—	12.6	3.23	-0.009
143**	100	15.0	0.96[b]	32.6	34.0	>190	156	43.5	—	—	12.2	3.23	0.091
142**	100	15.0	1.04[b]	35.4	—	>197	123	38.5	—	—	17.7	3.23	0.108
144**	100	15.0	1.04[b]	34.0	38.1	>190	156	47.6	—	—	8.2	3.23	0.108
147	100	15.0	1.12[b]	25.6	—	>193	58.5	16.0	—	—	—	3.23	0.125
151**	100	15.0	1.12[b]	31.6	34.3	>215	142	34.8	—	94	12.5	3.23	0.125
140**	100	15.0	1.21[b]	27.0	30.0	>192	67.5	15.0	—	—	10.5	3.23	0.144
145	100	15.5	1.21[b]	26.8	35.0	>200	59.9	16.9	—	—	8.5	3.34	0.144
146**	100	15.0	1.29[b]	30.0	30.0	>196	161	49.0	—	104	12.3	3.23	0.162
148	100	15.0	1.29[b]	26.7	—	>195	58.5	13.3	—	—	—	3.23	0.162
149**	100	15.0	1.31[b]	26.0	27.3	>221	63.3	14.9	—	96	10.9	3.23	0.166
141	100	15.0	1.37[b]	24.0	—	>192	51.0	12.0	—	—	—	3.23	0.179
137	100	15.0	1.46[b]	34.6	53.2	>184	82.5	20.0	>308	—	—	3.23	0.198
38	100	15.0	2.50	34.9	60.0	—	60.0	12.0	70	114	11.0	3.23	0.539

* Charge depth is to mid-point of charge unless the charge is on the bottom, as indicated by the letter "B".

** Smog.

b Measured to bottom of charge.

APPENDIX A: TABLE OF DATA FOR SCALED CHARGES (Cont.)

Shot No.	Chg.Wt. W (lb)	Water Depth d (ft)	Chg. Depth* c (ft)	Max.Col. Diameter D_{max} (ft)	Max.Col. Height C_{max} (ft)	Max.Jet Height J_{max} (ft)	Max.Surge Radius R_{max} (ft)	Max.Surge Height H_{max} (ft)	Max.Throw-out Dia. T_{max} (ft)	Max.Smoke Crown Dia. S_{max} (ft)	Min.Jet Dia. j_{min} (ft)	Scaled Depth λ_d (ft/lb$^{1/3}$)	Scaled Depth λ_c (ft/lb$^{1/3}$)
40	100	15.0	2.50	31.0	54.0	–	55.9	12.4	–	–	–	3.23	0.539
42	100	15.0	2.50	31.9	50.0	–	>42.2	9.0	–	–	–	3.23	0.539
67	100	17.0	2.50	36.8	50.0	>168	>41.6	16.0	–	–	12.8	3.66	0.539
68	100	17.0	2.50	36.2	–	>184	65.8	16.4	–	–	13.2	3.66	0.539
69	100	17.0	2.50	37.5	–	>150	>45.0	15.0	–	–	9.0	3.66	0.539
289[2]	83	32.0	2.08	28.8	48.0	>179	60.0	15.6	–	–	12.0	7.34	0.477
290[2]	83	32.0	2.08	29.4	54.0	>193	48.0	14.1	–	–	7.7	7.34	0.477
291[2]	83	32.0	2.08	–	–	>206	45.0	12.9	–	–	7.7	7.34	0.477
292[2]	83	30.0	2.12	29.9	51.0	>178	57.0	15.0	–	–	10.3	6.88	0.486
288[2]	83	32.0	2.12	30.0	54.0	>187	69.0	–	–	–	7.2	7.34	0.486
152	42	2.0	0.33	–	–	–	–	–	–	–	–	0.575	0.095
264[3]	42	1.67	B	18.0	40.0	240	–	6.0	–	–	5.6	0.480	0.457
259	42	1.79	B	18.4	32.0	200	–	–	–	–	8.0	0.514	0.420
vl 432**	32	0.28	0	19.8	16.5	–	42.0	12.6	126	66	–	0.088	0
vl 414**	32	1.85	0	20.6	19.1	–	73.0	28.0	–	–	–	0.583	0
vl 433**	32	0.28	0.70	21.5	33.0	–	35.0	9.3	>117	>100	–	0.088	0.221

* Charge depth is to mid-point of charge unless the charge is on the bottom, as indicated by the letter "B".
** Smog.

1 Film records obtained from Waterways Experiment Station, Vicksburg, Miss.
2 Spherical Pentolite charge, diameter 14.0 inches.
3 Ring-shaped charge.

APPENDIX A: TABLE OF DATA FOR SCALED CHARGES (Cont.)

Shot No.	Chg.Wt. W (lb)	Water Depth d (ft)	Chg. Depth* c (ft)	Max.Col. Diameter D_{max} (ft)	Max.Col. Height C_{max} (ft)	Max.Jet Height J_{max} (ft)	Max.Surge Radius R_{max} (ft)	Max.Surge Height H_{max} (ft)	Max.Throw-out Dia. T_{max} (ft)	Max.Smoke Crown Dia. S_{max} (ft)	Min.Jet Dia. J_{min} (ft)	Scaled Depth λ_d (ft/lb$^{1/3}$)	Scaled Depth λ_c (ft/lb$^{1/3}$)
80**	21	0.33	B	–	–	–	–	–	182	50	–	0.120	0.060
81**	21	0.33	B	–	–	–	–	–	174	50	–	0.120	0.060
84**	21	0.33	B	14.8	19.2	>126	–	–	180	50	9.6	0.120	0.060
92**	21	0.33	B	18.2	13.3	>127	49.6	13.3	195	48	6.1	0.120	0.060
95**	21	0.33	B	19.2	14.4	> 95	42.0	18.0	192	48	–	0.120	0.060
96**	21	0.33	B	20.2	20.0	>100	45.5	20.2	200	57	12.0	0.120	0.060
99**	21	0.33	B	22.5	–	>115	71.9	17.5	–	–	–	0.120	0.060
233**	21	0.33	B	18.5	18.5	160	–	–	–	–	–	0.120	0.060
244**	21	0.33	B	17.1	17.1	127	49.3	–	–	–	–	0.120	0.060
247**	21	0.33	B	17.1	15.4	133	–	–	–	–	10.3	0.120	0.060
83**	21	0.50	B	16.8	14.4	>128	24.0	–	168	54	6.0	0.181	0.120
93**	21	0.50	B	17.5	18.0	>125	–	–	225	69	4.4	0.181	0.120
97**	21	0.50	B	20.2	19.0	>115	–	12.6	–	50	6.3	0.181	0.120
98**	21	0.50	B	20.9	18.0	>115	40.0	–	–	50	6.2	0.181	0.120
82	21	0.75	B	20.4	20.4	>126	18.6	–	120	60	12.0	0.272	0.211
77	21	0.75	B	14.8	18.0	–	–	–	132	54	–	0.272	0.211
76	21	0.75	B	14.6	20.5	–	–	–	130	59	–	0.272	0.211
89	21	0.75	B	15.0	18.0	>112	–	–	140	54	12.0	0.272	0.211
196	21	0.75	B	19.8	–	–	–	–	–	–	–	0.272	0.211
234	21	0.75	B	20.3	18.5	194	–	–	–	–	11.1	0.272	0.211
226	21	0.75	B	16.6	21.2	166	–	–	–	–	–	0.272	0.211
30	21	0.83	B	17.0	–	>108	–	–	–	–	–	0.301	0.242
31	21	0.83	B	18.8	19.6	> 95	–	–	–	55	–	0.301	0.242
32	21	0.83	B	20.6	20.6	>101	–	–	129	50	12.0	0.301	0.242
33	21	0.83	B	18.6	19.8	>108	28.7	–	155	52	14.7	0.301	0.242

* Charge depth is to mid-point of charge unless the charge is on the bottom, as indicated by the letter "B".
** Smog.

APPENDIX A: TABLE OF DATA FOR SCALED CHARGES (Cont.)

Shot No.	Chg.Wt. W (lb)	Water Depth d (ft)	Chg. Depth* c (ft)	Max.Col. Diameter D_{max} (ft)	Max.Col. Height C_{max} (ft)	Max.Jet Height J_{max} (ft)	Max.Surge Radius R_{max} (ft)	Max.Surge Height H_{max} (ft)	Max.Throw-out Dia. T_{max} (ft)	Max.Smoke Crown Dia. S_{max} (ft)	Min.Jet Dia. J_{min} (ft)	Scaled Depth λ_d (ft/lb$^{1/3}$)	Scaled Depth λ_c (ft/lb$^{1/3}$)
241	21	1.12	B	18.8	30.6	>212	–	–	–	–	–	0.406	0.344
1	21	1.50	B	20.9	31.3	–	40.6	8.9	57	39	6.8	0.543	0.482
2	21	1.50	B	21.5	33.4	–	43.8	11.0	48	43	7.2	0.543	0.482
90	21	1.50	B	19.0	44.0	–	52.5	15.0	150	44	–	0.543	0.482
21	21	1.50	B	21.8	26.6	–	34.9	10.3	100	–	–	0.543	0.482
22	21	1.50	B	21.7	26.0	–	–	–	93	73	–	0.543	0.482
23	21	1.50	B	21.9	31.0	–	17.0	4.2	94	70	–	0.543	0.482
73	21	1.50	B	19.3	–	–	30.4	–	–	–	–	0.543	0.482
74	21	1.50	B	17.3	–	–	–	–	–	–	–	0.543	0.482
91	21	1.50	B	19.6	30.5	–	–	–	98	49	6.1	0.543	0.482
94	21	1.50	B	20.4	36.0	–	43.5	–	145	42	6.4	0.543	0.482
223	21	1.50	B	18.0	30.0	240	–	–	–	–	7.0	0.543	0.482
240	21	1.50	B	18.8	32.9	>212	–	–	–	–	7.0	0.543	0.482
265[3]	21	1.50	B	16.8	48.0	300	–	–	–	–	8.6	0.543	0.482
18	21	3.0	B	22.2	–	–	31.2	7.9	–	–	–	1.09	1.03
19	21	3.0	B	22.6	47.0	–	30.6	11.8	47	35	5.2	1.09	1.03
260	21	3.0	B	17.1	–	223	–	–	–	–	7.7	1.09	1.03
261	21	3.0	B	25.0	50.0	250	–	–	–	–	8.0	1.09	1.03
24	21	4.5	B	23.1	46.2	–	>38.9	14.4	35	40	5.8	1.64	1.57
25	21	5.0	B	24.3	60.0	–	–	3.5	28	40	–	1.74	1.69
45	21	6.0	B	24.6	42.0	–	32.8	8.1	52	37	8.0	2.17	2.11
46	21	6.0	B	24.5	39.0	–	35.5	7.4	39	37	7.3	2.17	2.11
65	21	6.0	B	22.4	–	–	>21.5	6.9	–	–	–	2.17	2.11
267	21	12.0	B	0	0	0	–	–	0	0	–	4.35	4.29
237	21	0.33	0[b]	–	–	–	–	–	–	–	–	0.120	-0.062
194**	21	1.50	0[b]	27.7	21.0	169	135	48.5	–	–	13.8	0.543	-0.062

* Charge depth is to mid-point of charge unless the charge is on the bottom, as indicated by the letter "B".
** Smog.

3 Ring-shaped charge.

b Measured to bottom of charge.

APPENDIX A: TABLE OF DATA FOR SCALED CHARGES (Cont.)

Shot No.	Chg.Wt. W (lb)	Water Depth d (ft)	Chg. Depth* c (ft)	Max.Col. Diameter D_{max} (ft)	Max.Col. Height C_{max} (ft)	Max.Jet Height J_{max} (ft)	Max.Surge Radius R_{max} (ft)	Max.Surge Height H_{max} (ft)	Max.Throw-out Dia. T_{max} (ft)	Max.Smoke Crown Dia. S_{max} (ft)	Min.Jet Dia. J_{min} (ft)	Scaled Depth λ_d (ft/lb$^{1/3}$)	Scaled Depth λ_c (ft/lb$^{1/3}$)
BG186**	20	2.29	0[b]	17.5	21.0	>168	82.4	20.6	-	-	-	0.830	-0.062
225**	21	3.0	0[b]	27.0	-	140	-	-	-	-	-	1.09	-0.062
226**	21	3.0	0[b]	18.9	21.4	129	42.8	-	-	-	4.3	1.09	-0.062
193	21	4.5	0[b]	-	-	-	-	-	-	-	-	1.68	-0.062
BG179	20	5.5	0.21[b]	15.5	-	217	-	-	-	-	5.8	1.99	0.014
195	21	1.29	0.29[b]	-	-	-	-	-	-	-	-	0.467	0.043
153**	21	2.0	0.29[b]	18.3	17.0	>149	109	27.4	-	-	-	0.725	0.043
BG178	20	4.5	0.37[b]	15.5	25.2	203	-	-	-	-	5.8	1.68	0.072
154	21	2.0	0.54[b]	15.9	27.2	>140	24.9	5.4	-	-	-	0.725	0.134
BG177	20	4.75	0.54[b]	17.1	-	219	-	-	-	-	6.7	1.72	0.134
BG187	20	2.58	0.79[b]	16.5	-	>179	74.3	18.7	-	-	5.5	0.935	0.224
248**	21	1.5	0	24.0	28.3	163	-	-	-	65	-	0.543	0
249**	21	1.5	0	20.5	20.5	120	-	-	-	-	8.6	0.543	0
258	21	3.25	0.17	-	-	-	-	-	-	48	-	1.18	0.062
190	21	1.5	0.46	15.6	-	189	-	-	-	-	-	0.543	0.167
191	21	2.0	0.46	18.3	-	188	-	-	-	-	-	0.725	0.167
204	21	1.25	0.58	-	-	-	-	-	-	-	-	0.453	0.210
203	21	1.25	0.58	-	-	-	-	-	-	-	-	0.453	0.210
192	21	1.54	0.58	15.5	-	-	-	-	-	-	-	0.558	0.210
239	21	1.5	0.58	15.8	16.8	221	-	-	-	-	7.2	0.543	0.210
269	21	1.33	0.67	21.2	27.7	176	-	-	-	51	-	0.482	0.243
224	21	1.5	0.75	20.0	20.0	180	-	-	-	-	-	0.543	0.272
227	21	1.5	0.75	21.2	23.0	166	-	-	-	-	11.0	0.543	0.272
231	21	1.5	0.75	16.0	24.0	192	-	-	-	-	8.0	0.543	0.272
238	18	1.5	0.75	19.7	23.1	223	-	-	-	-	5.1	0.572	0.286
27	21	1.5	0.75	18.2	29.0	-	-	7.3	35	55	6.5	0.543	0.272

* Charge depth is to mid-point of charge unless the charge is on the bottom, as indicated by the letter "B".
** Smog.

b Measured to bottom of charge.
BG Blasting Gelatin.

APPENDIX A: TABLE OF DATA FOR SCALED CHARGES (Cont.)

Shot No.	Chg.Wt. W (lb)	Water Depth d (ft)	Chg. Depth* c (ft)	Max.Col. Diameter D_{max} (ft)	Max.Col. Height C_{max} (ft)	Max.Jet Height J_{max} (ft)	Max.Surge Radius R_{max} (ft)	Max.Surge Height H_{max} (ft)	Max.Throw-out Dia. T_{max} (ft)	Max. Smoke Crown Dia. S_{max} (ft)	Min.Jet Dia. j_{min} (ft)	Scaled Depth λ_d (ft/lb$^{1/3}$)	Scaled Depth λ_c (ft/lb$^{1/3}$)
28	21	1.5	0.75	15.9	21.0	–	–	–	55	46	5.6	0.543	0.272
29	21	1.5	0.75	17.8	27.0	–	–	–	66	58	–	0.543	0.272
182	21	1.5	0.75	13.3	20.0	173	–	–	53	46	6.6	0.543	0.272
270	21	1.5	0.75	22.2	32.3	184	–	–	101	58	4.6	0.543	0.272
78	21	9.0	0.50	–	–	–	–	–	–	–	–	3.26	0.181
79	21	9.0	0.50	–	–	–	–	–	–	–	–	3.26	0.181
118	21	30.0	1.00	15.6	–	–	26.6	7.3	–	–	–	10.9	0.362
117	21	30.0	1.17	14.5	–	–	20.6	6.1	–	–	–	10.9	0.424
119	21	30.0	1.17	13.8	–	–	25.2	5.6	–	–	–	10.9	0.424
116	21	30.0	1.33	12.7	–	–	19.8	6.0	–	–	–	10.9	0.482
37	21	15.0	1.50	17.2	–	>104	–	–	–	–	–	5.43	0.543
39	21	15.0	1.50	17.8	–	–	40.0	8.9	–	–	–	5.43	0.543
41	21	15.0	1.50	17.2	–	–	32.0	8.0	–	–	–	5.43	0.543
58	21	15.0	1.50	16.9	19.5	>116	36.7	9.2	–	–	6.2	5.43	0.543
59	21	15.0	1.50	18.1	–	>131	33.8	10.4	–	–	–	5.43	0.543
60	21	15.0	1.50	20.2	–	>131	25.3	4.2	–	–	–	5.43	0.543
71	21	15.0	1.50	19.8	35.0	>132	–	–	–	–	4.7	5.43	0.543
72	21	15.0	1.50	20.6	34.0	>126	27.4	13.6	–	–	6.9	5.43	0.543
115	21	15.0	1.50	16.9	–	> 97	19.4	4.8	–	–	–	5.43	0.543
70	21	17.0	1.50	17.7	–	>176	34.1	–	–	–	8.2	6.16	0.543
120	21	20.0	1.50	14.8	–	–	28.4	4.9	–	–	–	7.25	0.543
121	21	20.0	1.67	16.0	–	–	21.2	6.2	–	–	–	7.25	0.605
122	21	20.0	1.92	16.7	–	–	27.2	7.4	–	–	–	7.25	0.696
63	21	15.0	2.0	19.6	26.0	>131	38.0	11.8	–	–	5.2	5.43	0.725
64	21	15.0	2.0	19.2	–	>136	36.0	7.4	–	–	6.0	5.43	0.725

* Charge depth is to mid-point of charge unless the charge is on the bottom, as indicated by the letter "B".

APPENDIX A: TABLE OF DATA FOR SCALED CHARGES (Cont.)

Shot No.	Chg.Wt. W (lb)	Water Depth d (ft)	Chg. Depth* c (ft)	Max.Col. Diameter D_{max} (ft)	Max.Col. Height C_{max} (ft)	Max.Jet Height J_{max} (ft)	Max.Surge Radius R_{max} (ft)	Max.Surge Height H_{max} (ft)	Max.Throw-out Dia. T_{max} (ft)	Max.Smoke Crown Dia. S_{max} (ft)	Min.Jet Dia. j_{min} (ft)	Scaled Depth λ_d (ft/lb$^{1/3}$)	Scaled Depth λ_c (ft/lb$^{1/3}$)
61	21	15.0	3.0	19.8	26.0	>118	30.6	7.1	-	-	4.7	5.43	1.09
62	21	15.0	3.0	20.0	30.0	>123	37.5	7.5	-	-	7.5	5.43	1.09
125	21	15.0	4.0	17.6	-	-	28.6	7.7	-	-	-	5.43	1.45
268	21	12.0	5.17	-	-	131	-	-	49	0	6.0	4.35	1.87
123	21	20.0	2.17	17.3	-	-	25.4	7.4	-	-	-	7.25	0.786
124	21	20.0	2.5	18.2	-	-	25.7	7.4	-	-	-	7.25	0.906
75	15	1.5	B	16.6	-	> 43	24.0	3.8	-	-	-	0.608	0.541
10	10	1.17	B	14.4	-	> 37	17.4	6.0	-	-	-	0.544	0.428
11	10	1.17	B	14.1	-	> 44	16.6	6.2	-	-	-	0.544	0.428
12	10	1.17	B	14.4	-	> 48	12.9	6.2	-	-	-	0.544	0.428
20	10	1.17	B	15.2	-	> 44	24.8	5.7	-	-	-	0.544	0.428
15	10	2.33	B	16.7	-	-	-	4.1	-	-	-	1.08	0.967
16	10	3.08	B	17.3	-	> 79	-	7.5	-	-	-	1.43	1.23
17	10	3.58	B	18.5	-	> 92	15.7	4.6	-	-	-	1.67	1.55
54	10	6.0	1.17	15.5	-	-	0	0	-	-	-	2.79	0.544
55	10	6.0	1.67	16.3	-	-	-	-	-	-	-	2.79	0.777
53	10	6.1	2.17	17.1	-	-	0	0	-	-	-	2.84	1.01
56	10	8.0	2.67	18.2	-	>108	21.2	5.4	-	-	-	3.60	1.24
57	10	8.0	4.0	19.7	-	-	0	0	-	-	-	3.60	1.86
13	1.7	0.67	B	10.0	-	-	-	3.2	-	-	-	0.562	0.454
14	1.6	0.67	B	9.1	-	-	0	0	-	-	-	0.571	0.464
162[4]	10	-	1.0	-	-	-	-	-	-	-	-	-	0.465
316	101	26.0	0.17	26.6	28.2	>258	0	0	-	156	11.0	5.58	0.036
317	102	26.0	0	38.5	38.5	>321	0	0	-	212	13.5	5.57	0
318**	102	26.0	0	29.4	20.6	>244	112	26.5	-	147	13.2	5.57	0
319**	103	26.0	0	26.3	23.6	>221	92.0	23.6	-	131	10.5	5.54	0
320**	102	24.0	0	27.8	27.8	>232	97.2	22.2	-	145	8.9	5.14	0
321**	102	30.0	0	28.6	28.6	>249	> 67.2	17.1	-	149	14.3	6.42	0
322**	101	30.0	0	28.6	25.7	>246	-85.8	18.6	-	172	15.7	6.44	0

* Charge depth is to mid-point of charge unless the charge is on the bottom, as indicated by the letter "B".
** Smog.
4 Underground shot.

APPENDIX B

FLASHBULB SCALE MARKERS

by
R. L. Willey

I. INTRODUCTION.

To provide a distance scale on the film records, two No. 31 photoflash bulbs were fired a known distance apart, one on each side of the charge position. A trigger gauge utilizing the underwater shockwave to close a circuit was designed to initiate the firing of the flashbulbs.

II. THE GAUGE.

1. Gauge assembly. The gauge assembly consists of the gauge body, a connecting tube and the battery box (Fig. B-1). The gauge body contains the diaphragm and contact assembly. It was designed to permit the use of diaphragms of different materials and thicknesses, depending on the shockwave pressures and time constants expected. The contact assembly (Fig. B-2) is adjustable and has a sliding contact within an insulated housing. This contact is held in the extended position by a spring so that overpressures by the shock wave will cause the contact to recede into its housing and prevent permanent deformation to the diaphragm.

The brass connecting tube can be of any convenient length which will permit the orientation and positioning of the gauge body at the desired water depth and the placement of the flash bulbs at the proper height above the water surface. This tube also carries the wiring from the contact assembly to the battery and flash bulb socket.

The battery box houses a six volt drycell battery, switch, and socket all connected in series with the contact and dia-

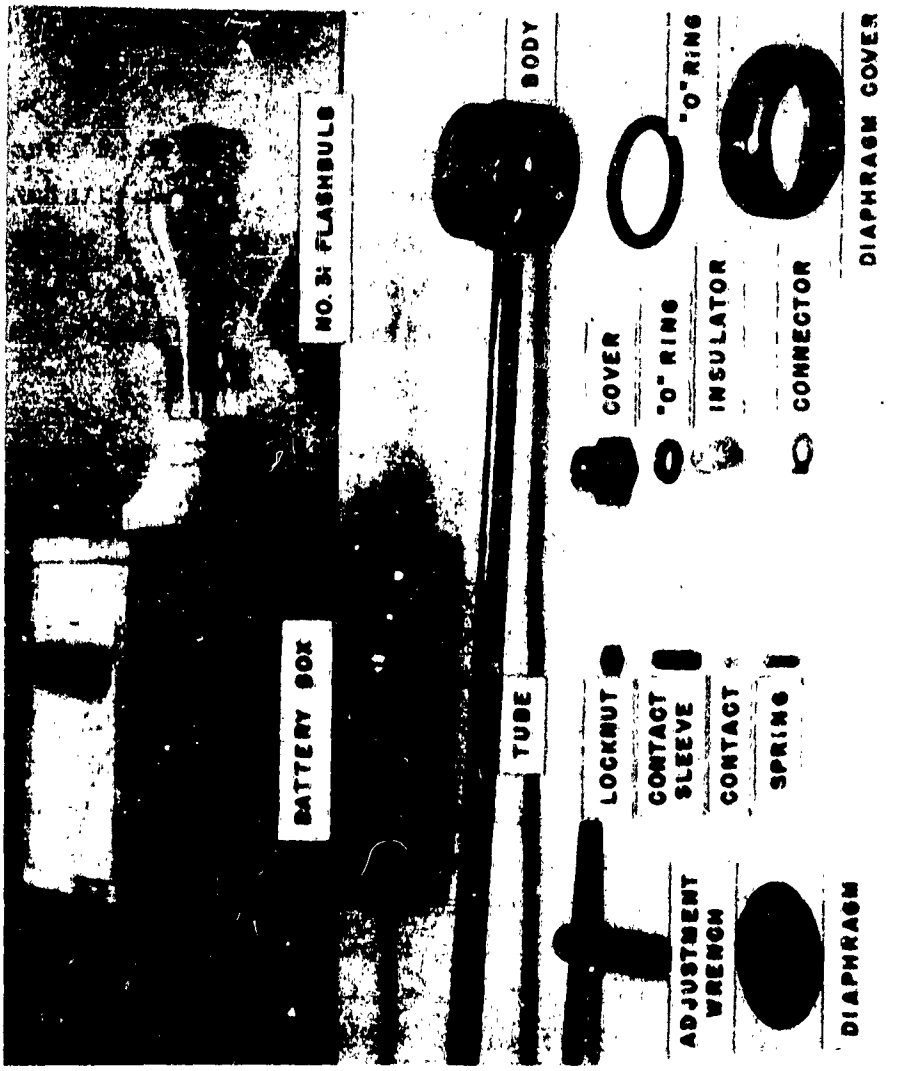

FIG. B-1 TRIGGER GAUGE COMPONENTS

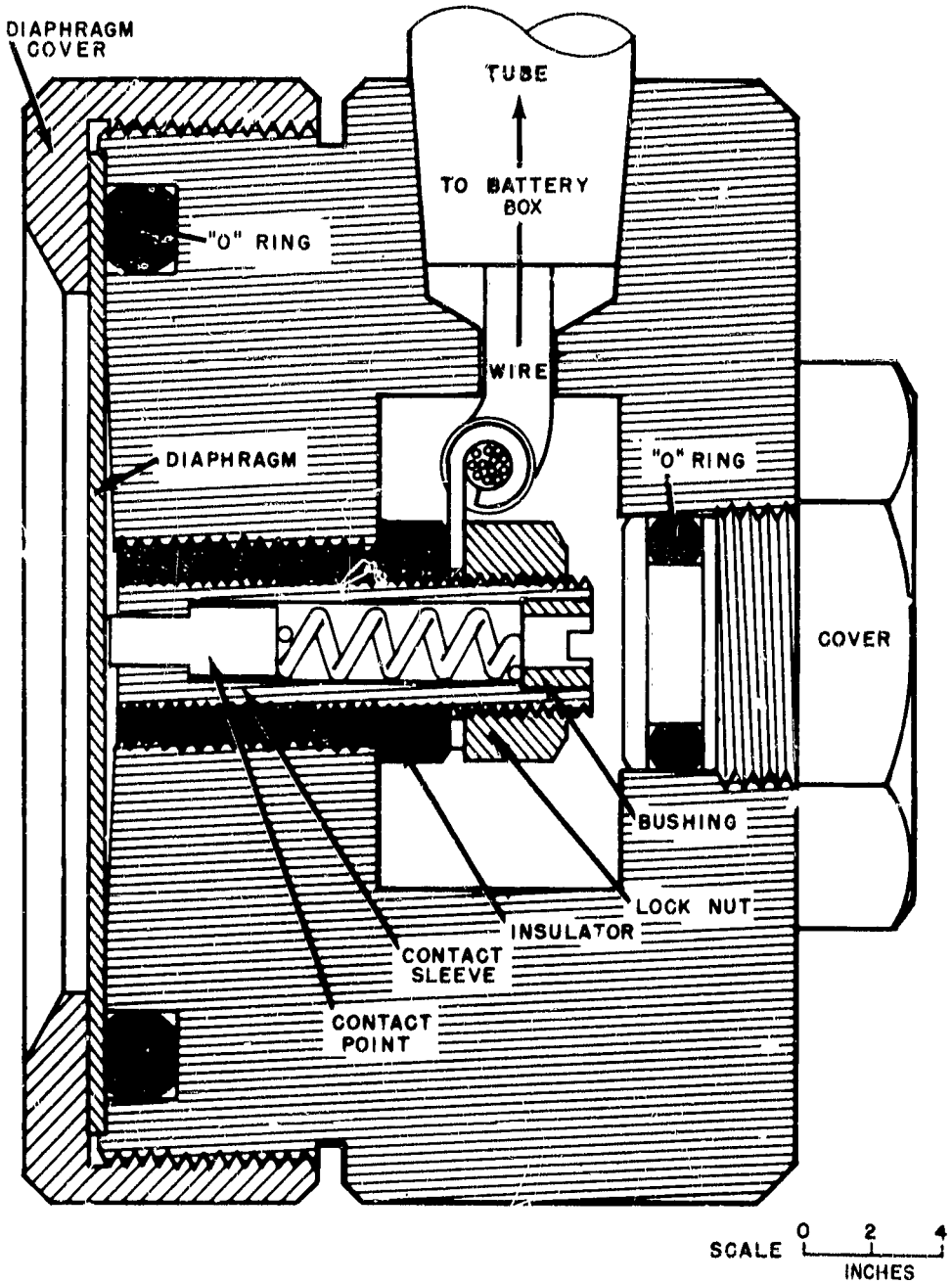

FIG. B-2 DIAPHRAGM AND CONTACT HOUSING

phragm.

2. Adaption for other use. A locking solenoid relay could be incorporated into the gauge so that a heavier current could be passed, since the actual time of contact is very short, and this in turn could operate a small motor or a bank of flash bulbs for greater camera distances.

III. USE IN THE FIELD.

The weight and location of the charge in relation to the camera positions were the governing factors in the final positioning of the gauges. These gauges were placed on either side of the charge on a line perpendicular to the camera line of sight. Because of the irregularities of the river bottom the gauges had to be placed at various depths, ranging from 3 inches to 2 feet. When the water depth was less than 4 feet the best results were obtained with the gauges at mid-depth.

To check the gauges before placing them in position, an ohmmeter was connected in series with the contact and diaphragm. The contact was adjusted by screwing the contact housing (Fig. B-2) in or out until the ohmmeter showed that the gap was at a minimum distance. A rough check can be made on the amount of pressure required to close the contacts by pressing on the diaphragm and watching the ohmmeter. In this manner it is possible to set the contacts so that a very small pressure will activate the gauge. The gauge was held in position by clamping the battery box to a pole that was set vertically in the river bottom.

IV. TEST RESULTS.

1. Use as a scale marker. On the latest field test the results of using these gauges as scale markers were very good. The flashes from the bulbs could be seen clearly on the film. The duration of the flashes is several frames at

normal camera speed.

Figure B-3 is an enlarged print from 35 mm film showing the flashes to the right and left as white spots. The camera, a 35 mm Mitchell equipped with a 1 inch lens, was approximately 500 feet from the explosion. Although this distance is fairly short, in other cases the cameras had to be over 6000 feet from the charge, yet the flashes were still measurable.

2. Troubles and their attempted cures. Although the gauges were not 100% reliable, modifications during the field test tended to correct the outstanding faults. Considerable trouble was encountered when salt water spray from the explosions corroded the brass contacts in the flash bulb sockets and rusted the steel spring in the contact assembly. The corrosion problem was reduced by installing wide mouth mason jars over the sockets and it is hoped that with the use of stainless steel or phosphor-bronze springs in the contact assembly the rust problem will be eliminated.

In very shallow water - 8 inches or less - there seemed to be a shockwave cut-off effect, so that the diaphragm was not depressed. When this condition prevailed, both gauges were placed on the deeper side of the charge, perpendicular to the camera line of sight.

V. CONCLUSION.

Although the gauges did not function 100%, they were better than any other system tried. Since each gauge is a complete unit within itself, set-up time is reduced considerably over other systems. The distance between flashes of the bulbs was always measurable on the film, although camera to subject distances of over 6000 feet were encountered.

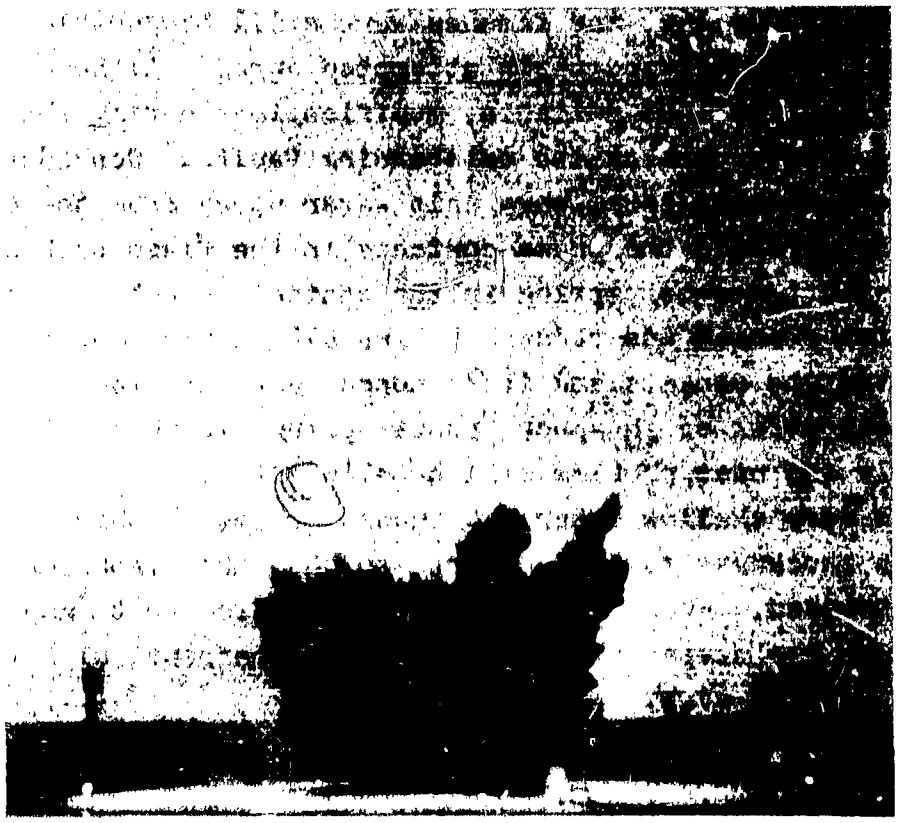

FIG. B-3 FLASHBULB SCALE MARKERS

APPENDIX C
MODEL LAWS IN RELATION TO SCALING OF THE BASE SURGE PHENOMENON

by
A. B. Arons, Consultant
Amherst College

I. INTRODUCTION.

1.1 The discussion given below consists of a development of the fundamental model laws and their application to the description and prediction of base surge effects. This is not a new contribution to the theory of models, but is simply an elementary development of pertinent ideas which, when thus assembled in one report, may prove useful to workers in the field and may help others more readily to use and interpret the results being reported by NOL Project 152. More detailed discussion of model laws and of hydraulic models may be found in references (1) and (2) upon which this note is largely based.

II. ELEMENTARY MODEL LAWS FOR GEOMETRICALLY SIMILAR MODEL AND PROTOTYPE.

2.1 "Geometrical similarity" means similarity of form, i.e., two objects are geometrically similar if the ratios of all homologous dimensions are equal. The term "kinematic similarity" denotes similarity of motion, i.e., the paths of homologous particles are geometrically similar and the ratios of the velocities of the various homologous particles involved in the motion are equal. "Dynamic similarity" implies similarity of masses and forces, i.e., two motion occurrences are dynamically similar if they are kinematically similar, if the ratio of masses of the various homologous particles are equal, and if the ratios of homologous forces

which affect the motion of the homologous particles are equal.

2.2 We adopt the following notation, the subscripts m and p denoting model and prototype respectively:

x_m, x_p homologous linear dimensions.

t_m, t_p homologous time intervals.

m_m, m_p homologous mass particles in corresponding positions.

F_m, F_p homologous mass accelerating forces.

ρ_m, ρ_p densities of homologous mass particles.

Then for geometrical similarity of model and prototype

$$\frac{x_m}{x_p} = x_r ,$$

a constant ratio for all homologous linear dimensions.

For kinematic similarity the ratio of homologous time intervals required for any two homologous particles to travel similar paths must be constant throughout the system:

$$\frac{t_m}{t_p} = t_r$$

Similarly, for dynamic similarity:

$$\frac{m_m}{m_p} = m_r \; ; \; \frac{F_m}{F_p} = F_r$$

From dimensional considerations it then follows that:

(a) the ratio of homologous volumes: $V_r = x_r^3$

(b) the ratio of velocities of homologous particles at corresponding positions: $v_r = \frac{x_r}{t_r}$

(c) the ratio of accelerations of homologous particles at corresponding positions: $a_r = \frac{x_r}{t_r^2}$

2.3 Both model and prototype must satisfy Newton's second law:

$$F_m = m_m a_m \quad ; \quad F_p = m_p a_p$$

Therefore:

$$F_r = m_r a_r = \rho_r x_r^3 \cdot \frac{x_r}{t_r^2} \qquad (1)$$

In addition, other conditions must be satisfied, depending upon the nature and relative importance of the other driving forces. Perfect similarity is rarely attainable in the model because it is generally impossible to satisfy all the additional restrictions, but simple scaling laws may be derived for situations in which one particular kind of force is dominant.

2.4 The Froude Law. For the case in which the force of gravity is the dominant one causing motion in both model and prototype, the gravitational forces acting on homologous mass particles are:

$$F_m = \rho_m V_m g_m \quad ; \quad F_p = \rho_p V_p g_p$$

and

$$F_r = \rho_r x_r^3 g_r \qquad (2)$$

where g_r is the ratio of gravitational accelerations in the

model and prototype; its magnitude is usually unity, but it will be retained here as an algebraic symbol for generality.

To satisfy both (1) and (2) it is necessary that:

$$\rho_r x_r^3 \frac{x_r}{t_r^2} = \rho_r x_r^3 g_r ,$$

from which

$$t_r = \left(\frac{x_r}{g_r}\right)^{1/2} \tag{3}$$

When $g_r = 1$,

$$t_r = (x_r)^{1/2} \tag{4}$$

indicating that the ratio of homologous time intervals will be equal to the square root of the length scale when gravitational effects are dominant. This is the basis of "Froude scaling".

Since the ratio of velocities of homologous particles:

$$v_r = \frac{x_r}{t_r} ,$$

equation (3) may be written in another form:

$$v_r = (x_r g_r)^{1/2} \tag{5}$$

or, alternatively:

$$\frac{v_m^2}{x_m g_m} = \frac{v_p^2}{x_p g_p} \tag{6}$$

Equation (6) represents what is perhaps a more familiar form of the Froude law, namely that for dynamic similarity of

gravitational effects, the Froude number v^2/xg must be equal for corresponding points in the model and prototype.

2.5 For the particular purpose of examining the scaling of such base surge properties as the radius - time curve we use equation (4), noting that corresponding radii R_m and R_p would occur at corresponding times t_m and t_p. If we select the column diameters D_m and D_p as measures of the linear scale, certain radii would correspond to each other if $\frac{R_m}{D_m} = \frac{R_p}{D_p}$. The corresponding time intervals measured from a common zero would have to satisfy the condition of equation (4)

$$\frac{t_m}{D_m^{1/2}} = \frac{t_p}{D_p^{1/2}}$$

Thus, if gravitational forces are dominant and Froude scaling is satisfied, all model and prototype results would fall on the same curve if plotted in the form of r vs τ, where $r \equiv R/D$ and $\tau \equiv t/D^{1/2}$. Data presented in various reports by this group has been treated accordingly.

III. MODEL LAWS FOR THE BASE SURGE.

3.1 We now consider the base surge phenomenon itself in more detail, taking into account the effects of column height, column density, ambient density, etc. It is assumed that, at least in the initial stages, gravitational effects are dominant. Consider a column of height C, diameter D, and density ρ, surrounded by a fluid medium of density ρ_o, and descending under the influence of gravity.

At a height y the material of the column would have a potential energy per unit volume $(\rho - \rho_o)$ g y. The velocity which would be acquired at the base by virtue of this change

in potential would be given by $1/2\,\rho\, v^2$. Thus taking a ratio of model to prototype:

$$\rho_r\, v_r^2 = \rho_r\, \frac{\left(1-\frac{\rho_{om}}{\rho_m}\right)}{\left(1-\frac{\rho_{op}}{\rho_p}\right)}\, g_r\, y_r$$

$$v_r^2 = \sigma_r g_r y_r \tag{7}$$

where

$$\sigma = \left(1 - \frac{\rho_o}{\rho}\right)$$

and y_r is the vertical length scale defined by C_m/C_p.

Thus for motion in the vertical direction:

$$\frac{y_r^2}{t_{ry}^2} = \sigma_r\, g_r\, y_r$$

and the ratio of homologous time intervals for vertical motion is given by:

$$t_{ry} = \left(\frac{y_r}{\sigma_r g_r}\right)^{1/2} \tag{8}$$

The horizontal and vertical scales are connected by the fact that the velocity v becomes a horizontal velocity at the base of the column. Then for horizontal motion:

$$\frac{x_r^2}{t_{rx}^2} = \sigma_r\, g_r\, y_r$$

and

$$t_{rx} = \left(\frac{x_r^2}{\sigma_r g_r y_r}\right)^{1/2} \tag{9}$$

where t_{rx} is the ratio of homologous time intervals for horizontal motion and x_r is the horizontal scale determined by D_m/D_p.

3.2 If we again consider homologous radii in terms of the horizontal scale such that $\frac{R_m}{D_m} = \frac{R_p}{D_p}$, such radii will be attained at time intervals such that

$$\frac{t_{rx}\,(\sigma_m c_m)^{1/2}}{D_m} = \frac{t_{px}\,(\sigma_p c_p)^{1/2}}{D_p}$$

(g_r is assumed unity).

Thus, measurements of R vs. t should fall on the same curve if plotted as r vs. τ^* where $r = R/D$ and $\tau^* = t\,(\sigma c)^{1/2}/D$.

REFERENCES

(1) Hydraulic Models. American Society of Civil Engineers. Manual of Engineering Practice No. 25.

(2) Scale Models in Hydraulic Engineering. J. Allen. Longman's, Green, and Co. 1947.

APPENDIX D

BASE SURGE DATA FROM TEST BAKER

The following data were extracted from the University of California Report No. 3 on the Photogrammetry of Test Baker [14] and "Characteristics of the Base Surge" by Roger Revelle [15]. They are in agreement with an independent check of base surge growth made by NOL personnel from 35 mm photographic records obtained at Bikini on the U.S.S. Kenneth Whiting. Smoothed mean curves are used in this report for comparison with scaled high explosive results. The average maximum column diameter is 2030 ft.

Time t (sec)	Scaled Time τ (sec/ft$^{1/2}$)	Surge Radius R (ft)	Scaled Surge Radius r	Surge Height H (ft)	Scaled Surge Height h
*					
10	0.22	1210	0.60	426	0.21
11.8	0.26	1500	0.74	255	0.13
14.7	0.33	--	--	445	0.22
17.6	0.39	2030	1.0	365	0.18
20.6	0.46	--	--	370	0.18
23.5	0.52	2450	1.21	660	0.33
26.5	0.59	--	--	770	0.38
29.4	0.65	2875	1.42	490	0.24
32.3	0.72	--	--	495	0.24
35.3	0.78	3288	1.62	480	0.24
38.2	0.85	--	--	530	0.26
41.2	0.91	3600	1.77	650	0.32
44.1	0.98	--	--	655	0.32
47.0	1.04	3950	1.95	680	0.33
50.0	1.11	--	--	825	0.41
52.9	1.17	4300	2.12	925	0.46
55.9	1.24	--	--	1020	0.50
58.8	1.30	4525	2.23	790	0.39
61.7	1.37	--	--	785	0.39
64.7	1.43	4800	2.36	870	0.43
67.6	1.50	--	--	1025	0.51
70.6	1.57	5025	2.48	780	0.38
73.5	1.63	--	--	955	0.47
76.4	1.69	5300	2.61	1005	0.495
79.4	1.76	--	--	1115	0.55
82.3	1.82	5550	2.73	1035	0.51
85.3	1.89	--	--	1045	0.515
88.2	1.96	5775	2.84	1180	0.58
91.1	2.02	5875	2.89	1275	0.63
100	2.22	6250	3.08	--	---
105.8	2.35	6450	3.18	--	---
*100	2.22	6295	3.10	1476	0.73
*120	2.66	7020	3.46	1575	0.78
*140	3.10	7410	3.65	1804	0.89
*160	3.55	7808	3.85	1804	0.89
*180	3.99	8164	4.02	1804	0.89
*200	4.43	8393	4.13	1804	0.89

* Data obtained by R. Revelle [15].

DISTRIBUTION LIST

ARMY

	Copies
Assistant Chief of Staff, G-3, D/A, Washington 25, D.C. Attn: Deputy Chief of Staff, G-3 (RR and SW)	1
Assistant Chief of Staff, G-4, D/A, Washington 25, D.C.	1
Chief of Ordnance, D/A, Washington 25, D.C. Attn: ORDTX-AR	1
Chief Signal Officer, D/A, P and O Division, Washington 25, D.C.	3
The Surgeon General, D/A, Washington 25, D.C. Attn: Chairman, Med R and D Bd	1
Chief Chemical Officer, D/A, Washington 25, D.C.	2
The Quartermaster General, CBR, Liaison Officer, R and D Division, D/A, Washington 25, D.C.	1
Chief of Engineers, D/A, Washington 25, D.C. Attn: ENGNB	2
Chief of Transportation, Military Planning and Intelligence Division, Washington 25, D.C.	1
Chief, Army Field Forces, Ft. Monroe, Va.	3
President, Board No. 1, OCAFF, Ft. Bragg, N. C.	1
President, Board No. 4, OCAFF, Ft. Bliss, Texas	1
Commander-in-Chief, FECOM, APO 500, c/o, PM, San Francisco, Calif. Attn: ACofS, J-3	2
Commandant, Command and General Staff College, Ft. Leavenworth, Kansas. Attn: ALLIS(AS)	1
Commandant, The AA and GM Branch, The Artillery School, Ft. Bliss, Texas	1
Commanding General, Medical Field Service School, Brooke Army Medical Center, Ft. Sam Houston, Texas	1
Director, Special Weapons Development Office, OCAFF, Ft. Bliss, Texas	1
Commandant, Army Medical Service Graduate School, Walter Reed Army Medical Center, Washington 25, D.C.	1
Commanding General, Research and Engineering Command, Army Chemical Center, Maryland. Attn: Deputy for RW and Non-Toxic Material	1
Commanding General, The Engineer Center, Ft. Belvoir, Va. Attn: Asst Commandant, Eng School	3
Commanding Officer, Engineer Research and Development Laboratory, Ft. Belvoir, Va. Attn: Chief, Tech Intel Br	1
Commanding Officer, Picatinny Arsenal, Dover, N. J. Attn: ORDBB-TK	1
Commanding Officer, Army Medical Research Laboratory, Ft. Knox, Ky	1
Commanding Officer, Chemical and Rad. Laboratory, Army Chemical Center, Maryland. Attn: Tech Library	2
Commanding Officer, Transportation R and D Station, Ft. Eustis, Virginia	1

DISTRIBUTION LIST (CONT.)

ARMY (CONT.)

	Copies
Director, Technical Documents Center, Evans Signal Laboratory, Belmar, New Jersey	1
Director, Waterways Experiment Station, P. O. Box 631, Vicksburg, Mississippi, Attn: Library	1
Director, Armed Forces Institute of Pathology, 7th and Independence Ave., S. W., Washington 25, D.C.	1
Director, Operations Research Office, Johns Hopkins University, 6410 Connecticut Avenue, Chevy Chase, Maryland. Attn: Library	1
Commanding Officer, Ballistics Research Laboratory Aberdeen, Maryland	1

NAVY

Chief of Naval Operations, D/N, Washington 25, D.C. Attn: OP-36	2
Chief of Naval Operations, D/N, Washington 25, D.C. Attn: OP-374 (OEG)	1
Director of Naval Intelligence, D/N, Washington 25, D.C. Attn: OP-322V	1
Chief, Bureau of Medicine and Surgery, D/N, Washington 25, D.C. Attn: Special Weapons Defense Division	1
Chief, Bureau of Ordnance, Washington 25, D.C.	1
Chief, Bureau of Ordnance. Attn: Re2c	3
Chief, Bureau of Ordnance. Attn: Rexn	1
Chief, Bureau of Ships, D/N, Washington 25, D.C.	1
Chief, Bureau of Ships. Attn: Code 423	2
Chief, Bureau of Yards and Docks, D/N, Washington 25,D.C. Attn: P-312	1
Chief, Bureau of Supplies and Accounts, D/N, Washington 25, D.C.	1
Chief of Naval Research, D/N, Washington 25, D. C. Attn: LTJG F. McKee, USN	1
Chief of Naval Research. Attn: Code 466	1
Chief, Bureau of Aeronautics, D/N, Washington 25, D.C.	2
Commander-in-Chief, U. S. Atlantic Fleet, U. S. Naval Base, Norfolk 11, Va.	1
Commanding Officer, Norfolk Naval Shipyard. Attn: Code 290	2
Commander-in-Chief, U. S. Pacific Fleet, FPO San Francisco, California	1
Commanding Officer, Naval Powder Factory, Indian Head, Md.	1

DISTRIBUTION LIST (CONT.)

NAVY (CONT.)

	Copies
Commandant, U. S. Marine Corps, Washington 25, D.C. Attn: Code A03H	4
Naval Proving Ground, Dahlgren, Virginia Attn: Experimental Officer	1
President, U. S. Naval War College, Newport, R.I.	1
Superintendent, U. S. Naval Postgraduate School, Monterey, California	1
Commanding Officer, U. S. Naval Schools Command, U. S. Naval Station, Treasure Island, San Francisco, California	1
Commanding Officer, U. S. Fleet Training Center, Naval Base, Norfolk 11, Va. Attn: Special Weapons School	1
Naval Ordnance Laboratory Representative to the United Kingdom	1
U. S. Naval Attache, London	1
British Joint Services Mission, Navy Staff. Via Ad8, BuOrd	10
Defense Research Board, Canadian Joint Staff. Via Ad8, BuOrd	5
Director, Applied Physics Laboratory, Johns Hopkins University, Silver Spring, Maryland	2
Commanding Officer, U. S. Fleet Training Center, Naval Station, San Diego, California. Attn: (SPWP School)	2
Commanding Officer, U. S. Naval Damage Control Training Center, Naval Base, Philadelphia, Pa. Attn: ABC Defense Course	1
Commanding Officer, U. S. Naval Unit, Chemical Corps School, Army Chemical Training Center, Ft. McClellan, Alabama	1
Commander, U. S. Naval Ordnance Test Station, Inyokern, China Lake, California	1
Officer-in-Charge, U. S. Naval Civil Engineering Research and Evaluation Laboratory, U. S. Naval Construction Bn Center, Port Hueneme, California. Attn: Code 753	1
Commanding Officer, U. S. Naval Medical Research Institute, National Naval Medical Center, Bethesda, Maryland	1
Director, U. S. Naval Research Laboratory, Washington 25, D. C.	1
Commanding Officer and Director, U. S. Navy Electronics Laboratory, San Diego 52, California Attn: Code 4223	1
Commanding Officer, U. S. Naval Radiological Defense Laboratory, San Francisco, Calif. Attn:Tech Info Div.	2

DISTRIBUTION LIST (CONT.)

NAVY (CONT.)

	Copies
Commanding Officer and Director, David W. Taylor Model Basin, Washington 7, D. C. Attn: Library	2
Commander, U. S. Naval Air Development Center, Johnsville, Pa.	1
Director, Office of Naval Research Branch Office, 1000 Geary St., San Francisco, California	2

AIR FORCE

Assistant for Atomic Energy, Headquarters USAF, Washington 25, D. C. Attn: DCS/O	1
Director of Plans, Headquarters USAF, Washington 25, D.C. Attn: War Plans Division	1
Director of Requirements, Headquarters USAF, Washington 25, D. C.	1
Director of Research and Development, DCS/D, Headquarters USAF, Washington 25, D. C. Attn: Combat Components Div.	1
Director of Intelligence, Headquarters USAF, Washington 25, D. C. Attn: AFOIN-1B2	2
The Surgeon General, Headquarters, USAF, Washington 25, D. C. Attn: Bio Def Br, Prev Med Div	1
Commander, Strategic Air Command, Offutt AFB, Omaha, Nebraska. Attn: Special Weapons Branch, Inspector Div., Inspector General	1
Commander, Tactical Air Command, Langley AFB, Va. Attn: Doc Security Br	1
Commander, Air Defense Command, Ent AFB, Colorado	1
Commander, Air Materiel Command, Wright-Patterson AFB, Dayton, Ohio. Attn: MCAIDS	2
Commander, Air Training Command, Scott AFB, Belleville, Ill. Attn: DCS/O GTP	1
Commander, Air Research and Development Command, P. O. Box 1395, Baltimore, Maryland, Attn: RDDN	1
Commander, Air Proving Ground Command, Eglin AFB, Fla. Attn: AF/TRB	1
Director, Air University Library, Maxwell AFB, Ala. Attn: CR-5464	2
Commander, Crew Training Air Force, Randolph Field, Texas. Attn: 2GTS,DCS/O	1
Commander, Headquarters, Technical Training Air Force, Gulfport, Miss. Attn: TA and D	1
Commandant, Air Force School of Aviation Medicine, Randolph AFB, Texas	2
Commander, Wright Air Development Center, Wright-Patterson AFB, Dayton, Ohio Attn: WCOESP	2

DISTRIBUTION LIST (CONT.)

OTHERS (CONT.)

	Copies
Dr. E. B. Doll, Stanford Research Institute, Palo Alto, California. Via INM	1
Dr. Kurt Otto Friedrichs, Institute for Mathematics and Mechanics, New York University, New York, N.Y. Via INM	1
Dr. David T. Griggs, Institute of Geophysics, University of California, Los Angeles 24, California Via INM	1
Professor Bruce G. Johnston, Department of Civil Engineering, University of Michigan, Ann Arbor, Michigan. Via INM	1
Dr. Joseph B. Keller, Office of Naval Research, Washington 25, D. C.	1
Professor C. B. Morrey, Department of Mathematics, University of California, Berkeley 4, California Via INM	1
Dr. N. M. Newmark, Ill. Talbot Laboratory, University of Illinois, Urbana, Illinois. Via INM	1
Professor Donald W. Taylor, Department of Civil and Sanitary Engineering, Massachusetts Institute of Technology, Cambridge 39, Mass. Via INM	1
Dr. Hans H. Bleich, Department of Civil Engineering, Columbia University, New York, N. Y. Via INM	1
Dr. Charles H. Norris, Department of Civil Engineering, Massachusetts Institute of Technology, Cambridge 39, Massachusetts. Via INM	1
Prof. Arnold B. Arons, Amherst College, Amherst, Massachusetts. Via INM Boston	1
Dr. A. B. Focke, Marine Physics Laboratory, San Diego, California. Via INM	1
Prof. Werner Goldsmith, Dept. of Engineering Design, University of California, Berkeley 4, California Via INM	1
Director, Construction Division, USAEC, Washington 25, D.C. Attn: Mr. C. Beck	1